MODIFYING THE DEPOLYMERIZATION OF SACRIFICAL POLYMERS FOR ELECTRONIC DEVICES

A Dissertation
Presented to
The Academic Faculty

by

Oluwadamilola Phillips

In Partial Fulfillment
of the Requirements for the Degree
Doctorate of Philosophy in the
School of Chemical and Biomolecular Engineering

Georgia Institute of Technology
December 2018

MODIFYING THE DEPOLYMERIZATION OF SACRIFICIAL POLYMERS FOR ELECTRONIC DEVICES

Approved by:

Dr. Paul A. Kohl, Advisor
School of Chemical and Biomolecular Engineering
Georgia Institute of Technology

Dr. Elsa Reichmanis
School of Chemical and Biomolecular Engineering
Georgia Institute of Technology

Dr. Ryan Lively
School of Chemical and Biomolecular Engineering
Georgia Institute of Technology

Dr. Karl I. Jacob
School of Materials Science and Engineering
Georgia Institute of Technology

Dr. Martin Maldovan
School of Chemical and Biomolecular Engineering
Georgia Institute of Technology

Date Approved: July 3, 2018

This PhD dissertation is dedicated to my hero and father, Kola Sanyaolu Phillips

ACKNOWLEDGEMENTS

There are many people who I need to thank for allowing me to fulfill one of my dreams of pursuing a PhD in chemical engineering. First, I'd like to thank my advisor Dr. Paul Kohl for accepting me as graduate student in his group. I have a great deal of respect and admiration for the depth of knowledge and creativity in your approach to research. I have learned a tremendous amount from you, and I thank you for having a great sense of humor. My graduate study experience has been truly enjoyable and it is thanks to you. Hopefully I have expanded your horizon on all the types of delicious jello that one could make.

I also like to thank the current and past Kohl group members such as Dr. Brennen Mueller, Dr. Jared Schwartz, Dr. Johanna Stark, Dr. Lisha, Liu, Dr. Bharatkumar Suhtar, John Ahlfield, Jisu Jiang, Anthony Engler, and Garrett Huang. You all have been so much fun throughout the whole process. From indulging me in all my fun little wagers or convincing me that I have a receding hairline. Bharat thanks for stealing hours of my time with your 'interesting' points of views and I eagerly await for the release of your book "The Memoirs of a Monster". Lisha, thanks for allowing me to color all your minion picture books in a way that I liked. Garrett, thanks for being a nerd with me and talking about all of our favorite shows. Thank you Brennen and Jared for taking the time to train me in my first year, you both were a tremendous help. I have a lot of respect and gratitude for the VAPR winning team consisting of myself, Schwartzinator, Speedy Jisu, and Anthony (Tony) for going through all the intense times and solving many problems together. The

contributions you all have made to my work cannot be overstated. It is with great pride that I can say that I am a past Kohl Group member.

I would also like to thank my family. My wonderful and supportive wife, Wenjiao Huang, for dealing with a person like me and giving me strength in so many ways. I like to thank my mother for ruthlessly educating me after school and providing discipline in my studies throughout my entire life. Lastly, I'd like to thank my father, Kola Sanyaolu Phillips, for being my inspiration in all my work though life. Your positive attitude, hard work ethic, no-excuse persona has helped me through so many challenges. Your life story and triumph over immense adversity gives me strength to accomplish anything. You have taught me many things and led by example. If I could be half the man that you are, I think I'll do alright in life.

TABLE OF CONTENTS

LIST OF TABLES

LIST OF FIGURES

LIST OF ABBREVIATIONS

AA	Acid Amplifiers
DCM	Dichloromethane
DMA	Dynamic Mechanical Analyzer
DSC	Dual Scanning Calorimetry
GBL	Gamma-butyrolactone
HAR	High Aspect Ratio
NMR	Nuclear Magnetic Resonance
NMP	N-Methyl-2-pyrrolidone
PAG	Photoacid generator
PBG	Photobase generator
PET	Photo-induced electron transfer
PPHA	Poly(phthalaldehyde)
p(PHA-co-BA)	Poly(phthalaldehyde-co-butanal)
p(PHA-co-EA)	Poly(phthalaldehyde-co-ethanal)
PS	Photosensitizer
PPC	Poly(propylene carbonate)
Rhodorsil-Faba	tetrakis(pentafluorophenyl)borate-4-methylphenyl[4-(1-methylethyl)phenyl]iodonium
QCM	Quartz Crystal Microbalance
TGA	Thermal gravimetric Analysis
THF	Tetrahydrofuran
UV	Ultraviolet

LIST OF SYMBOLS

ΔG	Change in Gibbs Free Energy
E_{ox}	Oxidation potential
E_{red}	Reduction Potential
E_{oo}	Optical band-gap
ε	Dielectric constant
d	Distance between two ion pairs
k_{diff}	Diffusion-controlled rate constant
k_{el}	Activation-Energy Controlled rate constant
k_q	Bimolecular rate quenching constant
KSV	Stern-Volmer quenching constant
T_d	Thermal decomposition temperature
T_g	Thermal glass transition temperature
T_c	Ceiling Temperature
Rnorm	Normalized Resistance
b	Rate constant for depolymerization (s^{-1})
c	Photoresponse delay (sec)
°C	Celsius
Đ	Polydispersity Index
D_{100}	Minimum Dosage
γ	Lithographic Contrast
Ecc	Contrast-Curve Efficiency

SUMMARY

Decomposable polymers in the electronic industry can be used in the manufacturing of traditional integrated circuits and packages. Polymers that can be triggered to depolymerize into volatile, monomeric units are particularly useful as template materials for the creation of embedded-air cavities in the fabrication of traditional integrated circuits, MEMS packaging solutions, and transient (disposable) electronics. The understanding of thermal depolymerization of these polymers are used as a basis to modify their properties for a wide range of applications. The thermal decomposition of polypropylene carbonate has been stabilized by end-capping and organic additives to reach higher thermal process windows. The stimulus for the thermal decomposition has been controlled via photochemical reaction that can be targeted to specific wavelengths of light. A controlled delay of the depolymerization under the presence of irradiation has been demonstrated with the addition of basic additives that undergo competitive reactions with the free acid. The liquid-state after depolymerization of polyaldehdyes has been extended to low temperatures by freezing point depression of the monomer. Liquid products are desirable because the monomer can be absorbed into the surrounding environment and elicit 'disappearance' of the polymer for clandestine applications of transient devices. Dual-layer structures have been demonstrated to limit the photo-chemical trigger to one region, where the acid-catalyst for degradation can propagate to unexposed regions. The multi-layer structure allows for fabrication of a wide-range of devices where the photosensitive trigger can be added at the last fabrication step. The results in this dissertation has created a pathway for the development and application of a new family of transient, photodegradable

materials that can be tuned from wavelengths in the ultraviolet light region into the entire visible spectrum at ambient or subzero temperatures.

CHAPTER 1. INTRODUCTION

Decomposable polymers are a type of "sacrificial" materials that are widely used in the microelectronic industry as creating temporary place-holders in the fabrication of embedded air-gaps in a variety of electronic devices. These polymers can be triggered optically or thermally to depolymerize and volatize into small, harmless gaseous components that can permeate through most polymeric overcoat materials[1–8]. Decomposable polymers have been employed in many areas of electronic devices from traditional integrated circuits to the emerging field of transient (disposable) electronics. One of the many advantages is that gases, such as air, have a very low relative dielectric constant. Therefore, embedded air-cavities can be employed to lower the dielectric constant of an insulator for integrated circuits. This becomes increasingly important as the scaling of transistors to smaller dimensions can elicit cross-talk noise between copper interconnections, as well as power dissipation from resistance-capacitance coupling. Embedded-air cavities can also serve the purpose of the fabrication of a wide array of microstructures such as nanofluidic channels in microfluidic devices or the packaging of microelectromechanical systems [2,4,6,9,10]. The temporary nature of these materials has make for an ideal candidate for many transient electronics where the disposal of the device is desired.

1.1 Microelectromechanical Systems (MEMS) Packaging

MEMS packaging is essential for providing physical protection of the devices such as accelerometers and gyroscopes. The packaging of these devices amounts to a major cost (60 to 80%) of the total cost to fabricate a MEMS device[11]. Wafer-level packaging is a

necessary technique to for the packaging of multiple devices, thereby reducing the overall costs reliability testing and packaging. The most conventional approach is the "Wafer-Bonding" technique as shown in Figure 1.1[12]

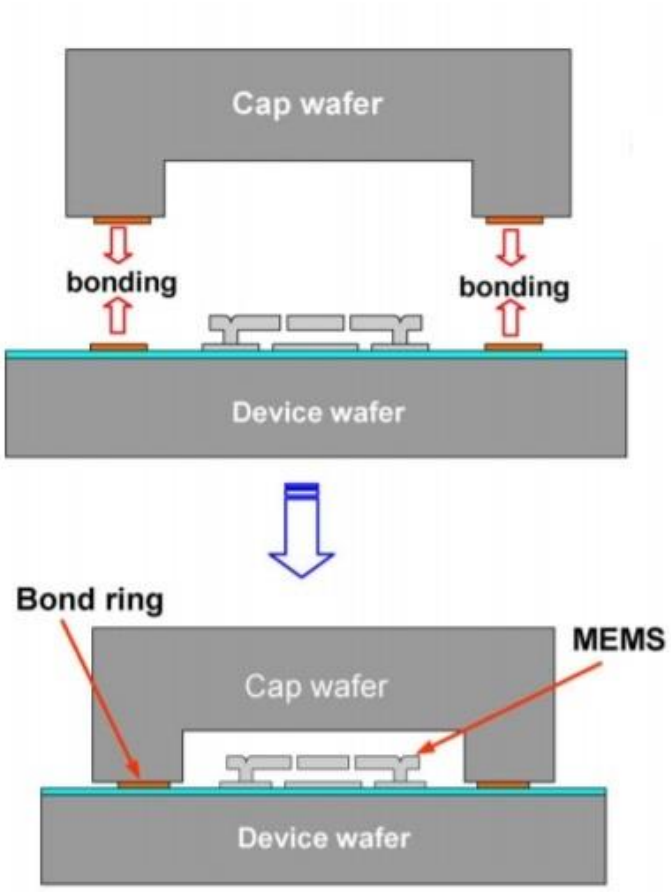

Figure 1.1 Wafer-Bonding Approach for MEMS device Packaging. Adapted from He. et al[12]

In this approach, a separate Si substrate is bonded directly to the MEMS wafer using a variety of techniques. The wafer-bonding approach is a costly, heterogeneous process. Additionally, high temperatures are typically required for the bonding (~400°C) which can be detrimental to the MEMS device.

A more cost-effective method has been developed by Fritz et.al for the creation of a polymer-based MEMS packaging solution using sacrificial materials[6]. The fabrication process for creating embedded air-cavities with decomposable polymers is straightforward as shown in Figure 1.2

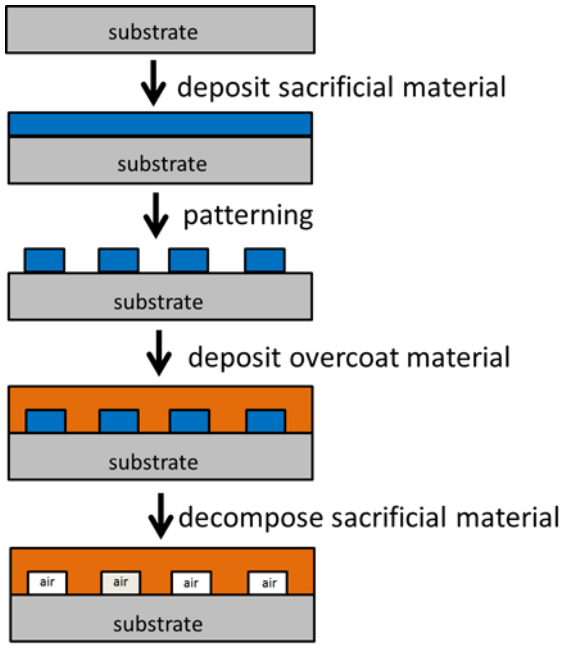

Figure 1.2 General Air-Cavity Fabrication Process

In Figure 1.2, the sacrificial polymers can be solvent-casted onto a silicon substrate. The polymer film can be directly photo-patterned from the addition of photo-acid generators or by other conventional etching techniques. An overcoat material is then deposited to form the shape of the sacrificial film underneath. The overcoat material is a cross-linking polymeric material (i.e. epoxy) that can maintain its mechanical integrity without support. The thermal window for the curing of the overcoat can vary by the type of material. The substrate can be annealed to trigger the decomposition of the sacrificial layer into small gaseous fragments that can permeate through the overcoat leaving an air-

cavity. A critical step in the fabrication process is controlling the thermal decomposition of the sacrificial polymer. A better understanding of the decomposition of the sacrificial polymer process can lead to modification and control of the rate and temperature of polymer decomposition making for a better match of the sacrificial polymer to the overcoat material.

1.2 Transient Electronics

The model for the electronics industry has historically been towards creating devices and materials that are operational and stable for long life. A new approach of decomposing electronics in a controlled, programmable manner is of interest for devices that don't have to be retrieved (i.e. returned to the environment in a friendly way) or can be destroyed so as to avoid reverse engineering, capture or detection [13]. The controlled, short life-span of these devices is of interest for use as biomedical implants, environmental sensors, and other commercial applications [14–17].

Many approaches have been made towards developing materials that are transient. The concept involves materials that function normally over a desired time of operation which can be triggered by a stimulus to dissolve or degrade into the environment leaving little to no chemical footprint behind. Many of the transient electronics today rely on solution-based triggers with biodegradable materials. Notable studies have included fully water soluble radio frequency electronic devices [15]. These devices are based on biocompatible and bioresorable materials such as magnesium for the electrodes and silk for the substrate. These components can be implanted into the human body and gradually dissolve in a controllable manner thereby eliminating the need for a surgical extraction.

Although much research has involved triggering the disappearance of devices with wet chemistry, the need for such an external or internal liquid source as trigger has limited the application of these temporary devices. Fast transience of materials in dry environments where an external liquid source is not viable has been largely unexplored. Past researchers have used outside stimulus such as light, temperature, and even mechanical forces to initiate transience of these materials [18]. Garner et al. used thermally tempered glass substrates that rely on an initial fracture to shatter the substrate into micron-sized pieces that are difficult to detect by the human eye [19]. Polymeric materials have also been used in transient device applications where the Moore group first introduced the use of poly(phthalaldehyde) to serve as the transient substrate for a an electronic device. Hernandez et. al demonstrated such a device where silicon-based active devices such as field-effect transistors and diodes were fabricated onto a PPHA substrate[20]. A photo-catalyst was incorporated into the PPHA substrate from exposure to ultraviolet light will undergo depolymerization as shown in Figure 1.3.

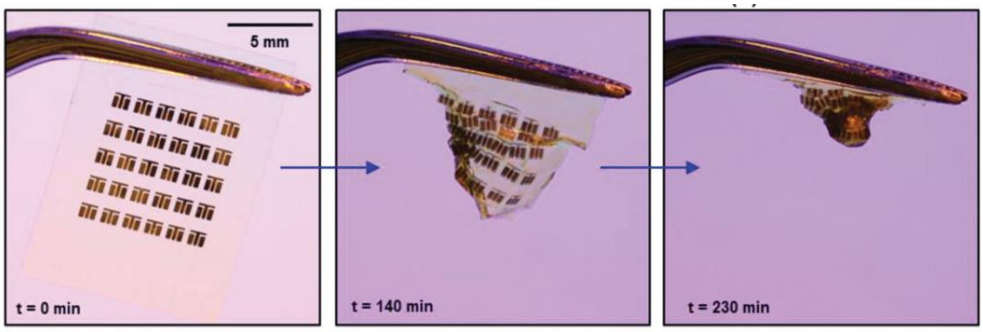

Figure 1.3 UV-triggered depolymerization of PPHA substrate with electronic circuits. Adapted from Hernandez. et al[20]

Decomposable polymers are an ideal candidate class of materials for transient electronics. The transient properties such as stimuli to initiate depolymerization,

depolymerization rate, thermal stabilization, and the control of the phase of the depolymerization products require careful tuning and modification for a wide variety of applications.

CHAPTER 2. BACKGROUND OF SACRIFICAL POLYMERS

2.1 Decomposable and Template Polymers

Decomposable and template polymers serve as temporary placeholders before the triggered decomposition into volatile units[21]. The general decomposition steps of decomposable polymers is a two-step process: (i) the polymer depolymerizes by going back to the monomers which, in some cases, were used to create the polymer, and (ii) the small molecule products from the first step evaporate. At higher temperatures, the first step is generally rate limiting since evaporation is rapid. However, at low temperatures the second step, evaporation of the monomer is the rate limiting step.

The desirable general, thermal degradation characteristics of sacrificial polymers include the following:

i) Polymer backbone or end-groups are susceptible to catalytic degradation from a specific stimulus (ie. light, acid, and/or heat)
ii) Stability from thermal degradation prior to the presence of trigger/stimuli
iii) Minimal to zero residual products after complete depolymerization/decomposition

In most traditional applications involving IC chips and MEMS packaging, a high sensitivity to the trigger and fast depolymerization is desirable to reduce the processing time and manufacturing costs to create the embdedded air-cavity during the fabrication of

microstructures. However, in transient electronics there are some instances where low sensitivity to the trigger and/or a controlled, slow depolymerization is also a desirable trait.

Modifying the three aforementioned characteristics can lead to a variety of new applications for decomposable polymers. However, modifying the depolymerization requires a fundamental understanding of the depolymerization pathways and the catalysts used to manipulate such mechanisms. Therefore, it is the aim of this dissertation to understand and control these thermal and optical properties to expand the compatibility of these materials for a wide range of sacrificial applications. Post-polymerization modification and the incorporation of unique organic, additives are facile and commercially viable pathways to manipulate these properties.

Heat-depolymerizable polymers are commonly used sacrificial polymers due to the ease of patterning and releasing. The ceiling temperature of the polymer is a thermodynamic property that dictates the critical temperature at which the polymer will depolymerize. In other words, the ceiling temperature is the temperature at the equilibrium between polymer and monomer. Below the ceiling temperature the polymer can exist in a thermodynamically stable state. Above the ceiling temperature, the polymer will become thermodynamically unstable and depolymerize back into its monomer state. High ceiling temperature polymers (ie. above ambient temperature) are typically used for embedded air-cavities for microstructures, while low-ceiling temperatures (ie. below ambient temperature) are more applicable to transient electronics.

2.1.1 High Ceiling Temperature Polymers

Thermodynamically stable polymers at room temperature (i.e. high ceiling temperature) that are most typically used to fabricate air-gaps or voids in microelectronic devices include the polynorbonene family[2,22–24]. Polynorbonenes have very high degradation temperatures (400^{o}C) and high glass transition temperature of 215^{o}C to prevent geometric distortion. This family of polymers is compatible with overcoats with high curing temperature and high-temperature oxide deposition. However, the elevated temperature can cause degradation of overcoat material as well as mechanical deformation in nearby structures. Polycarbonates, another family of sacrificial polymers, have a more favorable decomposition temperature range of 200^{o}C-300^{o}C and low-residue formation. Most notable polycarbonates include poly(ethylene carbonate) (PEC), poly(propylene carbonate) (PPC), poly(butylene carbonate) (PBC), poly(cyclohexene carbonate) (PCHC), poly(norbornene carbonate) (PNC), and poly(cyclohexene propylene carbonate) (PCHC) as shown in Figure 2.1.

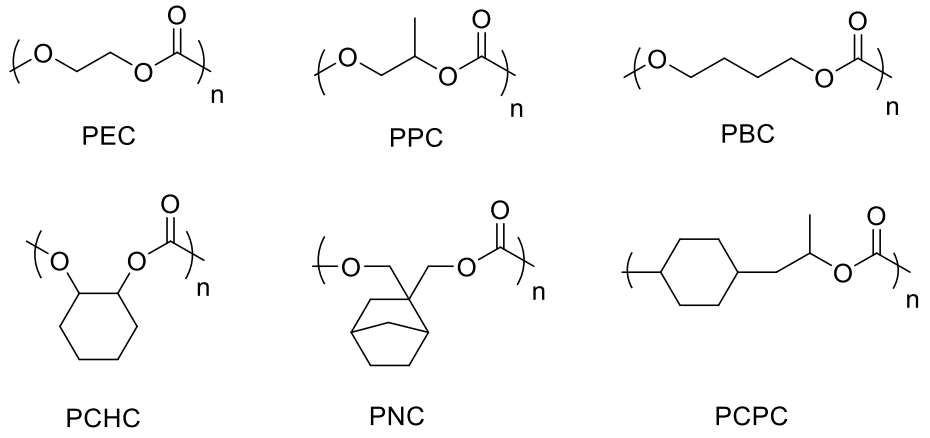

Figure 2.1 Various types of polycarbonates used as sacrificial materials

2.1.1.1 Poly(propylene carbonate) PPC

Poly(propylene carbonate) (PPC) is an amorphous, aliphatic polymer synthesized by the copolymerization of propylene oxide and carbon dioxide with an organometallic catalyst, typically zinc glutarate [25–31]. The polymer is attractive because it is made by the fixation of CO_2, and it is biodegradable and biocompatibile[32]. The low glass transition temperature makes PPC suitable for low-temperature packaging applications. The glass transition temperature of PPC can range from 25°C to 45°C depending on molecular weight and regioregularity of the polymer. Molecular weights ranging from 15 kDa to 200 kDa have previously been produced in commercial quantities. Recently lower molecular weight of 2 kDa PPC Polyol has been synthesized[33].

PPC has a relatively low onset temperature for decomposition, widely reported in the range from 180°C to 240°C depending on heating rates[8,29,34–36]. The low decomposition temperature makes it ideal for specific sacrificial polymer applications in microelectronics, especially those involving solder, epoxy, and movable components such as microelectromechanical systems (MEMS). The movable MEMS component can be encapsulated by a sacrificial polymer and a photo-definable dielectric as the overcoat in order to protect the movable component during processing. Later, a thermal treatment can be used to decompose the PPC and volatize the products, which diffuse through the overcoat, freeing the movable component in an air-cavity[4–7].

A critical step in the fabrication process is controlling the thermal decomposition of PPC, so that the MEMS device is released at the desired point in the fabrication

sequence. The thermal behavior of PPC has been studied; however, conflicting reports have led to an inadequate understanding of the thermal degradation process for PPC. A better understanding of the PPC decomposition process can lead to modification and control of the rate and temperature of polymer decomposition making for a better match of the sacrificial polymer to the overcoat material. For example, benzoyclobutene (BCB) has been used by Uzunlar, et al[4] as an overcoat material in the air-cavity process. A thermal treatment of the polymer/BCB structure at 190°C is done to cure the BCB and make it a mechanically stable overcoat before significant decomposition of PPC occurs. Afterwards, the temperature is increased to 240°C to quickly decompose PPC. At 190°C BCB needs 1.3 hours to cure to 70% cross-linking density. A modest increase of 20°C in the sacrificial polymer decomposition temperature can lower the curing time of BCB by a factor of 20 to just 4 minutes.

Desirable thermal properties of the sacrificial polymer that are needed for the process include: (i) thermal stability of the polymer during overcoat curing, (ii) rapid speed of decomposition at the degradation temperature, and (iii) minimal residue after decomposition. In this paper, the mechanisms for PPC decomposition have been studied and the means for altering the PPC decomposition temperature investigated. The results are compared to previous studies to shed light on the conflicting results.

Modifying the thermal properties requires a fundamental understanding of PPC degradation pathways. The thermal decomposition mechanisms of PPC have been previously proposed[26,32,37,38]. The polymer can be modified and catalysts can be added to the PPC polymer to inhibit or facilitate the decomposition. The thermal decomposition occurs via two mechanisms: (i) polymer unzipping (i.e. decomposition from the ends of

the polymer chain with the reaction proceeding inward), and (ii) random chain scission (i.e. internal repeat units of the polymer randomly undergo reaction), as shown in Figure 2.2.

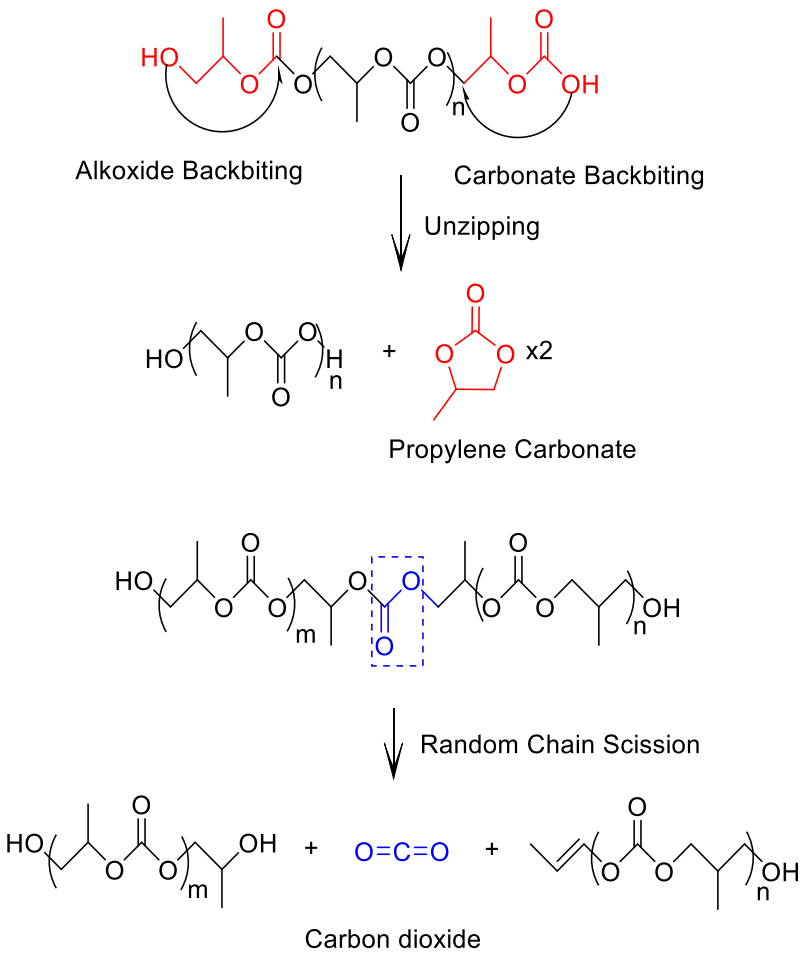

Figure 2.2 PPC decomposition pathways: unzipping and chain scission

In the unzipping reaction, chain ends become "active" via thermal energy and initiate a reaction with specific carbon sites across the polymer backbone, leading to degradation. Cyclic propylene carbonate is the typical product that is formed from this degradation mechanism[32,39,40]. It has been widely understood that the unzipping reaction proceeds by either an alkoxide or carbonate backbiting reaction, depending on how the polymer chain is terminated (i.e. terminated in a hydroxyl propyl or carbonate moiety). In alkoxide

backbiting, a carboxylate nucleophile attacks a carbonyl carbon atom. In carbonite backbiting, the weaker nucleophile of the alcohol end-group attacks an electrophilic carbon atom from the polymer backbone. It is believed that carbonate backbiting is the most common route due to its lower activation energy[28]. Reactive hydroxyl chain ends can be rendered "inactive" in the unzipping reaction by terminating the polymer chain (i.e. "end-capping" the polymer chain) with a less reactive moiety. Dixon et al.[41] first showed the end-capping of PPC with a variety of electrophilic organic compounds. The end-cap kinetically stabilizes the polymer ends so that chain unzipping is inhibited. Although reports of PPC end-capping have appeared in the literature[34,42,43], characterization of end-capped PPC has not been well-studied because the density of polymer ends is small for high molecular weight polymers. Analysis has been mostly limited to dynamic thermogravimetric analysis (TGA). In this study, lower molecular weight PPC with a higher density of end-groups has been used to characterize the end-groups.

Chain scission is the second thermal decomposition pathway for PPC. It has higher activation energy than chain unzipping and is not very sensitive to the type of polymer end-group. Chain scission occurs through the random, thermally-induced cleavage of C-O bonds within the backbone of the polymer, generally creating carbon dioxide and acetone as products. Organic additives have been used in previous studies to stabilize the polymer to random chain scission by creating complex interactions between the carbonyl moieties of the backbone[44–46]. Stearic acid has been used to improve the thermal stability at loadings between 0.28 wt% and 2.17 wt%[47]. The reports suggest that hydrogen bonding was the interaction between carboxylic acid and carbonyl moieties of the polymer.

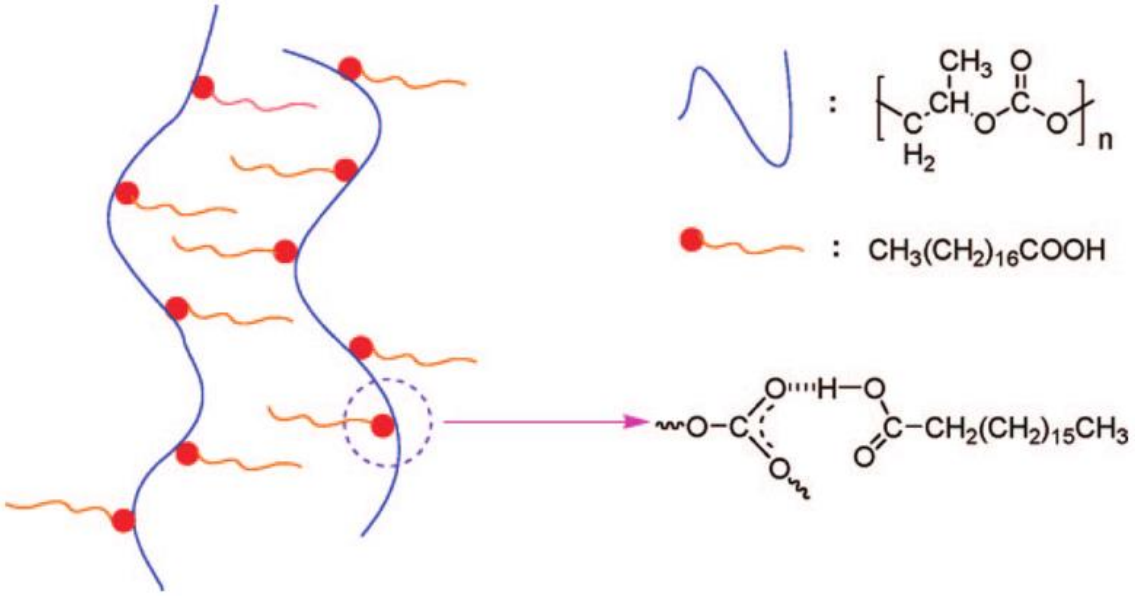

Figure 2.3 Thermal Stabilization of PPC via hydrogen bonding from stearic acid. Adapted from Yu, et al.[47]

Many of the additives have a higher decomposition temperature (300°C to 400°C) than PPC which creates substantial residue when the polymer decomposes and vaporizes. Additionally, stearic acid is a mono-functional carboxylic acid that has only one site available for interacting with the backbone of the polymer. In Chapter 3 of this dissertation, a biodegradable, tri-functional carboxylic acid with a low decomposition temperature of 175°C has been used to stabilize PPC from chain scission while leaving minimal residue.

2.1.2 Low Ceiling Temperature Polymers

An approach to producing materials that 'disappear' at room temperature is by using low-ceiling temperature polymers (i.e. ceiling temperature near or below room temperature)[21,48]. The ceiling temperature of a polymer is the temperature where the rate

of depolymerization and the rate of the polymerization are in equilibrium. At temperatures above the ceiling temperature, the polymer will rapidly decompose into monomers because the polymer is thermodynamically unstable. Low ceiling temperature polymers are thermodynamically unstable at ambient conditions and can be trapped in a kinetically stable state via end-capping or cyclization of the chain. The polymer can be triggered to decompose by removing the end cap or by providing a stimulus to break a bond from the backbone of the polymer as shown in Figure 2.4.

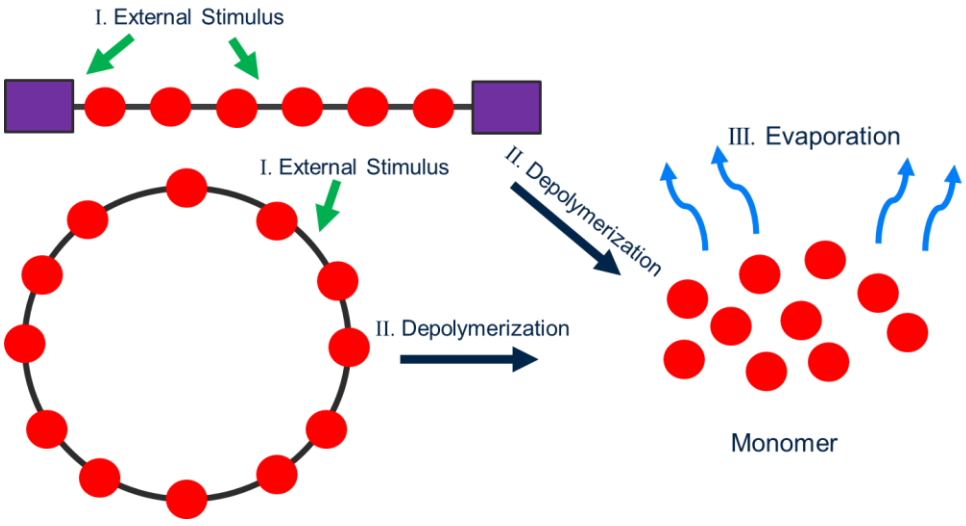

Figure 2.4 Stimulus-triggered depolymerization of polymers

Past studies have disclosed several families of low ceiling temperature polymers that can be potentially used in these dry transient applications. Examples of such polymers include poly (olefin sulfones), poly(carbamates), and poly(aldehydes) [49–53].

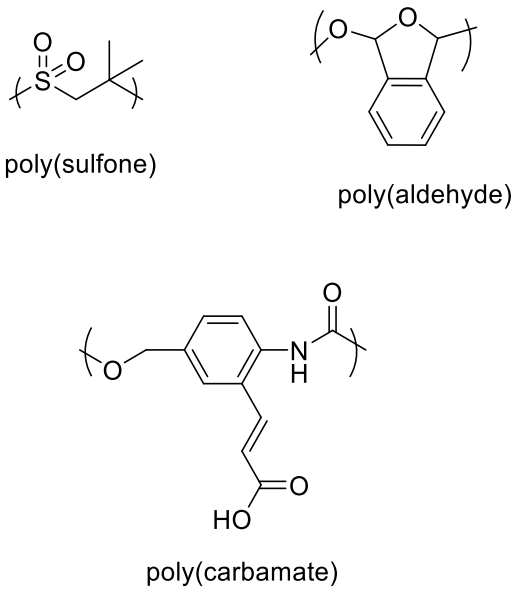

Figure 2.5 Examples of low-ceiling temperature polymers: poly(sulfones), poly(aldehydes), and poly(cabarbamates)

Low T_c polymers such as poly(olefin sulfones) and poly carbamates are hindered by slow depolymerization rates. Poly(ethyl glyoxylate) (PEtG), a type of polyaldehyde, has a facile synthesis route that yields non-toxic products post-decomposition. However, the low glass transition temperature (-1ºC) is not suitable for transient applications that require substrates with mechanical robustness. Furthermore, studies have shown that a film of PEtG requires 24 hours for 70% depolymerization after end-cap removal at room temperature [54]. Polyaldehydes such as poly(phthalaldehyde) (PPHA) are an especially attractive choice because of their ease of synthesis, superior mechanical properties, and fast depolymerization rates at room temperature. Additionally, the monomer that is formed after depolymerization, ortho-phthalaldehyde (o-PHA), is a non-toxic material used as an antimicrobial agent for disinfecting medical equipment[55].

A cationic synthesis route involves using boron triflouride etherate (BF_3-OEt_2) in solution with o-PHA as the temperature is brought down to -78ºC. After a specified amount of time, the reaction can be terminated by adding pyridine to deactivate the catalyst. Polymerization with BF_3-OEt_2 affords cyclic PPHA chains that is terminated by another o-PHA unit. Some studies have gone into understanding the role of the lewis-acid catalyst in the polymerization[56]. The stability of the polymer above its ceiling temperature is due to the polymer lacking end-groups.

The depolymerization of polyaldehydes can occur within seconds and the evaporation of the monomer is the rate-limiting step at low temperatures. The vapor pressure of phthalaldehyde at 20ºC is 0.0052 mmHg, which is 4 orders of magnitude lower than that of water. The acid-catalyzed depolymerization of phthalaldehyde is believed to be exothermic enough to vaporize a significant amount of the phthalaldehyde monomer. However, the low vapor pressure of phthalaldehyde significantly hinders the evaporation rate, and thus, the transient speed of the material. Aliphatic aldehydes such as butyraldehyde with higher vapor pressures (91.5 mmHg at 20ºC) would drastically increase evaporation rates at ambient conditions. However, polymerization of aliphatic aldehydes will lead to polymers that are too crystalline and have proven to be difficult to synthesize [57–60]. This relationship with various aldehydes and their corresponding vapor pressures is shown in Figure 2.6[61].

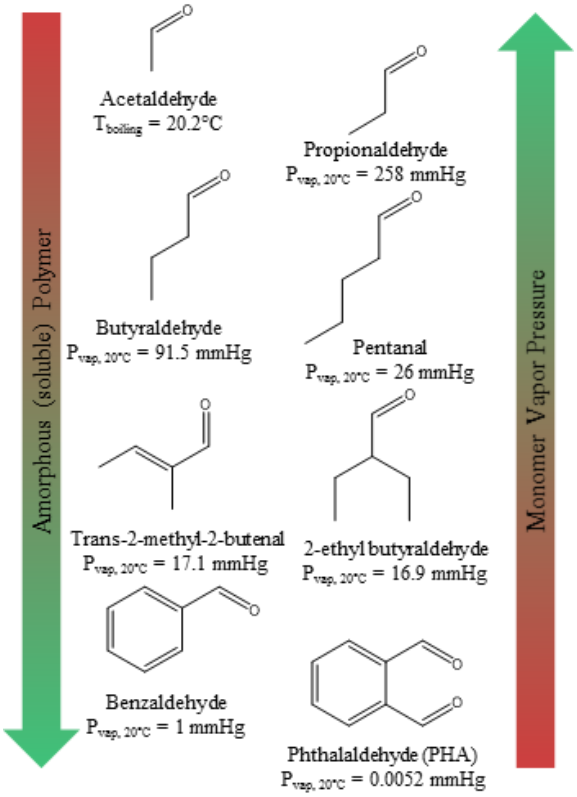

Figure 2.6 Various Aldehyde Monomers and Corresponding Vapor Pressures

Schwartz et. al investigated the cationic copolymerization of aromatic aldehydes with aliphatic aldehydes to synthesize polymers that can be used in solution deposition techniques as well as achieve fast evaporation rates at room temperature. Random cyclic copolymers of phthalaldehyde with butryaldehyde p(PHA-co-BA) were successfully synthesized with high molecular weight (>100 kDa) by controlling the monomer to catalyst ratio. The p(PHA-co-BA) recorded an evaporation time of 5 hours for >90% weight loss as compared to the PPHA homopolymer that needed 3.5 days for evaporation. Incorporation of higher vapor pressure butryaldehyde monomer revealed an improvement by a factor of 12 in the evaporation rate and thus, transience time, of the polymer.

2.2 Catalysts to Initiate Depolymerization

Optical, chemical, and thermal triggers are various ways for catalyzing the decomposition of sacrificial polymers. It was previously shown[8,62–64] that introducing a photo or thermal acid generator, such as an iodonium salt, into a PPC mixture can catalyze the degradation reactions. Upon exposure to UV light, these iodonium salts undergo a photolysis reaction releasing a strong protonic acid that attacks the PPC backbone in a "chain scission" manner [8]. Incorporation of a photo-acid generator (PAG) into a film of PPC can lower the photo-catalyzed PPC decomposition to 100°C. PAGs can also be thermally activated. If the PAG thermally decomposes at temperatures lower than that of the PPC, it has the effect of lowering the overall PPC decomposition temperature. It has also been shown that introducing a photo or thermal base generator, such as an amine salt, can catalyze degradation reactions [65]. From exposure to UV light, the salt releases a strong amine base that performs a nucleophilic attack on the polymer. This method of degradation is not as widely studied, but it has been suggested that the PBG acts primarily in a "backbiting" manner catalyzing the unzipping mechanism of PPC[66]. The most effective PAG and PBG in catalyzing the decomposition of PPC

A critical amount of 3 pphr PAG is required to catalyze the decomposition of PPC to achieve full-patternability within reasonable developing times[63]. Photo-patterning of sacrificial polymers is a very attractive attribute; however, these additives have very low volatility. The acid generated by Rhodorsil FABA has negligible vapor pressure at room temperature. Photo-base generators can be an advantageous to maintain effective PPC decomposition while reducing residue due to the high volatility of the released base. Residue created in encapsulated air cavities cannot be easily removed. Additionally, to

lower the chance of detection once transient electronics are triggered to vaporize, minimal residue is required. Thus, methods to lower the amount of residue of these photo-sensitive films are of great interest.

2.2.1 Photo-acid generators/Thermal Acid generators

Photo-acid generators are an important catalyst needed for the controlled trigger of the depolymerization of a wide variety of sacrificial polymers. Diaryliodonium and triarylsulfonium salts were the first practical photo-acid generators discovered for wide variety of commercial uses, in particularly, for inducing cationic polymerizations. The onium salts have very high quantum yields (0.5 to 0.9)[67]. The cation determines the wavelength and intensity of absorption, thermal stability, quantum yield, and the photosensitization properties. The anion determines the acidic strength of the resultant protonic acid. The mechanism of the photolysis reactions is shown in Figure 2.7.

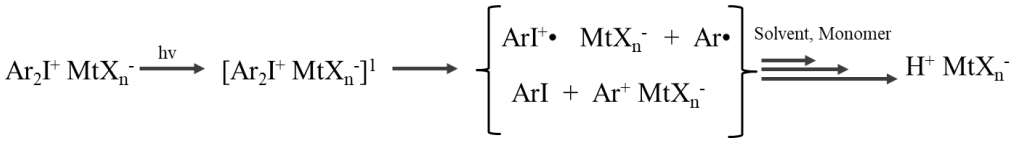

Figure 2.7 Mechanism for the UV-induced radical decomposition of diaryliodonioum salts for the generation of Brosnted acids

The carbon-iodine bond is very susceptible to cleavage from exposure to ultraviolet light energy. The excitation of the iodonium salt undergoes homolytic/heterolytic cleavage producing cationic and radical species. These species can react with itself from in-cage processes or react with other proton donors (solvents or monomers) from escape-cage

processes to generate strong Bronsted acids. The choice of the anion, MtXn- can tune the acidic strength but also controls the volatility of the products after photolysis. The incorporation of photoacid generators with bulky anion groups such as -$B(C_5F_6)_4$ will have negligible vapor pressure at room-temperature as opposed to a triflate anion that is volatile. However, in cases where the depolymerization of the polymer is slow and the rate limiting step then volatization of the acid will likely not complete degradation.

Typically most decomposable polymers with acid-labile backbones that can undergo catalytic degradation also are sensitive to bases. Therefore, photo-base generators can also be employed as catalysts for the controlled degradation of the polymer. The photogeneration of strong bases such as DBU (1-8-diazabicycloundec-7ene) and TBD (1,5,7-triazabicyclo[4.4.0]dec-5-ene) with pKa values of 24.3 and 26.03, respectively, have been synthesized from tetraphenylborate salts[65,66]. The thermal stability of the DBU•$HBPh_4$ and TBD•$HBPh_4$ as been reported as 244°C and 246°C, respectively. The photogeneration of TBD from the tetraphenylborate salt occurs by a photo-induced proton transfer reaction.

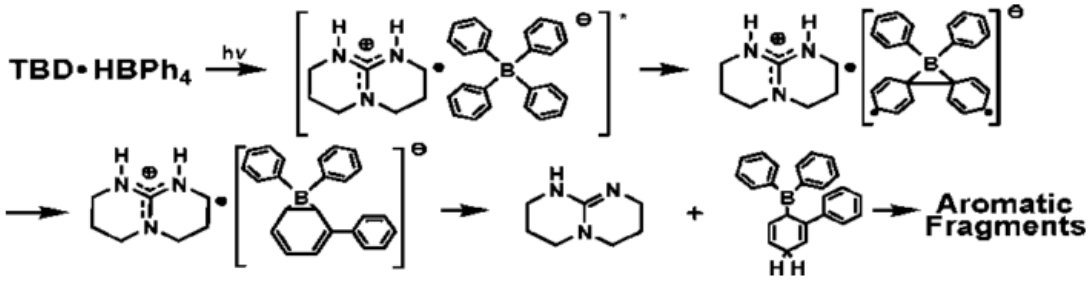

Figure 2.8 Mechanism for the UV-induced hydrogen abstraction mechanism of photobase generator for the production of TBD

As shown in Figure 2.8, upon ultraviolet light excitation the BPh_4^- ion can rearrange and abstract a proton from the TBD-H+, releasing the conjugate base. The quantum yield of TBD•$HBPh_4$ determined to be 0.18.

2.2.2 Photo-induced Electron Transfer Theory

The absorption properties of the onium cation are limited to wavelengths below 300 nm. The design of long-wavelength absorbing iodonium cations has not been achieved due to undesirable effects of modifying the initiating species and the resulting quantum yield of the photolysis reaction. Photo-induced electron transfer has been previously used to extend the absorption spectrum of the iodonium salts to the near-UV region and has been employed to a wide variety of cationic polymerization systems[68–70]. The concept is demonstrated in Figure 2.9.

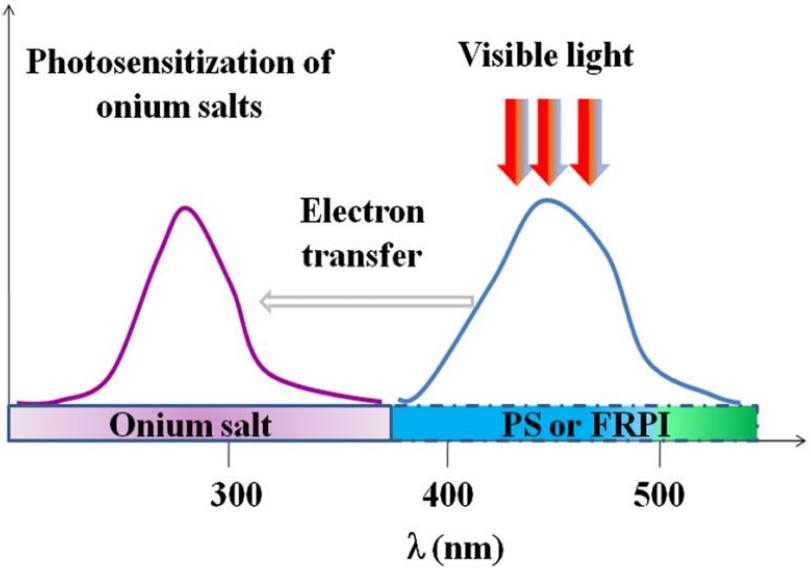

Figure 2.9 PET concept for expanding the wavelength of absorbance for onium salts. Adapted from Shi, et al.[68]

Photo-induced electron transfer is described as an electron transfer reaction between a donor and its acceptor from the absorption of higher energy wavelengths. The donor is generally called a 'photosensitizer' while the acceptor is the 'quencher'. In an environment where the reactants are mobile, an encounter complex can form between the reactants. The encounter complex can be described as an excited state donor and the ground-state acceptor that are surrounded by several layers of a solvent shell. The donor and acceptor can diffuse towards each other by a series of one-dimensional random steps where the molecules can physically collide into a 'collision complex'. The lifetime of uncharged particles are typically 10^{-9} to 10^{-10} seconds. If the electron transfer reaction is favorable, the reactants can undergo unique chemical structure and electronic changes. The solvated ions can dissociate where the formation of other products can occur. In the events preceding the dissociation of the solvated ions, back-electron transfer (BET) can potentially occur in many biomolecular quenching systems which results in a lower quantum yield for electron-transfer. It is clear that the thermodynamics (energetics) of the electron-transfer reaction and the kinetics (reactivity and mobility) of the sensitizer and quencher govern the photo-induced electron transfer reaction.

2.2.2.1 Thermodynamics

The thermodynamic favorability of any biomolecular electron transfer reaction is dictated by their electron affinity and ionization potential of the reactants. The electron transfer is feasible if the electron affinity, EA, (i.e. the ability to accept an electron) exceeds the ionization potential, IP, (i.e. energy to remove an electron) as shown in Eq. 1.

$$\Delta E = IP_D - EA_A \quad (1)$$

During photo-induced electron transfer, the donor (sensitizer) absorbs a photon of light equal to its band gap (E_{oo}). As a result of the excitation, the ionization potential decreases which makes it a better donor as shown below in Eq. 2 and Eq. 3.

$$IP_D^* = IP_D - E_{oo} \tag{2}$$

$$\Delta E = IP_D - EA_A - E_{oo} \tag{3}$$

The oxidation potential correlates with ionization potential of the sensitizer and the reduction potential correlates with the electron affinity of the acceptor (photo-acid/photo-base generator). Therefore, the favorability of electron transfer is determined by the oxidation and reduction potential of the excited and ground states of the donor and acceptor. The free-energy value from the difference of redox potentials can be evaluated by thermodynamic feasibility. This can be described by the Rehm -Weller Equation in Eq. 4.

$$\Delta G = E_{ox}\left(\frac{D^+}{D}\right) - E_{red}\left(\frac{A}{A^-}\right) - \Delta G_{00} - \frac{e^2}{\varepsilon d} \tag{4}$$

The expression of (D/D^+) describes the oxidation potential of the sensitizer while the expression of E (A/A^-) describes the reduction potential of the PAG/PBG. The expression of ΔG_{00} is the electronic energy that corresponds to the excited state of the sensitizer. The last term $e^2/ \varepsilon d$ corresponds to the coulombic attraction energy where ε is the dielectric constant and d is the distance between charges of the ion pair.

2.2.2.2 Rate Constants

The energetics of the PET is not the only contributor to the feasibility of the reaction. The diffusivity and reactivity of the molecules in the environment must be considered for the PET reaction. The series of steps for a general PET reaction with their associated rate constants are shown in Figure 2.10.

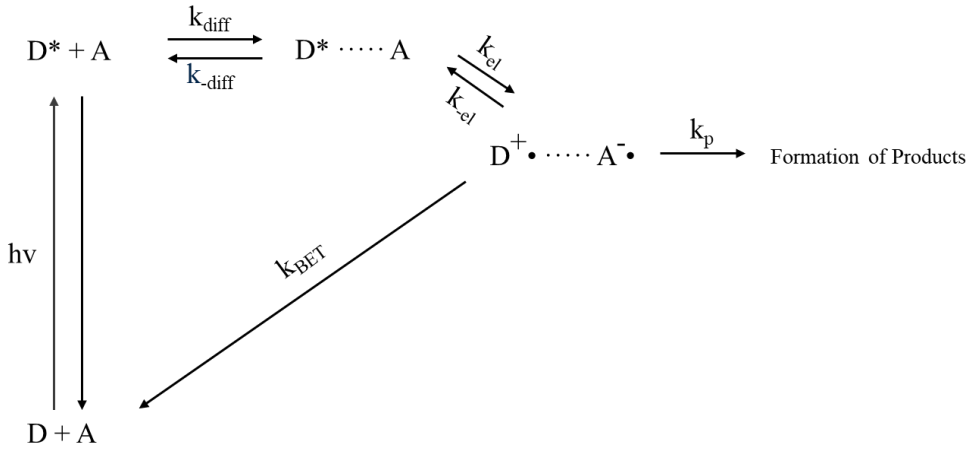

Figure 2.10 Schematic Diagram of the series of kinetic steps for a biomolecular PET reaction

In Figure 2.10, k_{diff} and k_{-diff} are the diffusion-controlled rate constants to form and dissociate from the encounter complex; k_{el} and k_{-el} are the biomolecular kinetics-controlled rate constants in the forward and reverse direction; k_{BET} is the rate constant for back-electron transfer processes; and k_p is the rate constant of the formation of products after PET reaction. A steady state approximation for the rate constants for the bimolecular quenching rate (k_q) PET reaction can be expressed in Eq. 5.

$$k_q = \frac{k_{diff}}{1 + \frac{k_{-diff}}{k_{el}} + \frac{k_{-diff} * k_{-el}}{(k_p + k_{BET})k_{el}}} \quad (5)$$

If the thermodynamics of the PET reaction are sufficiently exergonic ($k_{-el} << k_{el}$), then the expression becomes Eq. 6.

$$k_q = \frac{k_{el} * k_{diff}}{k_{el} + k_{-diff}} \quad (6)$$

Introducing a further assumption that the diffusion-controlled rate is equal in the forward and reverse direction ($k_{diff} = k_{-diff}$) leads to the following relationship (Eq. 7).

$$\frac{1}{k_q} = \frac{1}{k_{el}} + \frac{1}{k_{diff}} \quad (7)$$

From Eq. 7, it is clear that the in the condition where the PET reaction is controlled by diffusion ($k_{diff} >> k_{-el}$), then the biomolecular quenching rate is approximately the value of k_{diff}. In the condition where the kinetic rate based on the activation energy of the reactants involved is much faster than diffusive properties in the medium ($k_{el} >> k_{diff}$), then the biomolecular quenching rate is approximately the value of $k_{diff.}$

2.2.3 Acid Amplifiers

Acid amplifiers (AA) are such small molecule compounds that can be used to exponentially increase the number of acidic species created from photogenerated acids [71–

[73]. The acid amplifiers are any compounds that undergoe acidolytic reactions to produce more than one acidic species that are capable of generating nonlinear organic reactions. Acid amplifiers can also serve as latent thermal acid generators. These compounds were originally created for Extreme Ultraviolet (EUV) photoresists to bypass the trade-off effect of resolution, line-edge roughness, and sensitivity [74]. The acid amplifiers consist of three important parts: acid-sensitive trigger, body, and acid precursor as shown in Figure 2.11.

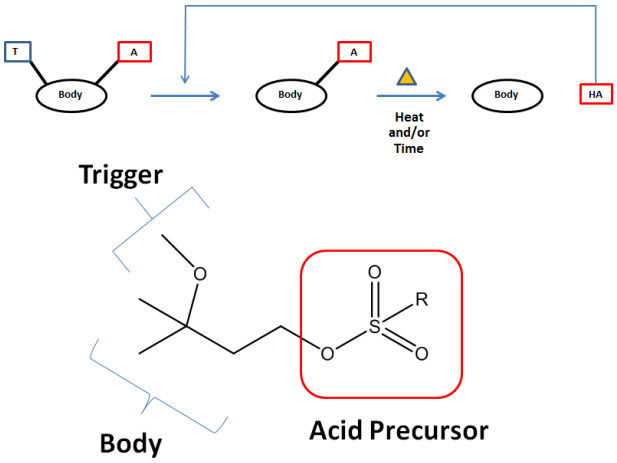

Figure 2.11 Acid Amplifier Structure

The desired acid generation pathway is the acid-catalyzed decomposition. During autocatalysis, the trigger undergoes acidolysis yielding an allylic sulfonic ester, while regenerating a monoprotonic acid. The intermediate further decomposes via elimination reactions to volatile alkene fragments and the release of the acid precursor as shown in Figure 2.12

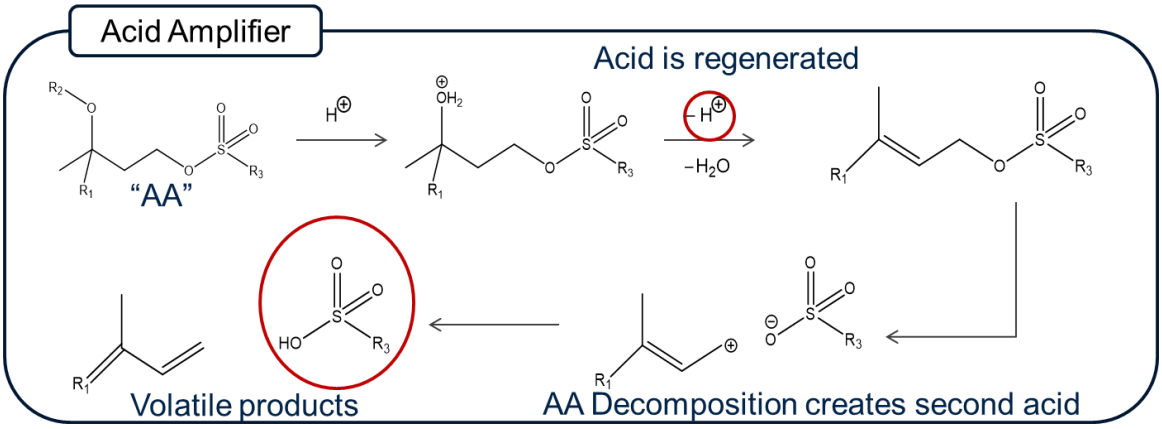

Figure 2.12 Mechanism for the autocatalytic reaction of an acid amplifier

The triggers are acid-sensitive groups that could be hydroxyl, methoxy, acetate, or ketal groups. The acid precursor can be a number of fluorinated sulfonic acids with pKa levels strong enough initiate the decomposition of polyaldehydes. Traditionally, these acid amplifiers are used in photoresists that require post-exposure bake temperatures of 100ºC for photopatterning. The thermal stability of these acid amplifiers are also related to their ability to be autocatalytic at lower temperatures.

CHAPTER 3. MATERIALS AND METHODS

3.1 Materials

3.1.1 Polymers

Polypropylene carbonate (PPC) was generously supplied by Novomer Inc. The weight-average molecular weight of PPC materials provided was 137 kDa, 160 kDa, 219 kDa, and 263 kDa. 137 kDA PPC has a polydisperity indexy (PDI) of 1.16. PPC polyol was also supplied by Novomer Inc. at a weight-average molecular weight of 2 kDa with a PDI of 1.1.

The procedure for the cationic synthesis poly(phthalaldehyde) (p(PHA)) polymer are provided in more detail in the work of Schwartz et al and so only a brief description of the procedure is provided[48,75]. Under a nitrogen-rich atmosphere, dry dichloromethane (DCM) is used to dissolve purified *o*-phthalaldehyde (monomer) at a concentration of 0.75 M. The initiator, boron trifluoride diethyl etherate (BF_3-OEt_2), is added at a molar ratio of 1:750, initiator to monomer. The mixture reacts in an acetone/dry ice jacket (-78 °C) for 2.5 hours. After that time, the reaction is quenched using pyridine at a mol ratio of 0.01 mol pyridine per mol aldehyde. The quenched mixture is then allowed to sit at temperature (-78 °C) for 30 minutes. The material is first precipitated into cold methanol, vacuum filtered, then redissolved in DCM to which is added 0.05 mL triethylamine per gram of polymer. The polymer is then precipitated into hexanes and vacuum filtered. Lastly, the polymer material is allowed to dry under vacuum until a constant weight obtained. Copolymers of more volatile aldehydes such as ethanal, butanal, and propanal were

synthesized from first purification by distillation which was subsequently added to reaction vessel at 2:3 molar ratio to phthalaldehyde following the same procedure described above.

The procedure of anionic synthesis of PPHA involved the addition of 1.48 grams of sublimed PHA from Alfa Aesar (98% purity) in 23 ml of anhydrous THF. 0.07 ml of P2-t-Bu was used as-received. N-hydroxysuccinimide was purchased from Sigma Aldrich and used at 20 mg. The reaction flask contained the aforementioned materials and kept in a deep freezer at 85°C for 3 hours and 30 minutes. Acetic anhydride and pyridine were added at 0.066 ml and 0.056 ml, respectively and kept stirring for 30 minutes. The solution was precipitated into methanol. Copolymers were synthesized with butanal at 4:1 o-pha to butanal molar ratios.

3.1.2 Photo-acid/base generators and Acid Amplifiers

The PAG investigated in this study was an iodonium salt, 4-methylphenyl [4-(1-methylethyl) phenyl] tetrakis(pentafluorophenyl) borate (referred to as Rhodorsil-Faba) from Solvay Inc. Photo-base generator (PBG) used in this study is an amine salt 1,5,7 -triaza-bicyclo [4.4.0]dec-5-ene tetraphenylborate (referred to as TBD•$HBPh_4$). Synthesis of PBG used in this study was made following the Sun et.al procedure[66].

3.1.3 End-Capping Preparation for PPC

End-capping reagents of nitrophenyl chloroformate, vinyl chloroformate, and benzoyl chloride were commercially purchased from Sigma-Aldrich. End-capping reactions with 137 kDa PPC were performed in a 20 ml scintillation vial under magnetic stirring. The scintillation vial contained 10 wt% of 137 kDa PPC in THF solution.

Equimolar quantities of pyridine to end-capping reagents were also added to the reaction vessel dropwise. End-capping reagents added to the reaction vessel were dependent on reactivity, and the number of end-groups for the specified polymer. For example, 1 gram of 137 kDa PPC has an estimated amount of 1.46E-05 moles of –OH endgroups. Benzoyl chloride was added at 700 times the molar amount of end-groups of PPC to drive the reaction to the end-capped PPC products. Thus, 0.0102 moles of benzoyl chloride was used. Chloroformates are generally more reactive; hence, vinyl chloroformate was added at 50 times the amount of end-groups of 137 kDa PPC in which 0.000730 moles was added to the reaction vessel. Magnetic stirring times were held for 48 hours to ensure that all ends have been reacted. Pyridinium-chloride precipitation is an indicator that the reaction is underway, because the produced white salt is insoluble in THF. The PPC was precipitated in methanol from the reaction solution at 10 times the volume of THF reaction solvent to ensure impurities have been removed.

End-capping reactions with 2 kDa PPC were held to at least 16 wt% in THF solution to ensure the polymer was at a concentration large enough to precipitate from solution in methanol. End-capping reagents must be added at lower amounts as to not exceed the solubility limit of reaction solvent because of the greater number of end-groups. The greater fraction of end-groups increases reactivity, thus, less amounts of end-capping reagents were used. For example, 1 gram of 2 kDa PPC has an estimated amount of 0.001 moles of –OH end-groups. Vinyl chloroformate was added at 5 times the number of end-groups of PPC to drive the reaction to the end-capped PPC products. Thus, 0.005 moles of end-capping reagent was added to the reaction vessel. Magnetic stirring was held at equally long times for 48 hours and subsequent precipitation of the polymer from methanol.

"Neat" PPC refers to polymers that were used as-received from the manufacturer. "AirDry-MeOH" samples are polymers that have been precipitated from THF in methanol. The sample was left to dry in a fume hood but contains residual methanol. "VaccDry" samples are polymers that have been precipitated from THF in methanol. However, the residual methanol has been essentially removed by vacuum drying at 100^oC for 12 hours. "Solvent-cast" samples are formulations with 20% weight PPC in GBL. These formulations were cast onto a silicon substrate and soft-baked at 100^oC for 3 minutes. In this study, additives were used to catalyze or inhibit the decomposition of PPC. The PPC material was made photosensitive by the addition of PAG (Rhodorsil-Faba) at a loading of 3 mass parts PAG per 100 parts polymer (pphr) to the formulation .The polymer was also made photosensitive by the addition of PBG (TBD•$HBPh_4$) at a loading of 1.35 pphr. The PAG and PBG loadings in PPC formulations correspond to approximately 332 monomer units per 1 mole of acid or base. Films were exposed using an Oriel Instrument flood exposure source at 2 J/cm^2. PPC formulations were stabilized from chain scission degradation by the addition of citric acid at 0.26 and 3 pphr loadings. Formulations were left on a ball-roller for 3 hours to ensure complete mixing.

3.1.4 Sensitizers

(Special acknowledgement to Anthony Engler for the synthesis)

2.05 equivalents of phenylacetylene was dissolved at 0.91 M in anhydrous tetrahydrofuran in a flame dried round bottom flask under an argon atmosphere. The solution was cooled to -78^{o}C followed by the slow addition of 2.02 equivalents of *n*-butyllithium in hexane via syringe. The reaction vessel was stirred at room temperature for

30 minutes before being cooled to -78^{o}C . 1 equivalent of the appropriate quinone was added with anyhdrous tetrahydrofuran to the reaction mixture. After stirring at room temperature for 60 minutes, the reaction was added dropwise into a 0.78 M solution of Sn(II) chloride dihydrate in 10% HCl solution. The solution stirred for 90 minutes before collecting the crystalline product via vacuum filtration. Products were recrystallized from chloroform.

1,8-dimethoxy-9,10-bis(phenylethynyl)anthracene (DMBA), 5,12-bis(phenylethynyl)tetracene (BPET) and 6,13-bis(phenylethynyl)pentacene (BPEP) were prepared according to the general procedure. 6,13-bis(3,4,5-trimethoxyphenylethynyl)pentacene (BTMP) was prepared from 3,4,5-trimethoxyphenylacetlyene using the same conditions as the general procedure. Molecular structure was verified by nuclear magnetic resonance and high resolution mass spectrometry, and matched previous reports on these compounds [76,77].

3.1.5 Acid Amplifiers

Acid Amplifiers were synthesized by following literature procedures[78]. However a brief detail is described here. 18 mmol of 3-methoxy-3methylbutyl butane-1-ol was dissolved into 25 grams of DCM with 12 mmol of TEA. 7.44 mmol of the corresponding sulfonyl chloride was added to the reaction vessel dropwise. The reaction solution was stirred for 3 hours until the solution turned from transparent to an opaque yellow.

The work-up of the product involved a series of organic extractions. 50 ml of sodium bicarbonate was added to the reaction vessel and stirred for 30 minutes. 60 ml of 0.5 ml HCL was washed twice with the reaction solution, followed by washing with 60 ml of

sodium bicarbonate once. The solution was dried by washing with brine solution and magnesium sulfate within a flask. The solution was vacuum dried. If the product was not sufficiently clean by NMR, then the product was further purified through a silica column by hexanes and ethyl acetate. A list of acid amplifiers synthesized is shown in Figure 3.1.

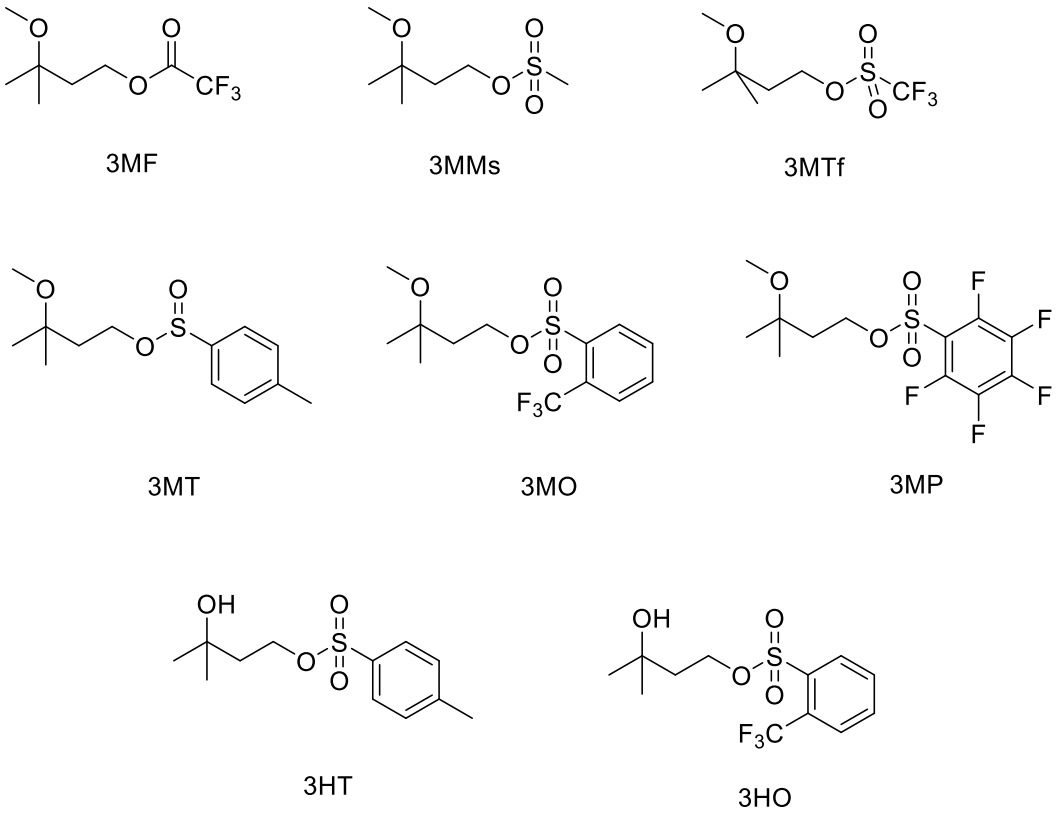

Figure 3.1 Acid Amplifiers

3.2 Methods

3.2.1 Optical Properties

The photo-patternability of a polymer film can be determined from contrast curves[79]. Contrast is the ability of a polymer film to absorb light and convert that energy into a chemical reaction (ie. decomposition from a generated acid from the catalyst). The contrast

of a film is measured by first spin-coating a polymer film with a loading of a photo-acid/base generator onto a substrate. The thickness of the film is measured and then exposed to a uniform exposure of light for a period of time. The exposure dose is the light intensity (mW/cm^2) multiplied by the exposure time. The exposure of the films can be performed under a neutral density mask where the transmission of light can vary in increments from 0% to 100%. The thermal development consists of baking the polymer film on a hotplate at the acid-catalyzed decomposition temperature of the polymer of interest. Contrast curves can be generated by plotting the normalized thickness loss after thermal development as a function of the log dose.

We can consider two properties to determine patternability of a polymer film: contrast (γ) and sensitivity. High contrast values are desired for the patterning of very distinct features. Sensitivity refers to the amount of light energy (mJ/cm^2) necessary to decompose the polymer from a generated acid. D_{100} is the minimum dose needed to remove 100% of the film. D_0 is ideally defined as the maximum dose of light at which no film can be removed. The mathematical relationship of contrast (γ) and the exposure doses is (D_0, D_{100}) are shown below:

$$\gamma = \frac{1}{log_{10}\frac{D_{100}}{D_0}}$$

The absorbance of a film can be gathered from ultraviolet-visible spectroscopy. A film can be spin-coated onto a transparent substrate (i.e. quartz) where broadband wavelengths can be illuminated through a film. The absorbance is defined as the logarithmic ratio of the incident intensity I_o to the transmitted intensity I:

$$A = log_{10} \frac{I_o}{I}$$

The absorption coefficient of films (a) is directly proportional to the length of the light path, t, (the thickness of the film):

$$A = log_{10} \frac{I_o}{I} = at$$

Contrast curves were generated with the photosensitizers from sunlight in Atlanta, Georgia between the hours of 11 am to 2 pm in September of 2016. A variable density mask filter (Model 400 F.S.) was used from Opto-line. Square band-pass filters of 50.8 x 50.9 mm at wavelengths of 500 nm, 560 nm, and 650 nm were used. All filters had a 10±2 nm full-width half-max value. Formulations of PPC films, sensitizer, and photo-acid generator were spin-coated onto silicon wafers where the variable density mask filter and corresponding bandpass filter were placed on-top. The intensity of sunlight was recorded with a SM206 Solar Power Meter. Ultraviolet light exposures filtered to 248 nm and 365 nm were exposed using an Oriel Instruments flood exposure source with a 1000 W Hg(Xe) lamp.

The Ultraviolet – visible (UV-vis) absorption spectrum of photosensitizers used in this study was investigated on Hewlett Packard 8543 UV-vis spectrophotometer in solutions of degassed DMF. Formulations of all polymer solutions with sensitizer and photo-acid/base generator were mixed on a ball roller for 12 hours. The photosensitizer-to-PAG molar ratio was1.2:1 for all formulations. Fluorescence spectra were evaluated with a Horiba FL3-2i Fluorometer. Time-correlated single photon counting (TCSPC) method with a Horiba NanoLed excitation source at 334 nm, 455 nm, 570 nm, and 625 nm was used to obtain the

fluorescence lifetimes. Stern-Volmer analysis was conducted with sensitizers maintained to approximately 4 μM solutions in degassed DMF with concentrations of PAG-FABA ranging from 0.008 M to 0.3 M.

3.2.2 Thermal Properties

TGA was performed by using a TGA Q50 from TA instruments to investigate the thermal decomposition of PPC materials. The platinum pan was re-zeroed after each run for accurate measurements of residue. Samples between 3 to 10 mg were loaded onto the pan. Nitrogen and air environments were used at a flow rate of 40 ml/min for the sample and the balance. PPC films were removed from silicon substrates with a razor blade and loaded onto the pan. Dynamic TGA samples were heated at rates of 1°C/min and 5°C/min from room temperature to 400°C. Isothermal TGA experiments were ramped at heating rate of 10°C/min to the temperature of interest and held at that temperature for two hours.

DSC was performed using a Discover DSC from TA instruments to investigate the glass transition temperature and the freezing point of materials. Samples were crimped in aluminum pans that weighed between 3 to 10 mg and ramped/cooled at 5°C/min. An nitrogen environment was used at a flow rate of 40 ml/min. Freezing point measurements were conducted in open lids as to not induce freezing of the material from mechanical agitation.

3.2.3 Electrochemical Properties

The electrochemical properties of the sensitizers and PAGs were evaluated by cyclic voltammetry using a Princeton PARSTAT 2263 potentiostat. Redox potentials were

recorded under dry nitrogen atmosphere with a three-Pt-electrode electrochemical cell in an anhydrous DMF solution of 0.13 M tetrabutylammonium perchlorate (TBAP). Ferrocene was used as an internal standard for determining the electrochemical potential.

3.2.4 Mechanical Properties

Quartz crystal microbalance (QCM) was performed on a Stanford Research Systems QCM 200 to quantify the solid-state kinetics of depolymerization of polyaldehydes. The Butterworth-van-Dyke model was used to describe the mechanical changes of the polymer coating on the quartz crystal. Polymer formulations were made with 9.1 wt% polymer solids in cyclopentanone with 5 parts per hundred resin (pphr) of PAG. Thin film samples were spin-coated onto a 2.54 cm QCM with 5 MHz unloaded resonant frequency and an active surface area of 0.4 cm^2. An open-faced holder was used to allow exposure of the polymer films with an Oriel Instruments flood exposure source with a 1000 W Hg(Xe) lamp filtered to 248 nm light. An exposure dose of 730 mJ/cm^2 is used for all samples.

An Instron Series 5840 Load Frame was used to evaluate the elastic (Young's) modulus of the polymer substrate. From a polymer-only formulation, long sheets of polymer film were cast, dried, and then cut into long strips while still attached to the Cu:FR4 support. The cut film was then soaked in a solution of (NH4)2S2O8 to separate the strips from the Cu:FR4 support following the procedure described previously. Several long rectangular pieces of approximate dimensions 100 x 14 x 0.2 mm (length by width by thickness) were obtained. Determination of the Young's Modulus was made following the ASTM D 882-02 method. The tests were conducted on the film samples with a gauge length

of 100 mm. The Young's modulus was calculated using the software supplied with the Instron equipment. Replicates of each sample were taken, and the averaged values reported.

3.2.5 Identification of Chemical Structures

Nuclear magnetic resonance (NMR) was used to determine the chemical structure of materials and polymers. NMR measurements were performed using a Varian Mercury Vx 400 (400 MHz) tool. Chloroform-D ($CDCl_3$) was used for the NMR solvent and was supplied by Sigma-Aldrich at a 99.8% purity level. The concentration of PPC in NMR sample tubes was held at 46 mg in 0.75 ml $CDCl_3$. ^{13}C NMR spectra was collected at 1,204 scans with a relaxation time of 5s. ^{1}H NMR spectra were collected at 16 scans with a relaxation time of 1s. The spectra in ^{1}H and ^{13}C NMR were calibrated and referenced to the chemical shift of the solvent $CDCl_3$, which were 7.26 ppm and 77.16 ppm, respectively.

Characterization of the residual products of the PET reactions within poly(phthalaldehyde) films were conducted with Proton Nuclear Magnetic Analysis (^{1}H-NMR), Matrix-assisted laser desorption/ionization – time of flight - mass spectrometry (MALDI-TOF-MS), and electrospray ionization (ESI) triple quadruple analysis. NMR measurements were performed using a Varian Mercury Vx 400 (400 MHz) tool. Chloroform-D (CDCl3) was used for the NMR solvent and was supplied by Sigma-Aldrich at a 99.8% purity level. The concentration of residue in NMR sample tubes was held at 46 mg in 0.75 ml $CDCl_3$. ESI measurements were performed on a Micromass Quattro LC and MALDI-TOF-MS measurements were performed on a Bruker AutoFlex III. MALDI-TOF-MS samples were prepared with a 10 mg/mL solution of the matrix trans-2-[3-(4-tert-butylphenyl)-2-methyl-2-propenylidene] malononitrile (DCTB) in dichloromethane

(DCM). The residue was prepared in a separate vial containing 10 mg/ml solution in DCM. The matrix solution and residue solution were mixed at equal parts and spotted 1 µL onto the plate for analysis.

3.2.6 Fabrication and Characterization of Poly(phthalaldehyde) Multi-layer Printed Wiring Board

3.2.6.1 Preparation of dielectric substrate and conductive formulations.

For the dielectric substrate, a polymer-only formulation was prepared by dissolving the neat p(PHA) polymer into N-methyl-2-pyrrolidone (NMP) at a mass concentration of 25-30 wt%. Before films of the polymer can be fabricated, a piece of copper-coated FR4 (Cu:FR4) board is cleaned for use with a five-step rinse procedure: 0.1 M hydrochloric acid, DI water, 0.9 M $(NH_4)_2S_2O_8$, DI water, isopropyl alcohol and then dried. Copper-coated FR4 was chosen because it provided a support with a smooth, flat surface where the polymer could be easily released from the surface through etching the copper away.

Films were prepared by casting an appropriate amount of the polymer-only formulation onto a piece of the prepared Cu:FR4 board using the doctor blade technique. The dimensions of the final film depended on both the amount of formulation applied to the Cu:FR4 board, the geometry of the applied material and the height of the blade before casting. The cast formulation was dried using a laboratory microwave (Microcure 2100) under the following two stage treatment.

1. 8 hours at 30 °C, 1 hour at 35 °C, 5 hours at 40 °C
2. 0.5 hours at 30 °C, 5 hours at 40 °C, 3.5 hours at 50 °C

The conductive formulation was prepared by first dry blending silver nano particles (1.3-3.3 µm) and the neat polymer in a mass ratio of 19:1 (95%), silver to polymer. The mixture was placed on a ball mill until the mixture was a homogenous fine powder. The final conductive formulation was prepared right before use by dissolving the dry-blend material with NMP at a weight concentration of 89% solids

3.2.6.2 Dielectric properties of polymer substrate

The dielectric properties (capacitance and dissipation factor) were determined for the polymer substrate. A polymer film was cast and dried on Cu:FR4. A series of conductive (Ag-filled) circles were screen printed onto the film. The LCR-800 instrument was configured for two probe operation with one probe on a Ag circle and the other on the copper surface of the Cu:FR4 support. The capacitance and the dissipation factor were measured at several places and the average values were calculated. Microscopic images were taken of the printed silver discs and the printed areas determined. The area values along with the thickness of the film were used to calculated a capacitance value using the permittivity of a vacuum ($\varepsilon_0 = 8.854\times10^{-12}$ F m^{-1}). The ratio of the measured capacitance value for the film and the calculated capacitance value for a vacuum-filled space of similar dimensions produces the relative permittivity of the film.

3.2.6.3 Electrical properties of conductive materials

The sheet resistance of the conductive formulation was measured both as a standalone film on uncoated FR4 board and after printing onto a polymer substrate film. The standalone film was cast Ag-filled formulation and was dried in the microwave under the following conditions: 8 hours at 30 °C followed by 7 hours at 35 °C. The sheet resistance

of the film was measured following the ASTM method F390-11 method using a four-point probe array. Multiple measurements were made and an average sheet resistance value was calculated from those values. During the fabrication of the multilayer board, the resistance of the ‘wiring’ that was screen-printed onto the polymer substrate layer were measured using a LCR-800 configured for two probe operation. The heights of both the standalone film and the printed wiring were measured and the collected measurements were used to calculate the sheet resistance and the resistivity.

CHAPTER 4. THERMAL DECOMPOSITION OF POLYPROPYLENE CARBONATE: END-CAPPING, ADDITIVES, AND SOLVENT EFFECTS

4.1 Molecular Weight Effect

The molecular weight of the PPC can be an important contributor to the overall decomposition and volatilization process because the polymer ultimately has to fragment into small, high vapor pressure moieties. A larger number of reactions would be required to vaporize a high molecular weight polymer. The decomposition and volatilization of five PPC polymers with molecular weight ranging from 2 kDa to 263 kDa were evaluated using TGA. Each of the five PPC samples was analyzed as-received (neat) at a ramp rate of 1°C/min in N_2 atmosphere and the TGA results are shown in Figure 3.

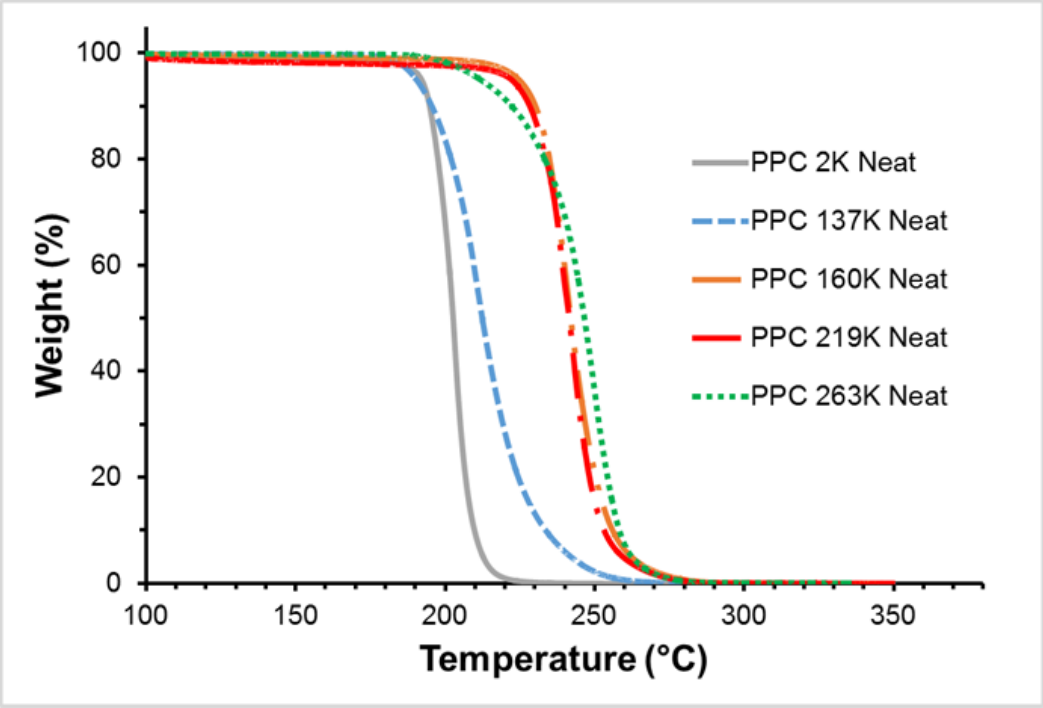

Figure 4.1 "Neat" Novomer PPC with molecular weights of 2 kDa, 137 kDa, 160 kDa, 219 kDa, and 263 kDa at a ramp rate of 1°C/min in N2 atmosphere.

While there is a general trend toward higher decomposition temperature with higher molecular weights, the trend does not correspond to simply the number of intramolecular reactions required to obtain small molecular weight products. For example, the onset of decomposition of 137 kDa and 2 kDa PPC are nearly the same even though the molecular weight of the 137 kDa material is 68 times greater than that of the 2 kDa polymer. The difference between the molecular weight of the 137 kDa polymer and three higher ones is less than a factor of two, yet there is a dramatic shift to higher temperature. Second, the TGA experiments were performed at a very low scan rate giving time for intramolecular reactions. It is interesting that the 2 kDa and 137 kDa had nearly the same on-set temperature but the rate of decomposition of the 2 kDa PPC was significantly faster (sharper slope) than the 137 kDa polymer which would be indicative of the number of

intermolecular reactions needed for volatilization. The speed of the unzipping mechanism of PPC is expected to be faster for lower molecular weight polymers due to the greater number of end-groups. For example, the 2 kDa PPC has only 20 weight average monomer units per polymer chain, while the 263 kDa PPC has 2578 weight average monomer units per polymer chain.

To further investigate the effect of molecular weight on the decomposition temperature, five PPC samples were dissolved in GBL, solvent-cast onto a silicon substrate, and soft-baked at $100^{o}C$ for 3 minutes. The PPC film was removed from the silicon wafer with a razor blade and evaluated using TGA with the same conditions used for Fig. 3. The results are shown in Figure 4. The decomposition temperature of the five PPC samples (each with a different molecular weight) was similar to each other and significantly different from the as-received form of the same polymers shown in Fig. 3. The wide range of decomposition temperatures shown in Fig. 3 no longer remained after this chemical treatment. The various molecular weight PPC samples had only a minimal difference in decomposition temperature and the decomposition temperature was like that of the original 2 kDa and 137 kDa PPC in Fig. 3.

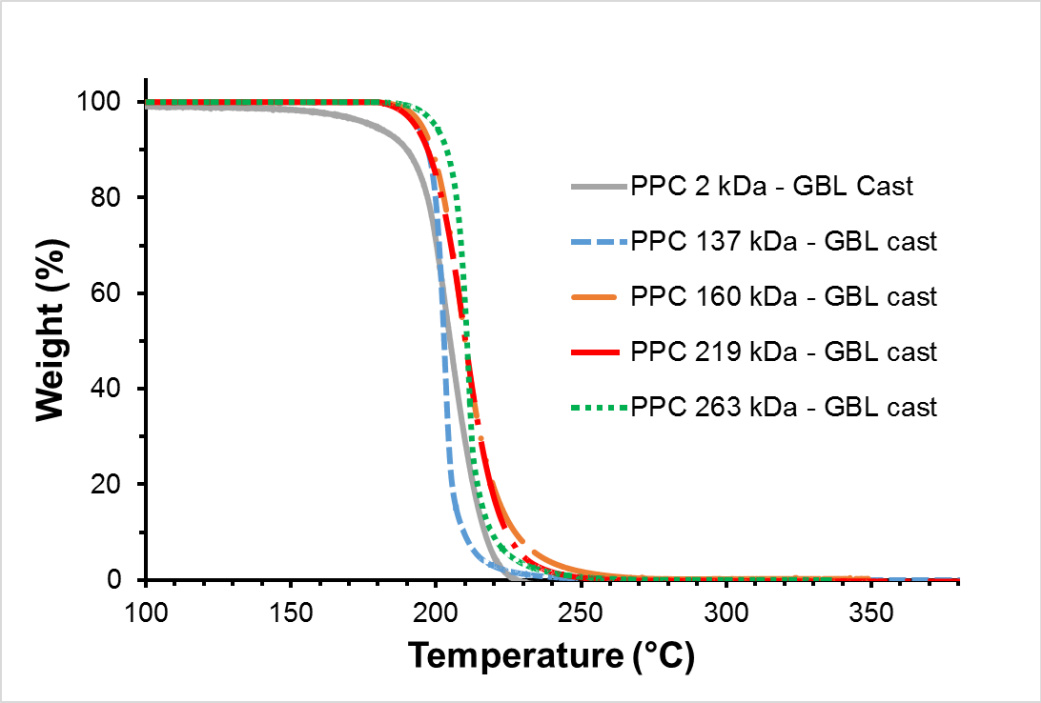

Figure 4.2 Solvent-cast Novomer PPC in GBL with molecular weights of 2 kDa, 137 kDa, 160 kDa, 219 kDa, and 263 kDa at a ramp rate of 1°C/min in N2 atmosphere.

It is clear that the solvent-casting process changed the decomposition temperature of some of the materials, mitigating the original differences in decomposition temperature. Solvent casting from GBL is purely a physical process of dissolving the PPC in a solvent followed by evaporation of most or all of the GBL, depending on the drying process. It is evident from this that molecular weight has a minimal effect on the stability of PPC films. At least two explanations exist for the role of GBL in shifting the PPC decomposition temperature. First, GBL could be participating in decomposition of PPC, which seems unlikely because GBL has no apparent reactivity with PPC. Second, GBL could remove (by dissolution) the presence of a stabilizing agent which had been present in some of the as-received PPC.

Many observations of decomposition temperature trends for PPC were made in the past including the effects of casting solvent, molecular weight, end-capping, and preparation. Molecular weight has been shown to have a considerable effect on the thermal stability of PPC[29,38]. In the previous study, PPC was shown to shift to higher decomposition temperature with increasing molecular weight. For example, a 144 kDa PPC compared to a 56 kDa showed a +20°C shift in thermal stability. Similar results were produced here in Figure 3 as the thermal stability appeared to trend with higher molecular weight with as-received PPC polymers. However, the process of dissolving the polymers in GBL and casting films showed that thermal stability actually does not depend on molecular weight, as shown in Figure 4. The highest molecular weight, solvent-cast PPC (263 kDa) displayed less than 8°Cshift in thermal stability compared to the lowest molecular weight PPC (2 kDa). These results suggest that impurities from synthesis can act as stabilizing agents and may be present in as-received polymers. The solvent-casting of samples can remove some impurities due to dilution and evaporation during the spin-coating and soft-bake procedures.

4.2 End-Capping

The mechanistic pathway and resulting temperature profile for PPC decomposition can be altered by end-capping with a chemical moiety which inhibits the unzipping reaction. Figure 4.3 shows the reaction scheme for end-capping PPC.

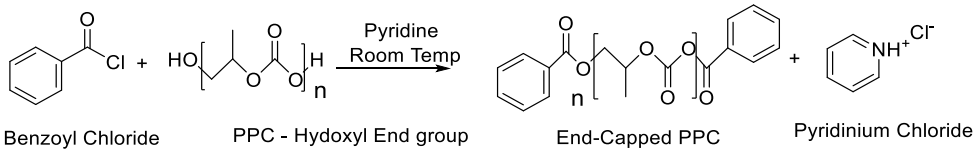

Figure 4.3 End-capping Reaction for PPC

The free hydroxyl end-groups can react with a chemical moiety to kinetically inhibit the unzipping reaction resulting in the thermal stabilization of PPC. Pyridine was used as a nucleophilic catalyst in the reaction. The end-capping process takes place via nucleophilic attack with the end-group of the polymer. Organohalide compounds containing carbonyl chlorides are excellent end-capping reagents due to the chloride leaving group and the partial positive charge of the carbonyl group. Benzoyl chloride, 4-nitrophenyl chloroformate, and vinyl chloroformate were used in this study for end-capping PPC. Chloroformates are known to be more reactive end-caps due to the additional electron-withdrawing oxygen bonded to the carbonyl group.

End-capping reactions with 137 kDa PPC were performed in a 20 ml scintillation vial under magnetic stirring. The scintillation vial contained 10 wt% of 137 kDa PPC in THF solution. Equimolar quantities of pyridine to end-capping reagents were also added to the reaction vessel dropwise. End-capping reagents added to the reaction vessel were dependent on reactivity, and the number of end-groups for the specified polymer. For example, 1 gram of 137 kDa PPC has an estimated amount of 1.46E-05 moles of –OH endgroups. Benzoyl chloride was added at 700 times the molar amount of end-groups of PPC to drive the reaction to the end-capped PPC products. Thus, 0.0102 moles of benzoyl chloride was used. Chloroformates are generally more reactive; hence, vinyl chloroformate was added at 50 times the amount of end-groups of 137 kDa PPC in which 0.000730 moles

was added to the reaction vessel. Magnetic stirring times were held for 48 hours to ensure that all ends have been reacted. Pyridinium-chloride precipitation is an indicator that the reaction is underway, because the produced white salt is insoluble in THF. The PPC was precipitated in methanol from the reaction solution at 10 times the volume of THF reaction solvent to ensure impurities have been removed.

End-capping reactions with 2 kDa PPC were held to at least 16 wt% in THF solution to ensure the polymer was at a concentration large enough to precipitate from solution in methanol. End-capping reagents must be added at lower amounts as to not exceed the solubility limit of reaction solvent because of the greater number of end-groups. The greater fraction of end-groups increases reactivity, thus, less amounts of end-capping reagents were used. For example, 1 gram of 2 kDa PPC has an estimated amount of 0.001 moles of –OH end-groups. Vinyl chloroformate was added at 5 times the number of end-groups of PPC to drive the reaction to the end-capped PCP products. Thus, 0.005 moles of end-capping reagent was added to the reaction vessel. Magnetic stirring was held at equally long times for 48 hours and subsequent precipitation of the polymer from methanol.

"Neat" PPC refers to polymers that were used as-received from the manufacturer. "AirDry-MeOH" samples are polymers that have been precipitated from THF in methanol. The sample was left to dry in a fume hood but contains residual methanol. "VaccDry" samples are polymers that have been precipitated from THF in methanol. However, the residual methanol has been essentially removed by vacuum drying at $100^{o}C$ for 12 hours

The mechanistic pathway and resulting temperature profile for PPC decomposition can be altered by end-capping with a chemical moiety which inhibits the unzipping reaction.

Figure 5 shows the reaction scheme for end-capping PPC. The free hydroxyl end-groups can react with a chemical moiety to kinetically inhibit the unzipping reaction resulting in the thermal stabilization of PPC. Pyridine was used as a nucleophilic catalyst in the reaction. The end-capping process takes place via nucleophilic attack with the end-group of the polymer. Organohalide compounds containing carbonyl chlorides are excellent end-capping reagents due to the chloride leaving group and the partial positive charge of the carbonyl group. Benzoyl chloride, 4-nitrophenyl chloroformate, and vinyl chloroformate were used in this study for end-capping PPC. Chloroformates are known to be more reactive end-caps due to the additional electron-withdrawing oxygen bonded to the carbonyl group.

Previously, end-capping of the PPC was verified only through thermogravimetic analysis. Characterization of the end-groups on high molecular weight polymers has proved to be difficult because the number of polymer ends is small compared to the number of monomers in the polymer. 137 kDa PPC has 672 monomers per end-group. In this study, we verified the end-capping process by NMR of the 2 kDa PPC because it has only 10 weight average monomer units per end-group.

Figure 4.4 shows the dynamic TGA in N_2 atmosphere of the decomposition of neat and end-capped 2 kDa PPC. The samples are in the "VaccDry" form meaning that the residual methanol was essentially completely removed from the PPC after end-capping and precipitation. The temperature was ramped at 5°C/min.

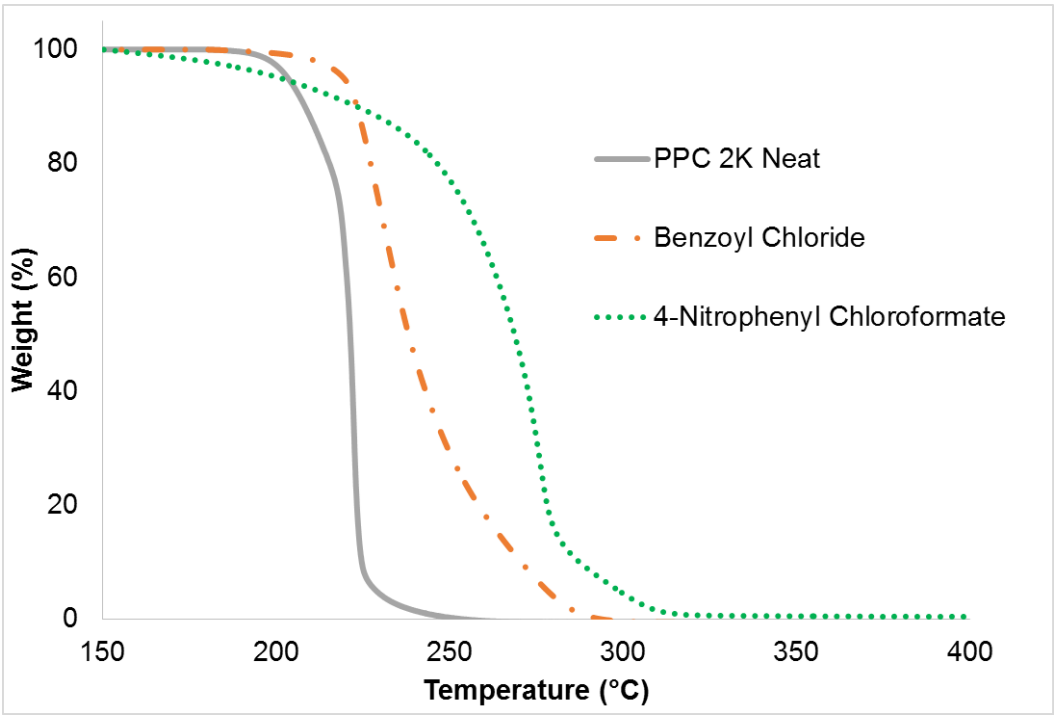

Figure 4.4 "VaccDry" Novomer 2 kDa PPC polyol end-capped with benzoyl chloride and 4-nitrophenyl chloroformate with a ramp rate of 5°C/min in N2 atmosphere.

As seen, the decomposition temperature of PPC end-capped with benzoyl chloride and nitrophenyl choloroformate showed 20°C and 50°C increase in thermal stability, respectively, when compared to neat PPC. The temperature shift in the TGA curves suggests that end-capping the hydroxyl end-groups of the PPC inhibit the unzipping reaction. The degree of stabilization due to the endcap is dependent on the structure of the endcap. In this study, the 4-nitrophenyl chloroformate shows a greater degree of stabilization from unzipping. The same end-capping reactions were repeated with the higher molecular weight PPC (137 kDa) and showed similar results, Figure 4.5.

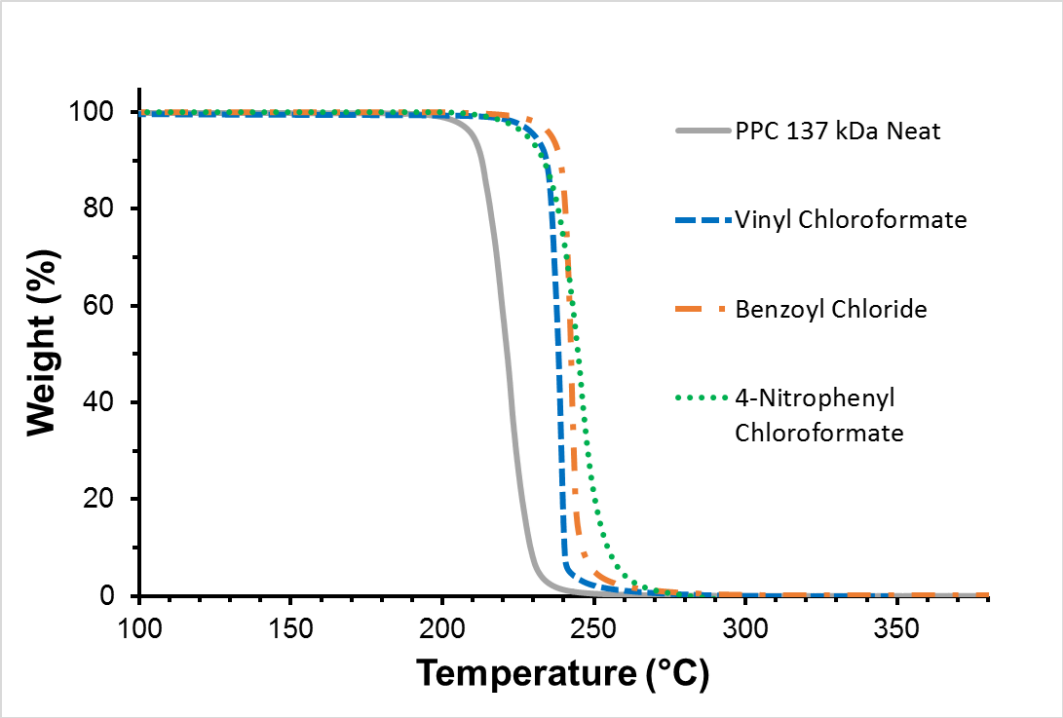

Figure 4.5 Novomer 137 kDa PPC "Neat", "VaccDry" benzoyl chloride end-capped 137 kDa PPC with benzoyl chloride, and solvent-casted benzoyl chloride end-capped 137 kDa PPC with 3 pphr of citric acid. Ramp rate used was 5°C/min in N2 atmosphere.

It is interesting to note that the stabilization effect is not as significant as with the higher molecular weight PPC. Previous research has shown that higher molecular weight PPC is less susceptible to the unzipping mechanism because it has fewer terminal hydroxyl end-groups[37]. It is likely that the 2 kDa PPC is more susceptible to unzipping because it has a greater fraction of end-groups compared to the high molecular weight PPC. The 4-nitrophenyl chloroformate shows the highest degree of stabilization with the 137k PPC, just as with the 2k PPC, however, the difference from endcaps is not as significant because the unzipping reaction is less of a factor overall with high molecular weight PPC.

Interestingly, the end-capped 2 kDa PPC in Figure 4.4 showed a much greater shift in thermal stability than 137 kDa PPC in Figure 4.5. The thermal decomposition of low vs

high molecular weight PPC has been studied with pyrolysis-gas chromatography –mass spectrometry. It has been reported by X.H. Li et.al [37] that lower molecular weight PPC is more susceptible to unzipping due to the larger fraction of end-groups. Furthermore, higher molecular weight PPC is more prone to chain scission due to the lower fraction of end-groups and greater number of repeat units in the backbone. Each end-cap has shown a different degree of stabilization from unzipping when used with the 2 kDa PPC. It is suggested here that the thermal and electronic properties of the end-group can become a more significant factor with lower molecular weight PPC that degrades primarily through unzipping.

Figure 4.6 shows the ^{1}H NMR analysis of "neat" 2 kDa MW PPC with hydroxyl end-groups. The major peaks were identified as followed: ^{1}H NMR ($CDCl_3$, δ, ppm), 1.3 ($3H; CH_3$, peak c), 4.18 ($2H; CH_2CH$, peak b), 4.98 ($1H; CH$, peak a), 0.95 ($3H; CH_3$, peak e), 3.92 ($2H; CH_2$, peak d).

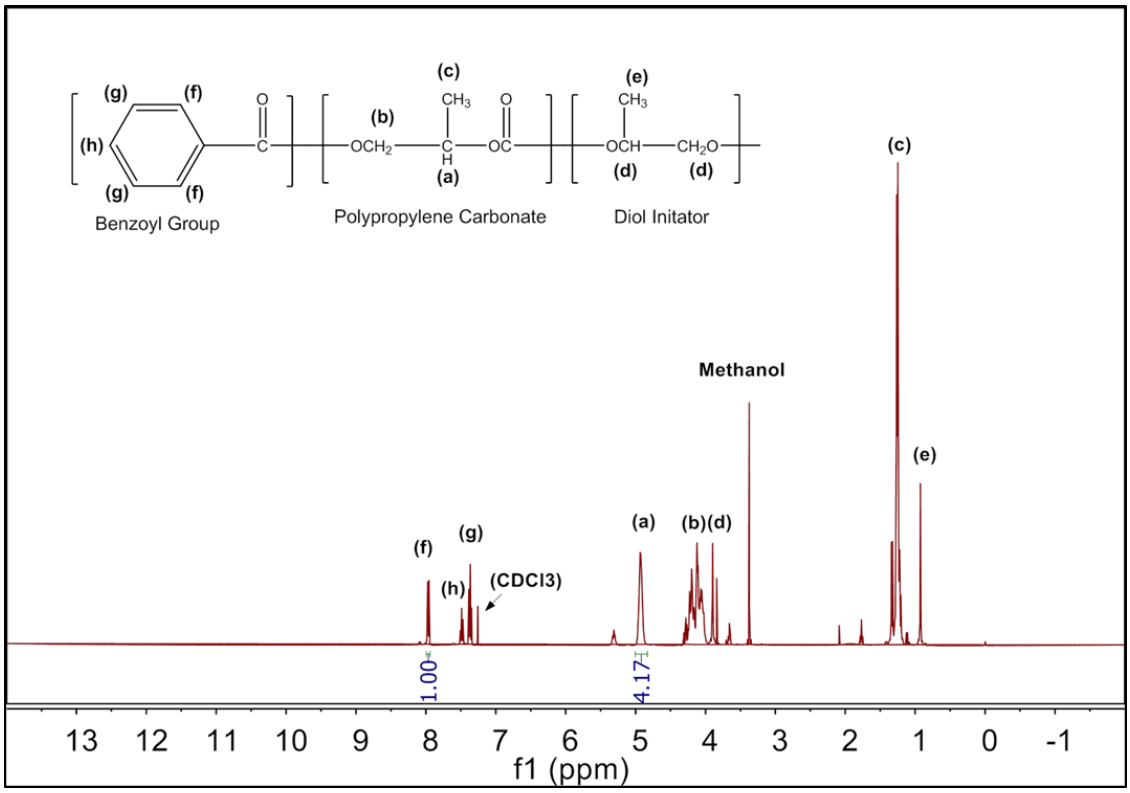

Figure 4.6 ^{1}H NMR analysis of "AirDry-MeOH" Novomer 2 kDa PPC polyol end-capped with benzoyl chloride in chloroform-D solution.

Chemical shifts of 1.3, 4.18, and 4.8 ppm confirm the existence of carbonate linkage of the PPC polymer which are denoted as peaks (a)-(c). Chemical shifts of 0.95 and 3.92 ppm, denoted as peaks (e) and (d), show that random ether linkages are also present in the PPC backbone which formed during synthesis. The chemical shifts of PPC agree with literature[27,36,39]. The carbonate content was calculated to be 91 mole % by integration of peaks following this formula: fcarbonate%= [a+b]/[a+b+d]. This corresponds to a 9 mole % of the diol initiator (or 1 diol monomer unit per polymer chain of PPC). No polyether content was observed in the spectrum. We should also note here that 137K PPC has approximately 99.99% carbonate linkages following the same formula and the polyether content is undetectable by NMR. In Figure 4.6, peaks (a)-(d) remained unchanged before

and after reaction showing that the polymer backbone has not been altered from the end-capping reaction. However, additional peaks from the end-group appear: ^{1}H NMR ($CDCl_3$, δ, ppm), 7.96 ($1H; CH$, hydrogen f), 7.48 ($1H; CH$ hydrogen g), 7.36 ($1H; CH$, hydrogen h)

Quantitative characterization of the molar ratio of the end-groups to the polymer chain ends can be determined from integration of ^{1}H NMR peaks. The number-average molecular weight of the lower molecular weight PPC is 1818.18 g/mol. This corresponds to a monomer to end-group ratio of 8.91:1. In Figure 4.6, integration of the PPC backbone Peak (a) was compared to integration of the protons from the end-cap Peak (f). Integration of Peak (a) shows an area of 4.17 which is normalized to protons from two different sites on the end-group. Thus, the ratio of monomer to end-group is 8.34:1. This value is very close to the number of monomers per end-groups (8.91:1) and within expected experimental error. These results reveal that end-capping has been achieved.

^{13}C NMR was used to confirm the site of the end-capping reaction on the PPC polymer chain. Figure 4.7 shows the ^{13}C NMR analysis of 2 kDa PPC unreacted and end-capped with benzoyl chloride, respectively. The major peaks were identified as followed: ^{13}C NMR ($CDCl_3$, δ, ppm), 16.3 (CH_3 , peak A), 69.1 (CH_2CH, peak B), 72.5 (CH_2CH, peak D), 154.7 ($OCOO$, peak E),

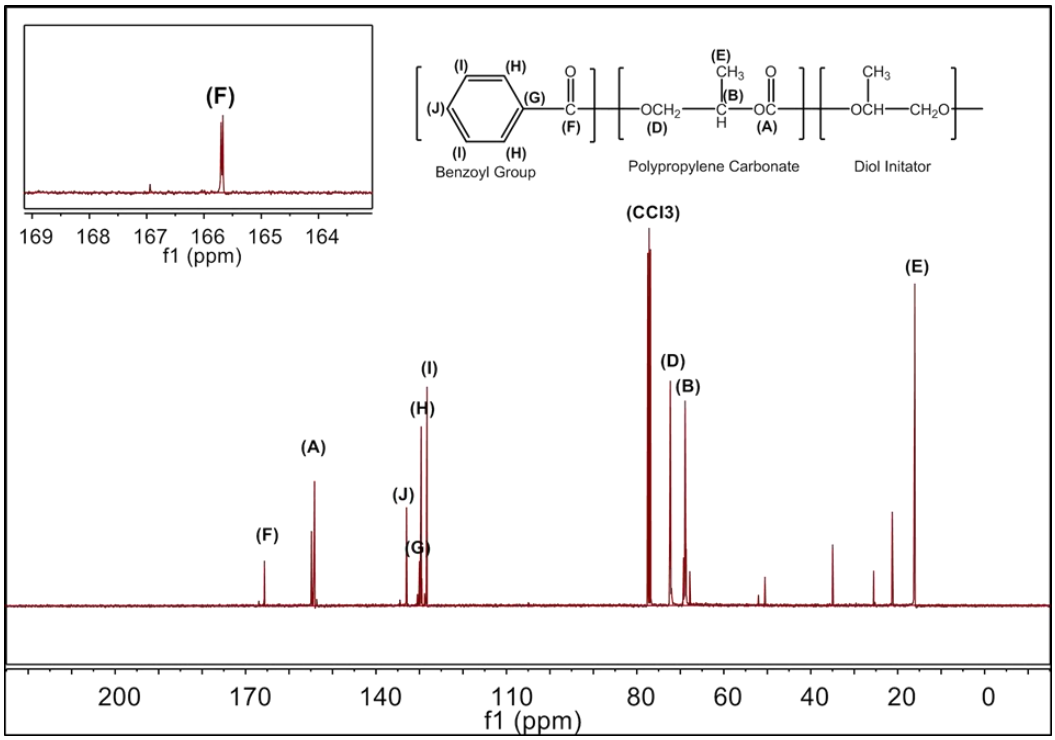

Figure 4.7 ^{13}C NMR analysis of "AirDry-MeOH" Novomer 2 kDa PPC polyol end-capped with benzoyl chloride in chloroform-D solution.

Chemical shifts of 16.4, 69.2, 72.8, and 154.7 ppm, denoted as Peaks (A)-(E), show the signals from the backbone of PPC before and after the end-capping reaction. In Figure 11, the benzoyl groups were observed at 129, 131.4, 133.2. 135.4, and 165.8 ppm, denoted as Peaks (F)-(I), respectively, after the end-capping reaction. The chemical shift of Peak (F) corresponds to the carbonyl carbon of the benzoyl group that has been reacted to the PPC ends. The chemical shift of the carbonyl carbon of benzoyl chloride is 168 ppm prior to end-capping and 165.8 ppm after end-capping. After end-capping, the carbonyl carbon of the benzoyl group is covalently bonded to the oxygen termination of the PPC as opposed to chlorine. As a result, Peak (F) shifts upfield to 165.8 ppm indicative of end-capping.

The nature of the unreacted PPC end-groups is of interest. PPC can be carboxylic acid and/or alcohol terminated, depending on the synthetic route. The carboxylic acid hydroxyl

has a chemical shift greater than 10 ppm in the ^{1}H NMR spectrum, which was not observed. The absence of a carboxylic acid peak suggests that the PPC is alcohol terminated. The alcoholic hydroxyl appears at 4-5 ppm which is masked by the signal from the backbone protons. The ^{13}C NMR spectrum also suggests that the end-groups are alcohol terminated. After reaction, peak (F) would shift further upfield to 161 ppm if it were carboxylic acid terminated because of its electron withdrawing nature. However, no such chemical shift was observed, suggesting that the 2 kDa PPC was alcohol terminated. The analogous NMR analysis could not be performed on the higher molecular weight PPC because the fraction of polymer ends was too low.

4.2.1 Acid/Base Catalyzed End-Capped PPC

Acid-catalyzed decomposition of end-capped PPC has also been studied via TGA. The as-received 137 kDa PPC and benzoyl chloride end-capped 137 kDa PPC samples were mixed separately with 3 pphr of PAG (Rhodorsil-Faba) in GBL and solvent-cast onto a silicon substrate. The resulting films were exposed to 248 nm UV light at a dosage of 2 J/cm^2. The acid-activated PPC-PAG samples were analyzed by dynamic TGA and are shown in Figure 4.8. Temperature was ramped at 5^{o}C/min

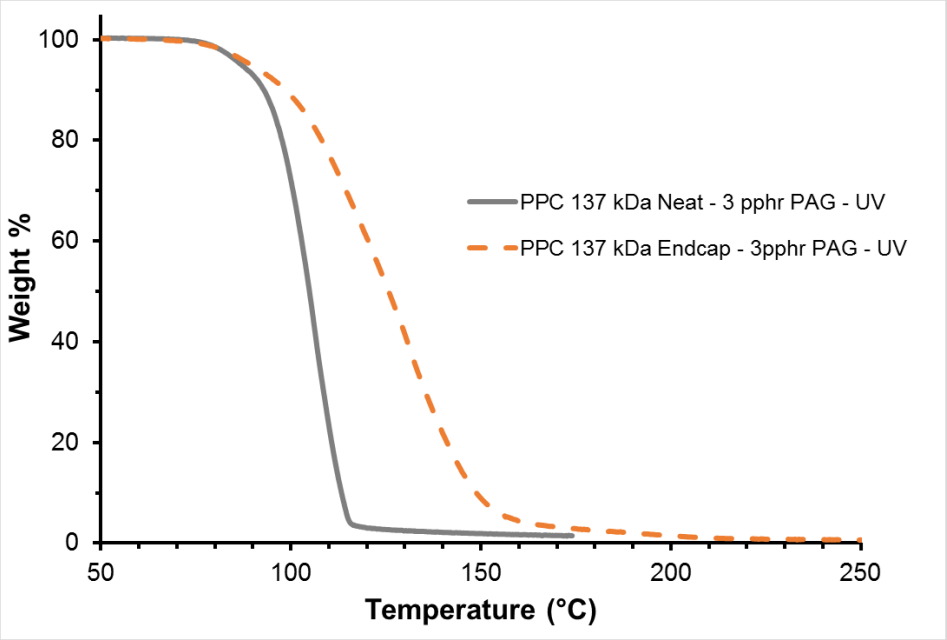

Figure 4.8 Solvent-casted Novomer 137 kDa PPC samples in GBL with 3 pphr PAG and a UV exposure dosage of 2 J/cm2. Ramp rate used was 5°C/min in N2 atmosphere.

As seen by the temperature of 5% weight loss, the onset of the degradation of the acid-catalyzed neat and end-capped PPC are almost identical at 88°C. However, the end-capped polymer depolymerized at a significantly slower rate as the temperature was raised. This is to be expected as acid-catalyzed degradation of PPC carries out primarily by chain scission, but also by unzipping mechanisms. The onset of degradation is the same due to the primary acid-catalyzed degradation pathway of chain scission, and the slower rate can be attributed to the inhibition of the second and minor acid-catalyzed degradation pathway of unzipping.

Acid-catalyzed decomposition of PPC has previously been the subject of studies[62,63,80]. The mechanism of degradation has been previously proposed by J. P. Jayachandaran et. al[8] from product formation analysis using a GC-MS system. The

generated acid from the PAG after UV exposure protonates the carbonyl oxygen groups across the backbone of the polymer leading to a degradation pathway similar to chain scission. It was also shown that unzipping can proceed from some acid-catalyzed intermediates leading to propylene carbonate as reaction products. Figure 12 reveals the acid-catalyzed decomposition of an end-capped and neat PPC samples. The onset temperature is similar due to initiation of chain scission as the primary degradation pathway. However, the end-capped PPC samples displayed a much slower rate (broader slope) because of the inhibition of the second, and minor, acid-catalyzed degradation pathway.

Base-catalyzed decomposition of end-capped PPC was analogously studied via TGA in Figure 4.9. The as-received 137kDa PPC and benzoyl chloride end-capped 137 kDa PPC samples were mixed with 1.35 pphr of the PBG in order to maintain the same concentration of 332 monomer units to 1 mole of acid or base. The films were treated with the same UV exposure conditions as the acid-catalyzed films and run with TGA.

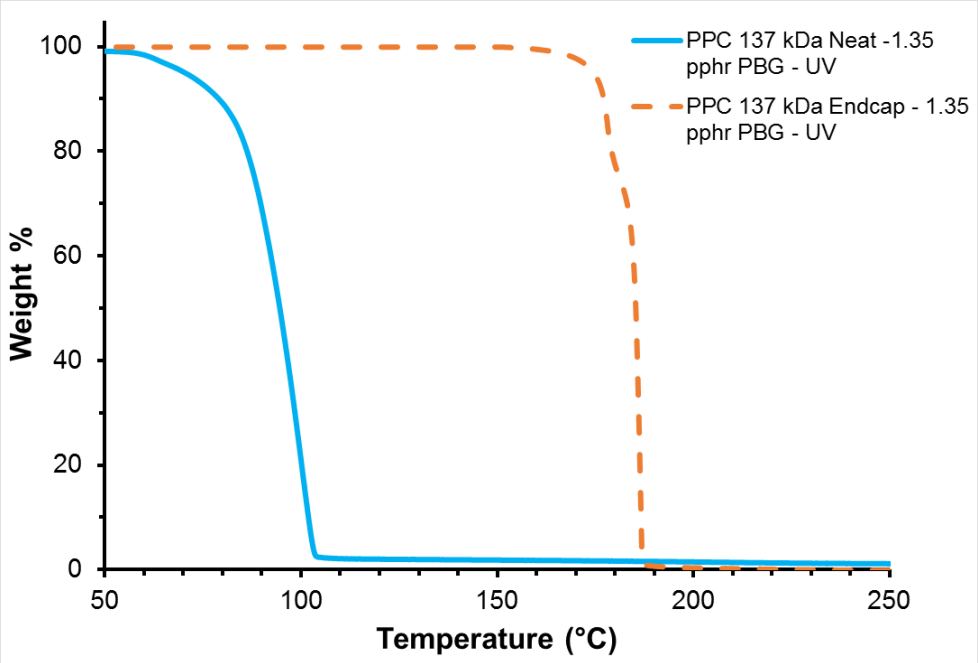

Figure 4.9 Solvent-casted Novomer 137 kDa PPC samples in GBL with 1.35 pphr PBG and a UV exposure dosage of 2 J/cm2. Ramp rate used was 5°C/min in N2 atmosphere.

The 137 kDa PPC neat and end-capped samples were drastically different. The 5 weight % temperature of the base-catalyzed neat 137 kDa PPC is 70^{o}C, while the end-capped PPC is 174^{o}C. Base-catalyzed degradation of the end-capped PPC samples performed poorly as expected. PBG catalyzes primarily the "backbiting" or unzipping mechanism of PPC. Thus, it is demonstrated here that the end-capped samples that are base-catalyzed are not as effective due to the inactive ends.

Base-catalyzed decomposition of PPC has not been well-studied in literature, but it has been suggested that PBG-caused degradation occurs primarily by the "backbiting" or unzipping reaction. Sun et.al monitored the thermolysis of PPC with 3 wt % of TBD by FTIR and GPC and revealed the formation of cyclic propylene carbonate[66]. In the previous study, it was proposed that the strong amine base performs a nucleophilic attack of the

carbonyl group that produces an alkoxide. This intermediate further backbites leading to the cyclic products in a similar way to the unzipping mechanism. PPC samples that have already been rendered "inactive" by end-capped chain ends should not be as susceptible to base-catalyzed decompositions. Figure 4.9 demonstrates the idea as the base-catalyzed degradation of end-capped PPC samples were not very effective compared to the neat PPC samples with free hydroxyl end-groups.

4.2.2 Solvent Effects

Solvent-casting PPC from a variety of solvents was previously shown to change the decomposition temperature of PPC[64]. To investigate the effect of the casting solvent on the decomposition temperature, end-capped polymers with residual solvent were investigated. After end-capping, the PPC was precipitated from THF by the addition of methanol. The precipitated PPC product was then air-dried which left a small amount of residual methanol in the PPC, identified as "AirDry-MeOH". The thermal stability of as-received, end-capped with 4-nitrophenyl chloroformate and end-capped PPC dried of residual methanol was compared and is shown in Figure 4.10 for the 137 kDa PPC. End-capping the PPC inhibits the unzipping reaction of the polymer.

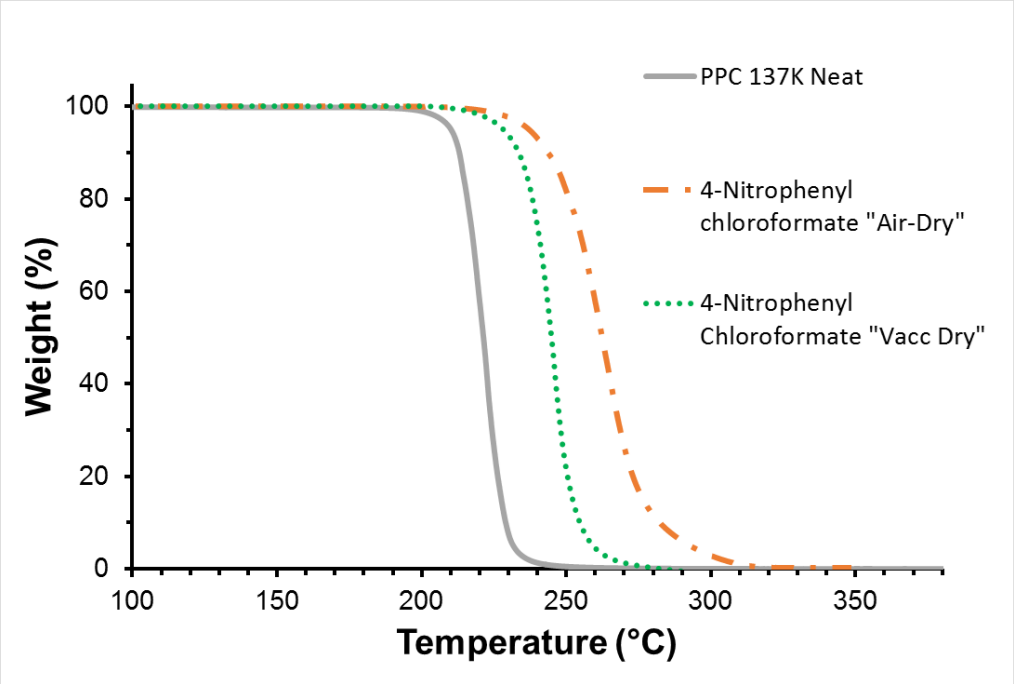

Figure 4.10 Novomer 137 kDa PPC samples end-capped with 4-nitrophenyl chloroformate with "VaccDry" and "AirDry-MeOH" conditions.

The 50% weight loss temperature of the dry end-capped PPC shifted to 240^{o}C compared to the as-received polymer at 220^{o}C. However, leaving the residual methanol solvent in the end-capped PPC shifted the decomposition temperature an additional 20^{o}C to 260^{o}C. The effect of solvent casting, as shown in Fig.4, is simply to remove the residual, stabilizing solvent from the PPC. Thus, the stabilizing effect of residual methanol adds to the end-capping stabilizing effect. End-capping stabilizes PPC from unzipping whereas methanol appears to stabilize the random chain scission reaction.

The end-capping and methanol stabilization effects were repeated on 2 kDa PPC to confirm that the end-groups were present before and after the different processing steps in Figure 4.11.

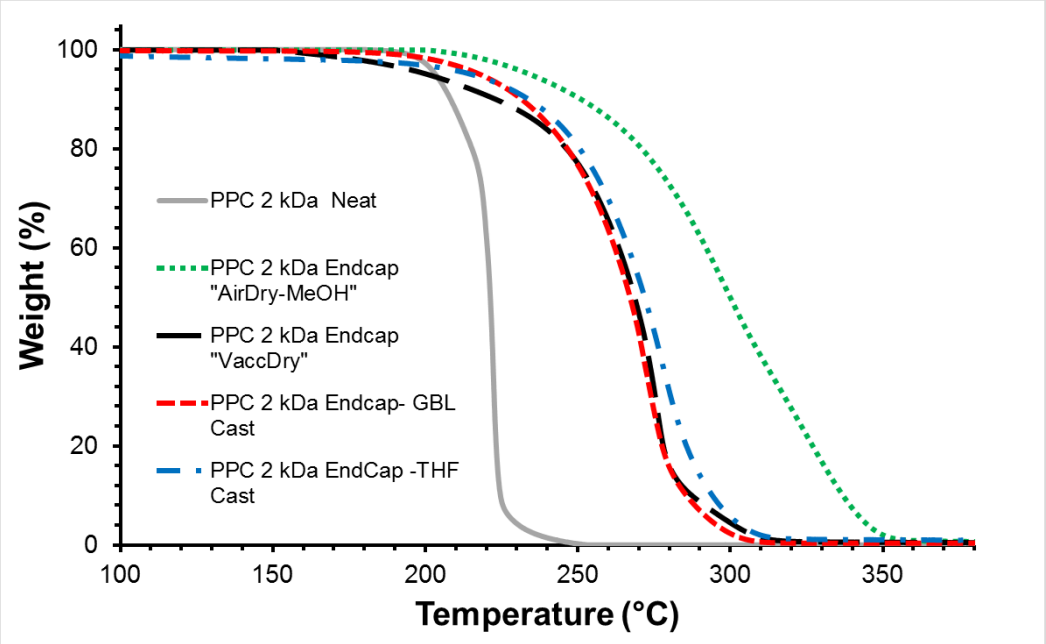

Figure 4.11 Novomer 2 kDa PPC polyol samples end-capped with 4-nitrophenyl chloroformate with "Solvent cast", "VaccDry", and "AirDry-MeOH" conditions.

The dry end-capped 2 kDa MW PPC shifted the 50% weight loss temperature to 270^{o}C compared to the as-received polymer at 220^{o}C. Leaving the residual methanol solvent in the end-capped PPC shifted the decomposition temperature an additional 30^{o}C to 300^{o}C. The end-capped PPC sample with the residual methanol was then solvent-cast onto a silicon substrate from GBL or THF, soft-baked at 100^{o}C for 5 minutes, and measured by TGA. As expected, the "VaccDry" end-capped PPC samples and the GBL or THF solvent cast samples produced similar 50 weight% decomposition temperatures at approximately 270^{o}C. The residual methanol that stabilized PPC from random chain scission was removed by the solvent-casting or vacuum drying procedure.

The presence of methanol in the "AirDry-MeOH" PPC samples was confirmed using NMR analysis. A peak at 3.46 ppm was identified in the ^{1}H NMR spectrum. The 3.46 ppm peak is consistent with that of methanol and corresponds to a concentration of 28

mole %. The monomer to end-group ratio was checked for this sample with methanol present. The ratio of monomer to end-group in ^{1}H NMR spectrum of "AirDry-MeOH" sample was found to be 8.2:1. The complete removal of methanol in "VaccDry" samples was confirmed by NMR analysis. Analogous integration measurements were done in the ^{1}H NMR spectrum of "VaccDry" sample gave a monomer to end-group ratio of 8.54:1. Thus, the NMR spectra reveal no significant change in the monomer to end-group ratio between "AirDry-MeOH" and "VaccDry" samples. The polymer end-groups are not affected by different processing techniques even though the TGA results show a significant shift in thermal stability for "AirDry-MeOH" samples with residual methanol. Thus, it is proposed that methanol is the stabilizing agent that inhibits random chain scission. The stabilization may occur through complex interactions with carbonyl sites on the PPC backbone.

It is suggested that methanol only inhibits chain scission and not unzipping since the stabilization effect is also seen with PPC that has been end-capped. Solvent-casting generally removes the methanol by dilution and evaporation during spin coating and soft-baking. PPC samples that were dried by forcibly removing methanol under vacuum or precipitation in a non-polar solvent may provide more accurate stability measurements of the polymer in future use.

Impurities have been the subject of investigations of thermal stability, specifically catalyst residues from polymerization[37,42,81–84]. Residual solvent from polymerization or purification procedures can affect the thermal stability of PPC[42,64] and are typically not reported in many studies. Methanol is one of the frequently used solvents to precipitate and purify PPC from reaction solution. It has been shown in this study to be

an impurity that can act as a stabilizing agent. In Figure 4.10 and Figure 4.11, PPC containing residual methanol had a higher thermal stability than PPC where the methanol was removed by vacuum evaporation. NMR analysis was used to confirm the existence of methanol as an impurity. The PPC material was end-capped, thus, any additional increase in thermal stability is the result of inhibition of chain scission through interactions with carbonyl moieties in the backbone of the polymer. The workup of these polymers from residual solvent has been demonstrated to be an important factor to the overall thermal stability of PPC polymers.

4.3 Chain Scission Stabilization

Monofunctional fatty acids have been used in the past to stabilize PPC by inhibiting chain scission degradation[47]. Fatty acids, such as stearic acid, typically have a very high decomposition temperature and leave substantial residue which is not suitable for a sacrificial polymer in some electronic applications. Citric acid, a tri-functional carboxylic acid, was used to kinetically stabilize PPC from chain scission. Citric acid has a decomposition temperature of 175°C[85–87], which is below the onset of decomposition of PPC (i.e. 180°C). In addition, the citric acid vaporizes mostly to carbon dioxide, acetone, and hydrogen, each of which are volatile. However, citric acid can decompose to anhydride derivatives which have a lower vapor pressure. Sustained heating can further break this compound to more volatile products. Citric acid will likely produce minimal residue after decomposition from the polymer matrix.

A sample of 137 kDa PPC and 3 pphr of citric acid were mixed in GBL and solvent-cast onto a silicon substrate. Figure 4.12shows the dynamic TGA of this mixture.

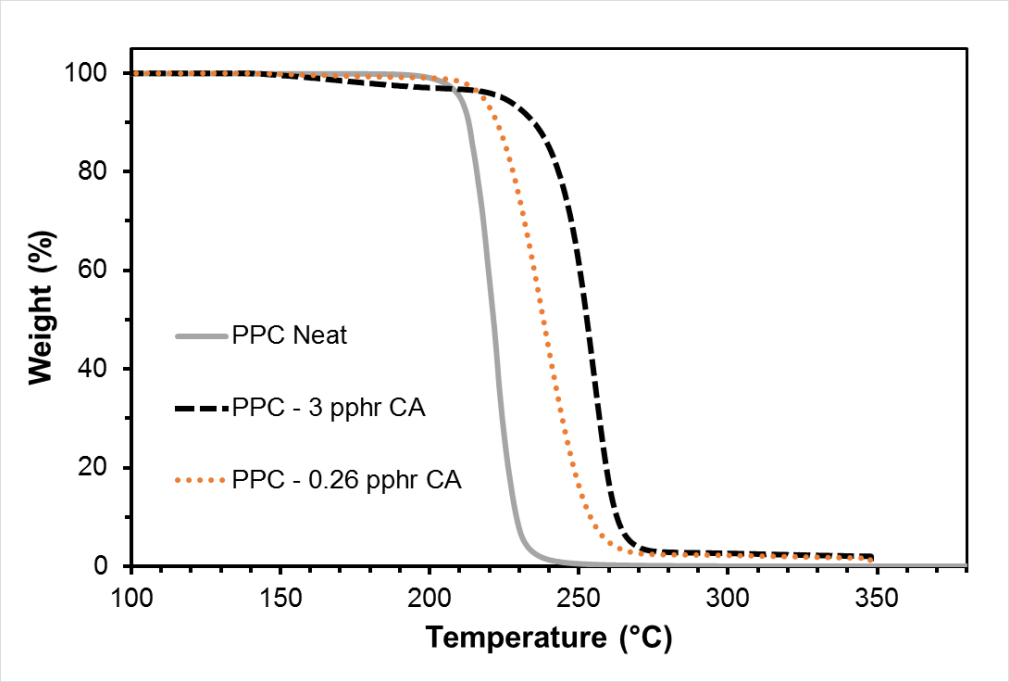

Figure 4.12 Solvent-casted Novomer 137 kDa PPC samples in GBL with 0.26 and 3 pphr citric acid

The PPC film with 3 pphr citric acid as an additive showed a 35°C increase in thermal stability with a 50 % weight loss temperature of 253°C compared to the neat sample. As expected, excess citric acid (2.74 wt %) vaporized at 175°C. The amount of citric acid added to the film (3 wt%) was subtracted from the excess citric acid shown from the TGA profile suggesting that only 0.26 wt% of citric acid was actually needed for stabilization from random chain scission mechanism. An exact amount of 0.26 pphr was blended with 137 kDa PPC and cast on a silicon substrate, also shown in Figure 16. The PPC film with 0.26 pphr citric acid displayed only a 20°C increase in thermal stability compared to the as-received polymer. The 50% weight loss temperature was 238°C and the evaporation of excess citric acid was not seen.

PPC is typically heated to higher temperatures to rapidly degrade and volatize the sacrificial polymer leaving an air-cavity. An isothermal TGA at 180°C of the film was done to quantify the amount of residue and the time to completely vaporize PPC. After 2 hours the residue is minimal (0.34 weight %) and not visible from the TGA pan.

4.4 Decomposition Atmosphere

Although the ambient atmosphere within the TGA is not involved in the PPC decomposition reaction [26,34,42] (i.e. no involvement of nitrogen or oxygen in the primary unzipping or chain scission reactions), there have been some reports of shifts in the TGA curves due to the ambient gas[64]. As-received PPC samples were decomposed in nitrogen and air environments at a heating rate of 5°C/min. The TGA curves in Figure 4.13 show a significant thermal stability shift for the air ambient for all PPC molecular weights.

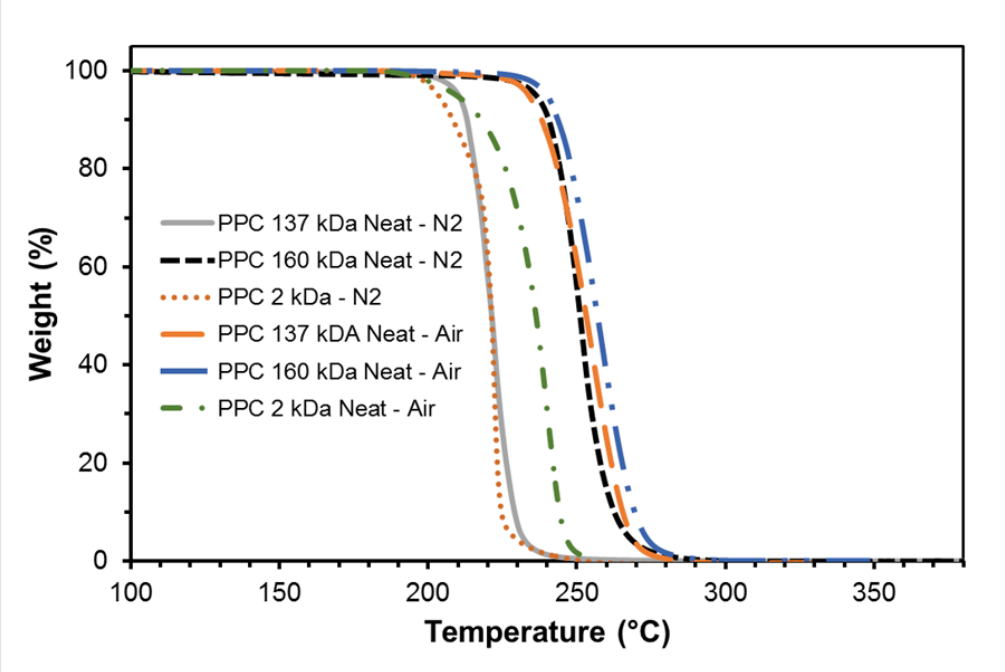

Figure 4.13 "Neat" Novomer PPC with molecular weights of 2 kDa, 137 kDa, 160 kDa at a ramp rate of 5°C/min in N2 and ambient air atmosphere.

Notably, the thermal shift of 137 kDa PPC had a 35°C increase in thermal stability. Interestingly, the 160 kDa has only a minimal shift in thermal stability of 3°C. However, the 50 wt% thermal decomposition temperature of the 137 kDa and 160 kDa PPC in air are nearly identical at 253°C.

The 137 kDa PPC end-capped with vinyl chloroformate with "VaccDry" processing was also decomposed in nitrogen and air environments at a heating rate of 5°C/min. The end-capped sample showed a 20°C shift in thermal stability in air with a 50 wt% decomposition temperature of 256°C, as compared to its thermal profile in nitrogen environment - 50% weight loss at 236°C. This result suggests that the stabilization of PPC material in air is not related to any interaction with end-groups of the polymer.

The stabilizing effect of oxygen ambient (from air) was further investigated. PPC films with 3 pphr citric acid (i.e. already stabilized from chain scission degradation) showed no difference in thermal stability in nitrogen and air ambient conditions. The nitrogen and air ambient had nearly identical 50% weight loss temperatures, 256°C. It appears that oxygen can react with specific intermediates during the PPC decomposition process slowing the decomposition reaction. Further investigation of this effect will be necessary to understand the role of oxygen.

4.5 End-Capping and Organic Additives

Previous studies have focused on stabilizing PPC by considering only a single route to decomposition. This has led to confusing and sometimes contradictory conclusions. In this study, we have considered both routes to decomposition, and the stabilization or catalysis of each route. Polymer unzipping can be kinetically stabilized through covalent

end-capping, and chain scission can be stabilized by additives. Inhibiting both mechanisms leads to the highest decomposition temperature PPC, thereby expanding the thermal window. Figure 18 compares the dynamic TGA profiles of the decomposition of end-capped 137 kDa PPC with benzoyl chloride, 137 kDa PPC with 3 pphr citric acid, and end-capped 137 kDa PPC with 3 pphr citric acid as an additive.

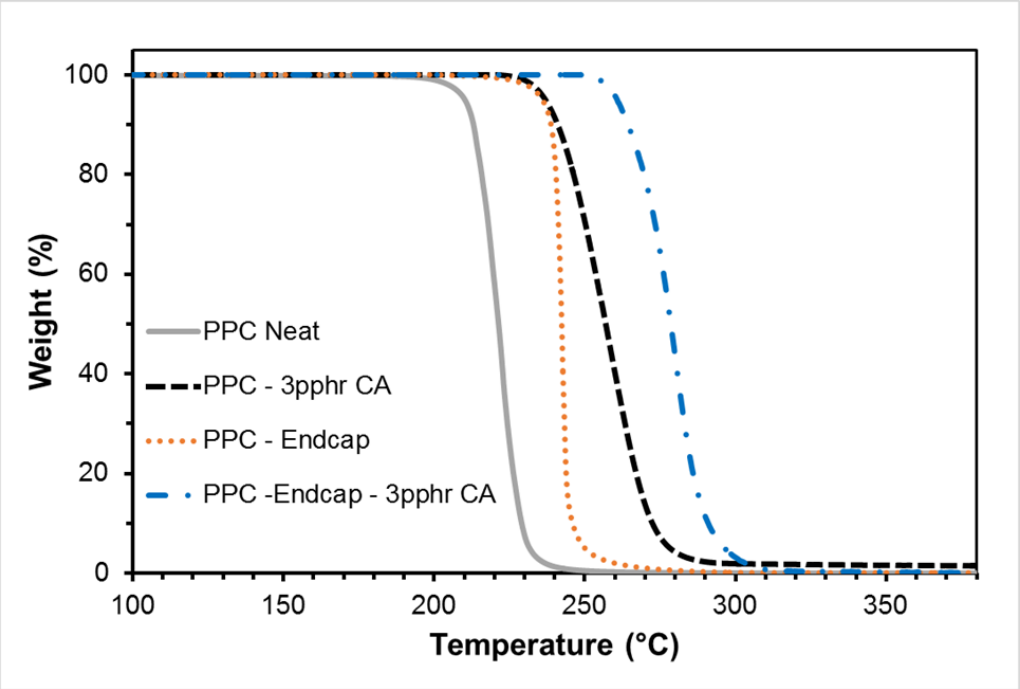

Figure 4.14 Novomer 137 kDa PPC "Neat", "VaccDry" benzoyl chloride end-capped 137 kDa PPC with benzoyl chloride, and solvent-casted benzoyl chloride end-capped 137 kDa PPC with 3 pphr of citric acid. Ramp rate used was 5°C/min in N2 atmosphere.

The plots were normalized after the initial loss of excess citric acid for comparison of the thermal stability. There is 20°C and 35°C increase in thermal stability by using end-capping or hydrogen bonding, however, when both decomposition mechanisms are suppressed, a 60°C increase in thermal stability (50 weight % loss temperature of 277°C) is achieved.

Studies have used octadecanoic acid and poly(ester) amide to stabilize PPC, and all suggested that hydrogen bonding is the reason[44,45,47]. However, confirming the presence of hydrogen bonding with the carbonyl group of PPC has not been easily demonstrated. It is clear from this study that these organic additives are inhibiting chain scission, due to the added thermal stability with end-capped samples as shown in Figure 18. This implies that there is a complex interaction with carbonyl moieties across the backbone of the polymer. However, further investigation is needed to determine the exact mechanism of inhibition that these additives provide.

4.6 Conclusions

Thermal stabilization of PPC as a sacrificial material for an air-cavity MEMS packaging process has been demonstrated. End-capping of PPC has been achieved and confirmed with NMR analysis that has not been seen before in literature. Chain scission inhibition was demonstrated through the use of citric acid additives with low residue after decomposition of the polymer matrix. Combing both methods of stabilizing interactions of the backbone of the polymer with citric acid and end-capping of chain ends in a PPC film provided thermal stability that surpassed both methods by themselves. Residual solvents in PPC such as methanol, have been demonstrated to be an impurity that can affect the thermal stability through possible interactions with the backbone of PPC. This study has widened the thermal process window of PPC as a sacrificial material while maintaining low-residue for use in MEMS packaging.

CHAPTER 5. ULTRAVIOLET TO VISIBLE LIGHT INITIATED DEPOLYMERIZATION OF TRANSIENT POLYMERS

5.1 Motivation and Background

Transient devices, such as electronic components, are an emerging field where the disposal of a device after use is desired so as to avoid reverse-engineering and minimize the environmental impact. Polyaldehydes with photo-triggers are investigated in this chapter because wavelength of the radiation can be adjusted to meet the transient application. Polynuclear aromatic hydrocarbons (PAHs) were used as the optical sensitizer for photoacid generators (PAG). Photo-induced electron transfer (PET) with iodonium-based PAG was used to expand the spectral sensitivity range

Photo-initiated onium salts can be used to catalyze the depolymerizations coatings in negative-tone, wet-developable photoresists [69,88,89]. Onium salts are very soluble and can be easily mixed with decomposable polymers to form photosensitive films by solvent casting. Diaryliodonium and triarylsulfonium salts are efficient PAGs because of the presence of UV absorbing aryl groups on the onium cation. Upon UV excitation, the carbon-iodine or carbon-sulfur bond undergoes homolytic or heterolytic cleavage that generates cation radicals which react with monomers or solvents to produce a strong Bronsted acid. However, the photo-active spectrum of the onium salts is limited to the UV portion of the electromagnetic spectrum making them insensitive to sunlight. Sensitizing the onium salts to longer wavelengths of light makes a more efficient photolysis in sunlight applications[68,90].

The goal of this chapter is to extend the PAG spectral sensitivity to longer wavelengths of light via photo-induced electron transfer (PET)[69]. A simplified reaction scheme, Scheme I, uses MtXn- as the weakly nucleophilic counterion (e.g. BF_4^-, PF_6^-, SBF_6^-, $(C_6F_5)_4B^-$) in the PAG. The photo-induced electron transfer is initiated by photosensitizer (PS) absorption of light creating the excited state [PS]*. The [PS]* undergoes energy transfer to the onium salt generating an excited complex state (exciplex). The onium is reduced by a formal one electron-transfer reaction. The electron-transfer reaction is rendered irreversible due to the rapid decay of the onium radical as shown in eq4 of scheme I. The PS cation radical can decay in a number of pathways to produce a strong Bronsted acid.

$$PS \xrightarrow{hv} [PS]^* \qquad \text{eq. 1}$$

$$[PS]^* + Ar_2I^+ MtX_n^- \longrightarrow [PS\cdots Ar_2I^+ MtX_n^-]^* \qquad \text{eq. 2}$$

$$[PS\cdots Ar_2I^+ MtX_n^-]^* \longrightarrow [PS]^+\bullet\ MtX_n^- + Ar_2I\bullet \qquad \text{eq. 3}$$

$$Ar_2I\bullet \longrightarrow ArI + Ar\bullet \qquad \text{eq. 4}$$

$$[PS]^+\bullet\ MtX_n^- \Longrightarrow H^+ MtX_n^- \qquad \text{eq. 5}$$

Scheme I. Mechanism for Photo-induced Electron Transfer of Onium Salts

A variety of compounds, including carbazoles, phenothiazines, isobenzofurans, cyanines, and conjugated olefins, can be used to photosensitize onium salts [68,90,91]. Diaryliodonium salts are more favorable for electron-transfer reactions because the reduction potential is low compared to triarylsulfonium salts. Polynuclear aromatic hydrocarbons are an efficient class of electron-transfer photosensitizers [69,91]. The

absorption characteristics and oxidation potentials of the acenes are related to the size of their aromatic frameworks. For example, anthracene has an absorption wavelength cut-off at 390 nm while pentacene is at 585 nm. However, increasing the number of aromatic rings lowers the solvent solubility due to the higher crystallinity from π- π stacking. Pentacene suffers from poor solubility in most common organic solvents that makes it difficult for solvent casting films. The spectral absorption and solubility of acenes can be adjusted through functionalization. Incorporation of other electron-donating groups, such as alkoxy groups, has been shown to improve the photosensitization process by refining the redox potentials, as well as improving the solubility [69]. Electron donating groups can potentially increase the excited-state lifetime to improve energy transfer with onium salts, especially in dilute solutions[92].

The sensitization of iodonium salts has been used in cationic photopolymerizations to achieve faster rate with anthracene derivatives [69]. NIR sensitization of iodonium salts have been assessed previously with cyanines, however, the basic functionality is likely not compatible with acid-catalyzed processes[68,93–97]. Wallraff et. al studied the sensitization of onium salts for acid-catalyzed deprotection of polymethacrylates as wet-developable photoresist[91]. However, sensitization of onium salts have not been extensively studied for acid-catalyzed depolymerization of polymers. The aim of this chapter is to evaluate the sensitization of iodonium PAGs into the entire visible spectrum with anthracene, tetracene, and pentacene derivatives. It is desirable for transient polymers to have low solid residues after depolymerization. Similarly, it is desirable for the decomposable polymers have a low chemical footprint after depolymerization to avoid detection and reverse-engineering.

Hence, the by-products of the PET reaction is studied to minimize solid residue post-depolymerization.

5.2 Optical Properties of Photosensitizers

The optical properties of the modified acenes were investigated by UV-vis absorption and fluorescence spectroscopy in degassed dimethylformamide (DMF). The six sensitizers, anthracene, CPTX, DMBA, BPET, BPEP, and BTMP, exhibited strong absorption bands from 312 nm to 673 nm, as shown in Figure 5.1 and listed in Table 1. The fluorescence spectrum corresponding to the first excited singlet state for BPET is shown in Figure 5.2.

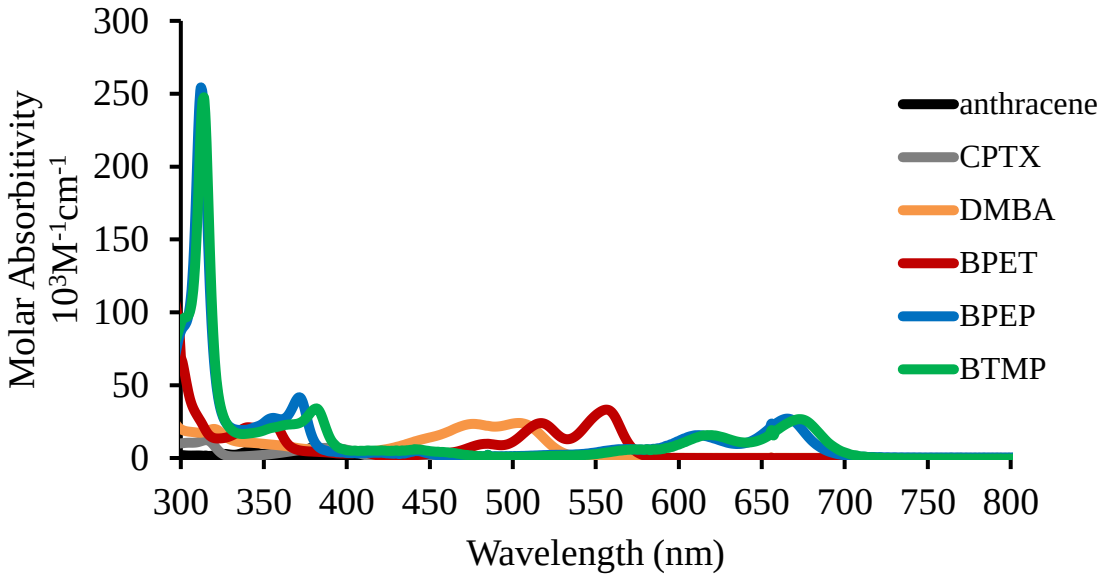

Figure 5.1 Molar Absorptivity of photosensitizers in DMF solution

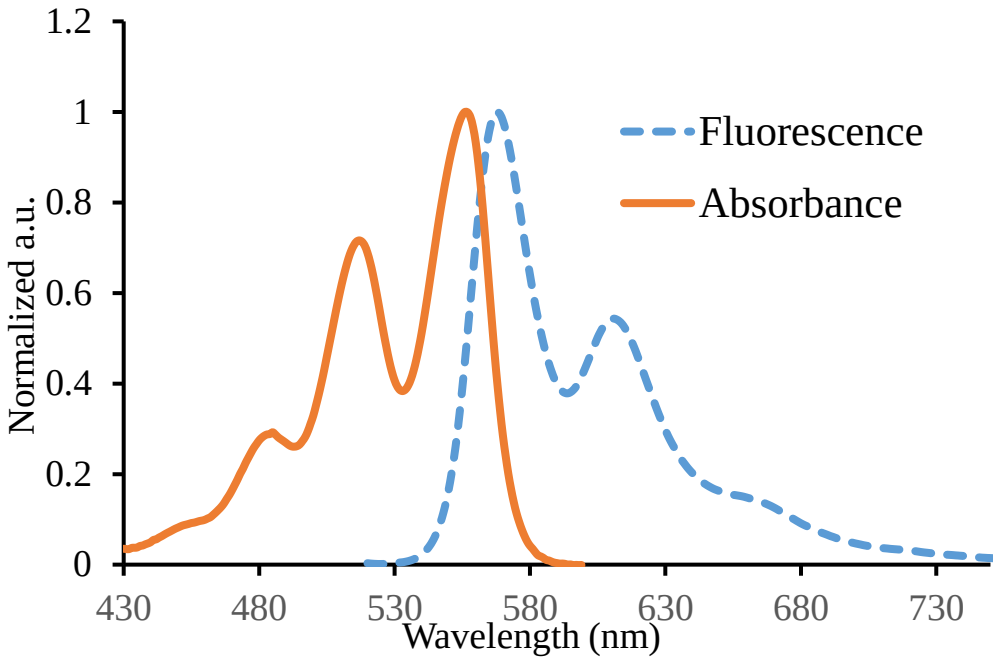

Figure 5.2 Normalized absorbance and fluorescence emission spectra of BPET photosensitizer after excitation at 514 nm in DMF solution

The four sensitizers that absorb in the visible region have high molar extension coefficients between $24 \cdot 10^3$ $M^{-1}cm^{-1}$ to $33 \cdot 10^3$ $M^{-1}cm^{-1}$ which is 3-4 times greater than the molar extinction coefficient CPTX, $6.9 \cdot 10^3$ $M^{-1}cm^{-1}$ at 387 nm, and anthracene, $7.1 \cdot 10^3$ $M^{-1}cm^{-1}$ at 370 nm. However, all of the absorption bands are red-shifted compared to their unmodified acene counterparts (anthracene, tetracene, pentacene) due to the halogenation of the acene core or the extension of the π - conjugated system by the appended phenylethynyl groups [76]. The two pentacene derivatives, BPEP and BTMP, show very similar spectra. The addition of methoxy groups to the molecules results in a red-shift in the absorption spectrum by 5 nm, and markedly improved solubility in common organic solvents and polymer films.

Table 1 Absorption and fluorescence maxima of modified PAH photosensitizers

Photosensitizer	Abs. λ_{max} (nm)	Abs. ε ($10^3 M^{-1}cm^{-1}$)	Emission λ_{max} (nm)
Anthracene	326	2.8	381
	342	5.3	403
	360	7.6	427
	370	7.1	453
CPTX	315	12	---
	387	6.9	---
DMBA	320	20	536
	476	23	563
	504	24	
BPET	341	21	411
	355	24	433
	410	3.6	568
	485	9.8	611
	517	24	660
	556	33	
BPEP	312	254	467
	371	42	492
	569	6.2	684
	612	15.7	738
	665	27	
BTMP	314	274	477
	382	33	503
	441	5	690
	576	6	750
	619	16	
	673	27	

5.3 Gibbs Free Energy of Photo-induced Electron Transfer

Molecular compounds, such as PAH, can be used as photosensitizers for the iodonium PAGs given that the energetics are thermodynamically feasible. Photo-induced electron transfer is the oxidation-reduction process between a donor and its acceptor through molecular orbitals. A simplified diagram is show in Figure 5.3.

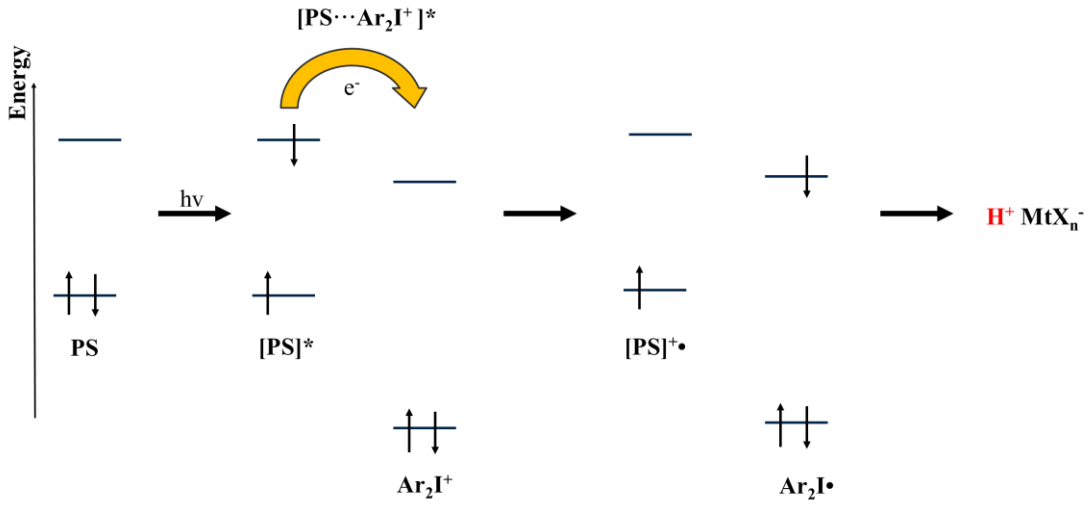

Figure 5.3 Photo-induced electron transfer of iodonium salts as expressed by molecular orbitals to generate super acid

The donor (sensitizer) is at a ground-state with two paired electrons in the highest occupied molecular orbital (HOMO). The oxidation potential of the donor (sensitizer) is increased, compared to the ground state value by absorption of a photon thereby creating an electron to the lowest unoccupied molecular orbital (LUMO) resulting in the formation of the first excited singlet state. The excited singlet state of the sensitizer can lose energy by fluorescence or non-radiative processes before reduction of the onium salt. The photosensitizer and onium salt can create an excited complex, as shown in Scheme I Equation 3, where an electron is transferred from the sensitizer to the LUMO of the PAG.

A reactive cationic radical is created as a result of this electron transfer that can further react to product a Bronsted acid. The favorability of electron transfer is determined by the oxidation and reduction potentials of the states of the compounds**.** In this case, the oxidation potential of sensitizer was compared to the reduction potential of the PAG to determine if the reaction is favorable. The thermodynamic favorability for the electron-transfer photosensitization of the modified PAHs with photo-acid/base generators can be evaluated by the Rehm Weller equation[68,70,90,91,98].

$$\Delta G(eV) = (E_{ox}^{1/2} - E_{red}^{1/2}) - E_{oo} \tag{8}$$

The half-wave oxidation potential (E_{ox}) and the optical band gap (E_{oo}) of the sensitizer was compared with the half-wave reduction potential (E_{red}) of the photo-acid/base generator. If the Gibbs free energy is less than zero ($\Delta G < 0$) then the photo-induced electron transfer is favorable. Another requirement is that there is no ground-state electron-transfer between PS and PAG. In this regard, the oxidation potential of the sensitizer must be unfavorable for electron transfer until the excited state is photo-created so that the sensitizer can act as an 'optical trigger'. Cyclic voltammetry was used to measure the redox potentials of the sensitizers and photo-acid/base generators using ferrocene (Fc/Fc+) as an internal reference potential. UV-vis was used to evaluate the optical band gap of the sensitizers using the onset wavelength of absorbance. Redox potentials and band gaps are reported in Table 2. The corresponding molecular orbitals of PAG and sensitizers are plotted in Figure 5.4.

Table 2 Thermodynamic and Photophysical Properties of photosensitizers for photo-induced/ Ground State Electron Transfer with FABA-PAG.

	Rehm-Weller Equation				Stern-Volmer (S_1 to S_0)			Stern-Volmer (S_2 to S_0)		
Sensitizer	E_{oo} (nm)	E_{ox} (V) vs Fc/Fc+	ΔG_{PET} (kcal/mol)	ΔG_{GET} (kcal/mol)	K_{SV} (M^{-1})	τ (ns)	$k_q \times 10^9$ ($M^{-1}s^{-1}$)	K_{SV} (M^{-1})	τ (ns)	$k_q \times 10^9$ ($M^{-1}s^{-1}$)
Anthracene	385	0.82	-24.59	49.72	16.27	2.92	5.58	---	---	---
CPTX	417	1.12	-12.17	56.44	---	---	---	---	---	---
DMBA	531	0.49	-11.80	42.08	5.48	5.35	1.03	---	---	---
BPET	574	0.54	-6.72	43.13	5.58	7.59	0.74	5.99	1.16	5.13
BPEP	690	0.31	-3.71	37.75	1.17	3.92	0.3	9.28	3.11	3
BTMP	700	0.31	-2.94	37.94	0.58	2.71	0.21	4.24	2.39	1.77

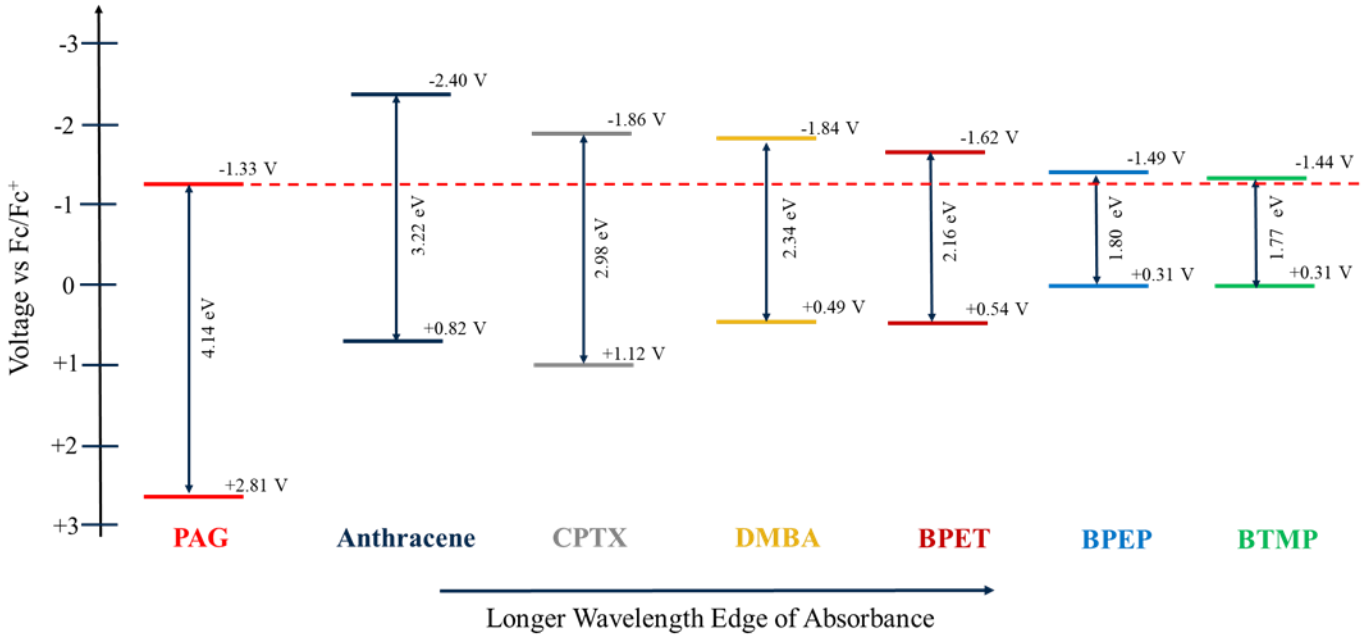

Figure 5.4 Energy levels of the FABA-PAG and all photosensitizer based on their redox potentials and band-gaps

Photoinduced electron-transfer of the acenes in this study with the iodonium PAG are thermodynamically favorable, as shown in Table 2. The low reduction potential of iodonium PAG is a contributing factor. The reduction potential of iodonium PAG in this case was -1.33 V vs Fc/Fc^{+}. However, electron-transfer becomes less favorable as the modified acenes become more red-shifted. The change in Gibbs free energy value for PET is an order of magnitude lower for BTMP (ΔG = -2.36 eV), which has an absorption onset at 700 nm, compared to anthracene (ΔG = -26.57 eV) which has an absorption onset at 385 nm. Ground-state electron transfer from all sensitizers to the PAG are thermodynamically unfavorable.

PET reactions are governed by collisional quenching where the fluorescence lifetime decay of the fluorophore (sensitizer) decreases with increasing concentration of the quencher (PAG). Thus, the effectiveness of the modified PAHs for PET reactions with iodonium salts were investigated by this method. Quenching rate constants (a measure of PET efficiency) for reducing the fluorescence lifetime of the sensitizers can be obtained from the Stern-Volmer relationship [98]:

$$\frac{\tau_o}{\tau} = 1 + K_{sv}[PAG]\,,\ K_{sv} = k_q\tau_o \qquad (9)$$

In Eq. 7, τ_o and τ are the fluorescence lifetimes in the absence and the presence of the quencher PAG-FABA, respectively; K_{SV} is the Stern-Volmer quenching constant; [PAG] is the concentration of the onium salt; and k_q is the bimolecular quenching rate constant. Rate constants and fluorescence lifetimes are listed in Table . The Stern-Volmer plots of each photosensitizer with various concentrations of FABA-PAG are shown in

Figure 5.5. The fluorescence lifetime decay of PET with quencher is also shown in Figure 5.6.

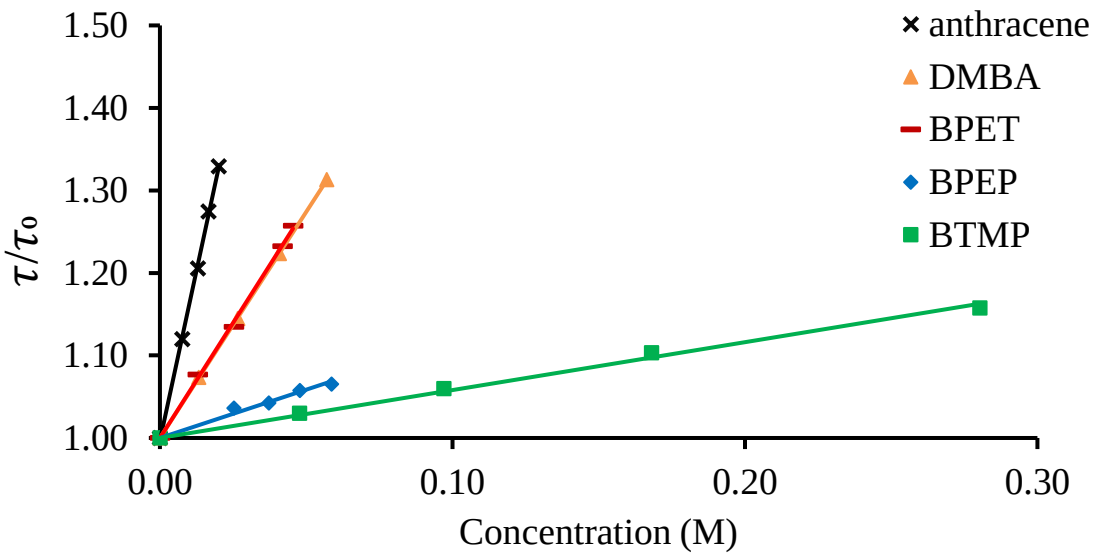

Figure 5.5 Stern-Volmer plots of all photosensitizers in DMF of their first excited singlet state with FABA-PAG as the quencher

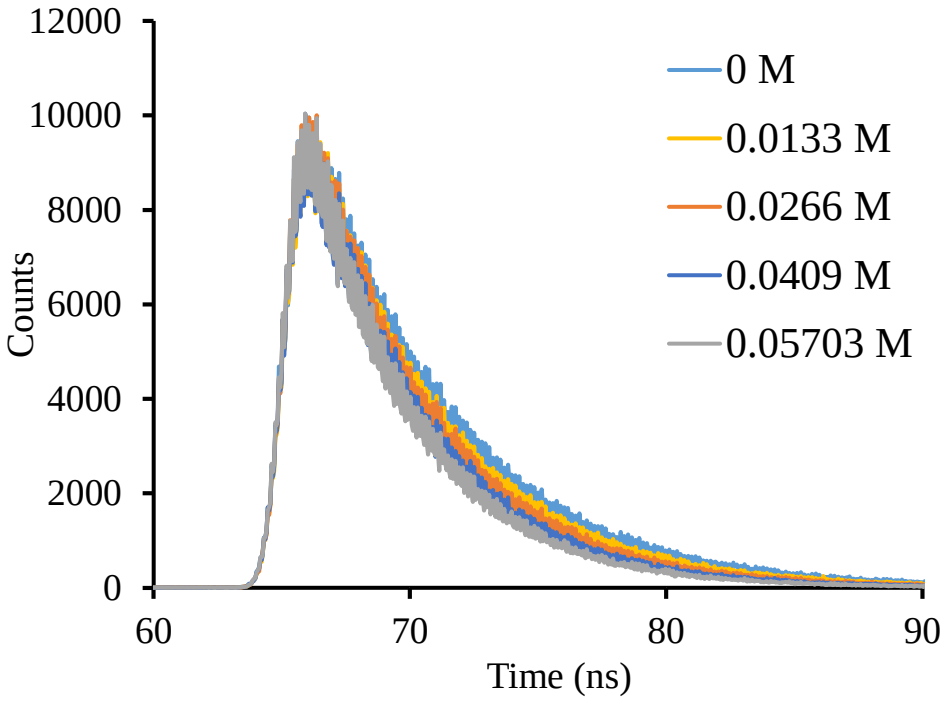

Figure 5.6 The effect of various concentrations of FABA-PAG on the fluorescence lifetime decay of DMBA. Fitted to a mono-exponential decay with $2.61 < \chi 2 < 2.86$

The theoretical diffusion-controlled rate constant (k_d) in DMF is approximately $7.06 \cdot 10^9$ $M^{-1}s^{-1}$, as estimated from a derivation from the Stokes-Einstein equation [99]. In PET systems where the electron transfer is sufficiently exergonic, $k_d \approx k_q$ [70]. Anthracene and DMBA are practically diffusion controlled, however, the k_q values of tetracene and pentacene derivatives (BPET, BPEP, and BTMP) are an order of magnitude lower. As expected, the decrease in k_q values can be rationalized by following the thermodynamic considerations (ΔG_{PET}) as listed in Table .

The Rehm-Weller equation only considers the thermodynamic favorability of the first excited singlet state for electron-transfer. It is possible that upper excited state energy levels (S_2) of the sensitizers could contribute to more exergonic electron transfer reactions.

The photosensitizers have high molar absorptivity peaks in the near-UV region which can activate upper excited state levels. In many cases, the internal conversion from S_2 to S_1 is rapid, e.g. picoseconds [98]. However, it was found that the pentacene derivatives had long-lived second excited singlet states. The fluorescence spectrum of BTMP under excitation at 334 nm shows strong S_2 to S_0 fluorescence λ_{max} values at 477 nm and 503 nm, as well as the S_1 to S_0 fluorescence λ_{max} at 690 nm and 750 nm, shown in Figure 5.7. The response between 642 and 677 nm was removed due to emission peaks from second-order diffraction of the excitation wavelength that is unrelated to BTMP [98].

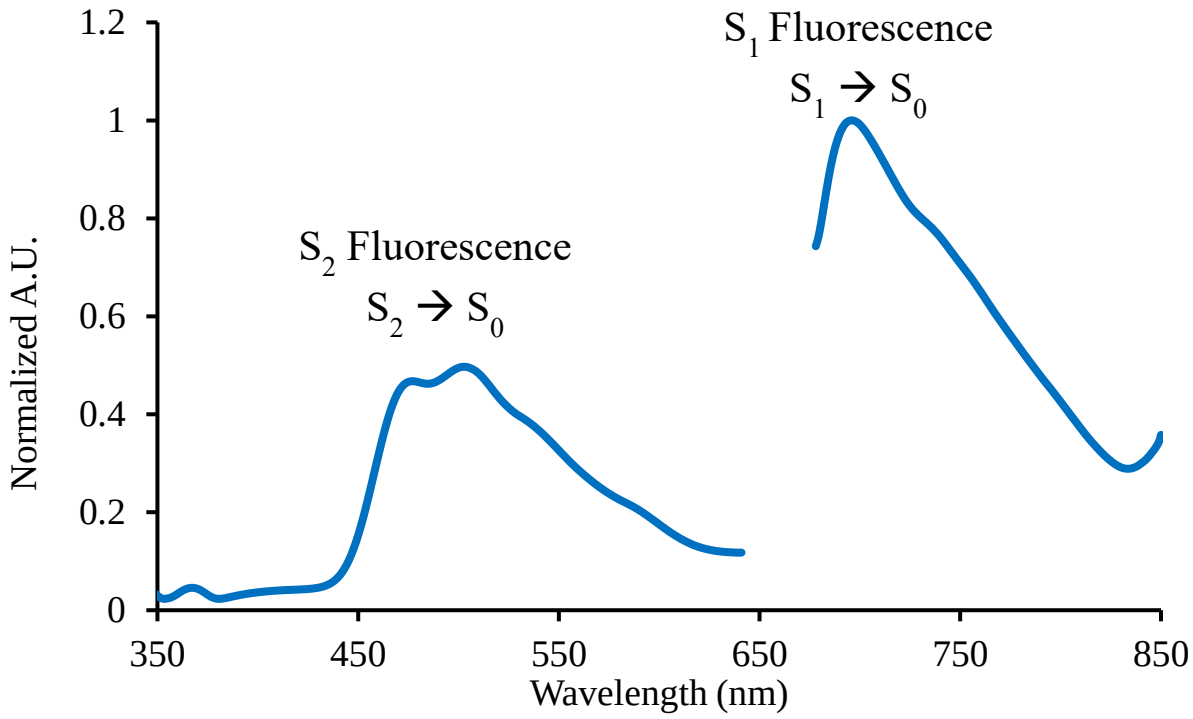

Figure 5.7 The fluorescence spectrum of BTMP at 334 nm excitation in DMF solution. The emission between 642 and 677 nm was removed due to peaks from second-order diffraction of the excitation wavelength.

The BTMP sensitizer at the S_2 fluorescence region recorded nanosecond scale lifetimes as well as an order of magnitude increase in the bimolecular quenching rate as shown in Table and Figure 5.8. BPET and BTMP showed similar increases in their biomolecular quenching rate of their S_2 fluorescence. The S_2 quenching rate of DMBA was not recorded due to the rapid internal conversion of S_2 to S_1 giving fluorescence lifetimes less than 0.0013 nanoseconds.

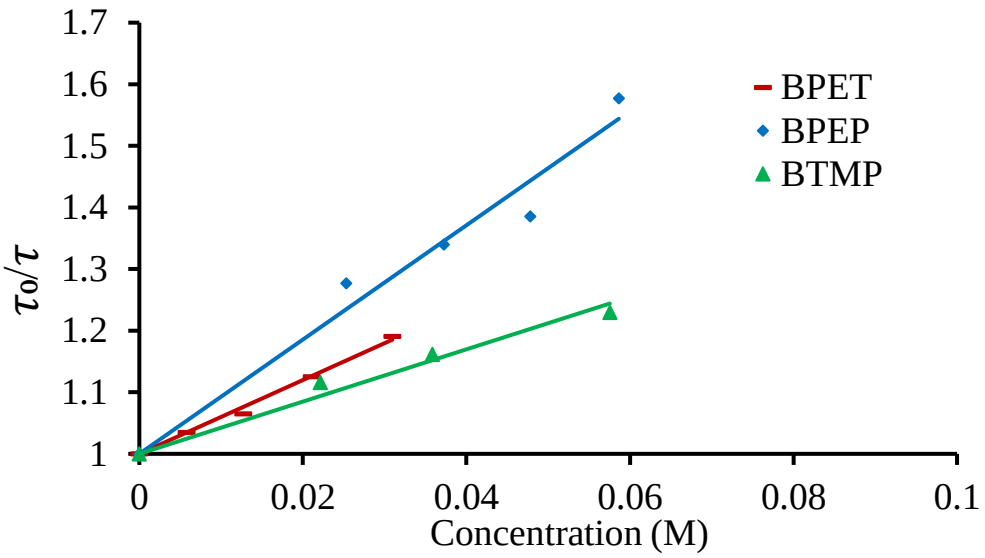

Figure 5.8 Stern-Volmer plots of all BPET, BPEP, and BTMP in DMF of their second excited singlet state with FABA-PAG as the quencher

5.4 Photo-sensitivity of Sensitized Polymer Films

The performance of the sensitizers were evaluated in solvent cast films consisting of PPC with 3 pphr PAG and exposed to sunlight under a variable neutral density mask and bandpass filter for wavelength selection. Sensitizers were exposed at select wavelengths that correspond to regions near the long wavelength end of the absorption

spectrum for each. Films with DMBA were exposed at 500 nm, BPET films were exposed at 560 nm, and BTMP films were exposed at 650 nm wavelength. Anthracene and CPTX were evaluated at 365 nm under a UV exposure tool. The normalized thickness after development versus log exposure dose (ie. contrast curve) was generated, Figure 5.9[79].

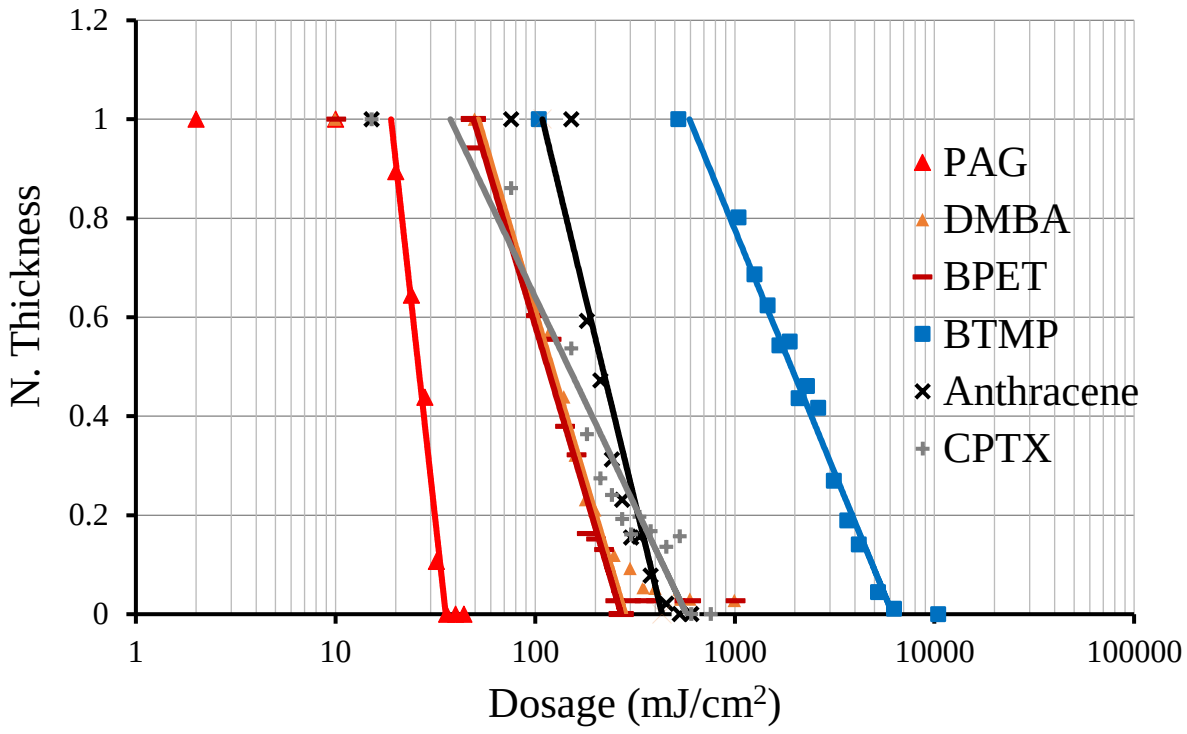

Figure 5.9 Contrast curves of PPC films with 3 pphr PAG with the following sensitizers: DMBA, BPET, BTMP at 1.2 PS to 1 PAG molar ratio.

The normalized thickness of the film was plotted where each point corresponds to the transmission of light from 1% to 100% through the variable neutral density mask. The full intensity of light (100% transmission) through the bandpass filters at 500 nm, 560 nm, and 650 nm were recorded: 1.38 mW/cm^2, 1.40 mW/cm^2, and 1.45 mW/cm^2, respectively. The linear region was extrapolated to zero on the x-axis where the dosage value was taken as the minimum dose required for exposure (D_{100}). Films of DMBA and BPET had a

similar D_{100} of 284 and 270 mJ/cm^2, however, BTMP had a minimum dose of 6,180 mJ/cm^2. Thus, the most red-shifted BTMP peak was 22 times less sensitive than films sensitized with DMBA or BPET. The photosensitivity of all sensitized PPC films are shown in

Table 3 The photosensitivity and efficiency of polypropylene carbonate films loaded with 3 pphr PAG and sensitizers (1.2 PS to PAG molar ratio) exposed at select wavelengths

Sensitizer	Wavelength of Exposure (nm)	Minimum Dose mJ/cm^2	Ecc
PAG only	248	36	0.42
Anthracene	365	433	0.13
CPTX	365	573	0.056
DMBA	500	284	0.021
BPET	560	270	0.023
BTMP	650	6180	0.004

A method to normalize the sensitivity in terms of the absorbed light vs the incident light stated above, was used to compare the efficiency of the PET reactions within films. The contrast-curve efficiency (Ecc) of the PET reactions in the PPC films was calculated from the ratio of the amount of photo-active compounds (PAG or PS) to the number of absorbed photons from the $D_{100.}$ Quantum efficiencies approaching unity are desired. As shown in Table , direct photolysis of the iodonium PAG at 248 nm gave a quantum efficiency of 0.42. The result is in agreement with previous measurements of iodonium salts, between 0.42 to 0.54 [100]. Efficiency dropped as the wavelength of the sensitizer was extended to higher values. The BTMP sensitizer had the lowest efficiency of 0.004. This is due to the less favorable thermodynamics of the electron-transfer from BTMP to PAG compared to the other sensitizers, as discussed above.

The Ecc values show excellent agreement with the Stern-Volmer quenching rates (Ksv) as shown in Figure 5.10.

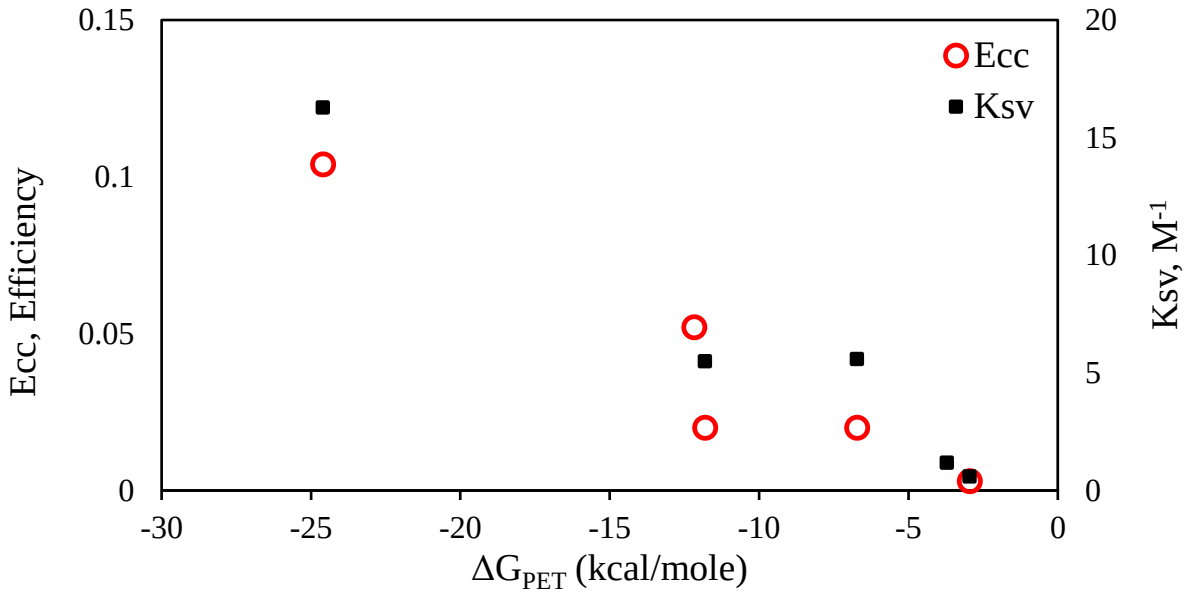

Figure 5.10 Contrast-curve Efficiency (Ecc) values plotted against ΔG_{PET} of sensitizers from left-to-right: anthracene, CPTX, DMBA, BPET, and BTMP. Stern-Volmer quenching rates (Ksv) plotted against ΔGPET from left-to-right: anthracene, DMBA, BPET, BPEP, and BTMP.

The Ecc and Ksv values increase with more negative value of the Gibbs energy. It is noted that the Ecc and Ksv values for DMBA and BPET are nearly equal even though the electron transfer of iodonium salts with DMBA is 5.08 kcal/mole more exergonic than with BPET. Stern-Volmer analysis shows that that BPET has a longer excited-state lifetime which allows it greater opportunity to interact with and undergo electron-transfer with the iodonium salt. The bimolecular quenching rate (k_q) of BPET is 1.39 times lower than DMBA which also follows the relationship between the PET reaction rate efficiency and the thermodynamic favorability in Table .

The effect of path length within the anthracene or DMBA in PPHA films was investigated, as shown in Light transmission vs film thickness was plotted for DMBA and anthracene at various loadings within PPHA films. The optical path length of anthracene and DMBA loaded PPHA films was investigated near the λ_{max} absorption value in Figure 5.11

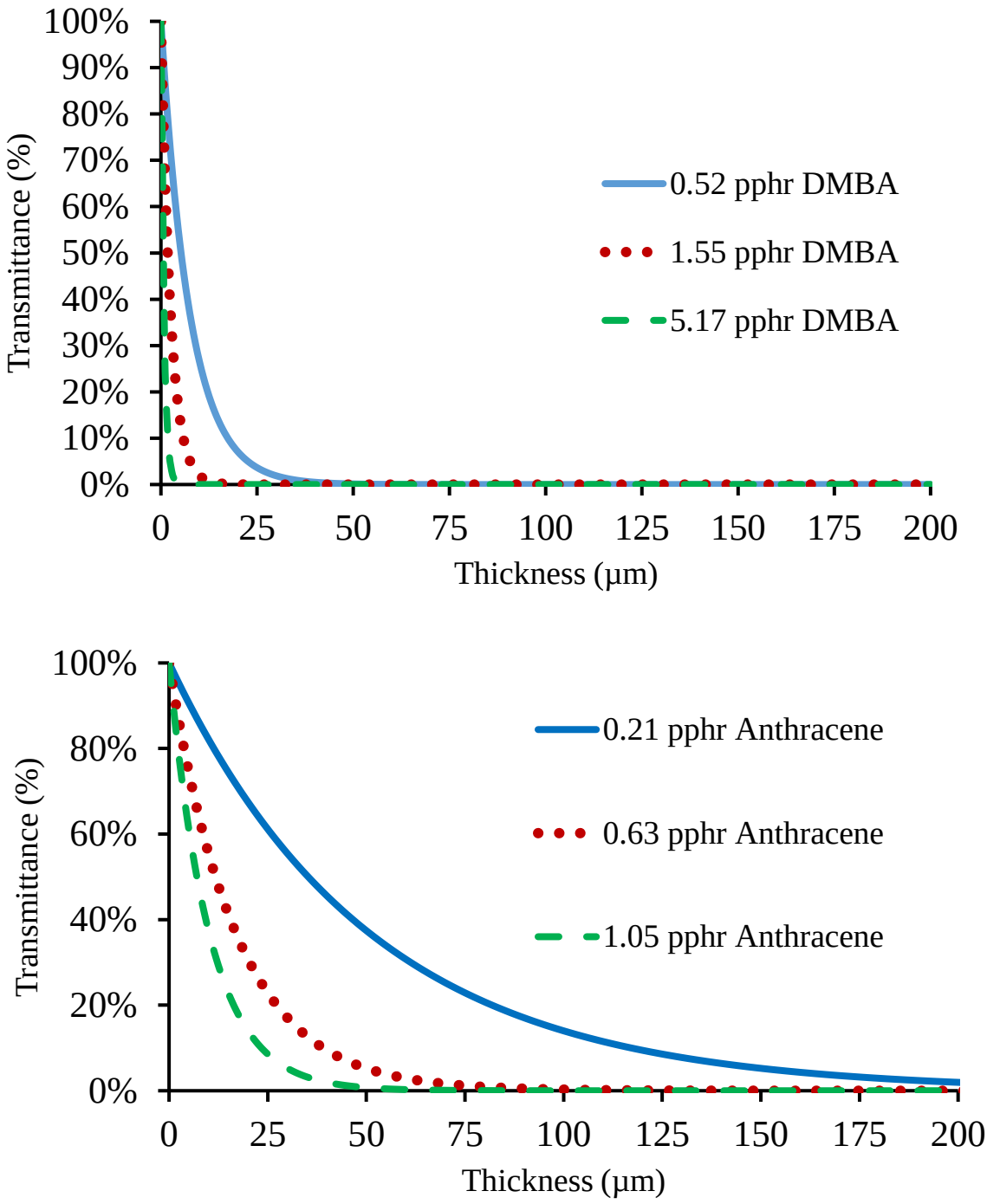

Figure 5.11 Transmittance as a function of thickness for various loadings of DMBA in PPHA films at 480 nm (top) and various loadings of anthracene in PPHA films at 363 nm (bottom)

In Figure 5.11, the optical path length decreased with higher loadings of DMBA within the PPHA film. The 0.52 pphr DMBA film had <1% transmittance at thickness of 35 μm. PHA films loaded with 5.71 pphr DMBA had less than 1% transmittance of 4 μm. The optical path length at 0.21 pphr Anthracene (molar equivalent to 0.51 pphr DMBA) was <1% transmittance at thicknesses above 214 μm. Sensitizers with high molar absorptivity are advantageous for faster photolysis, however, this is at the expense of optical path length.

Photo-bleaching can mitigate problems with highly absorbent sensitizers, especially in thick films. Sensitizer photo-bleaching has been investigated by using ultraviolet light spectroscopy (UV-vis), Figure 5.12.

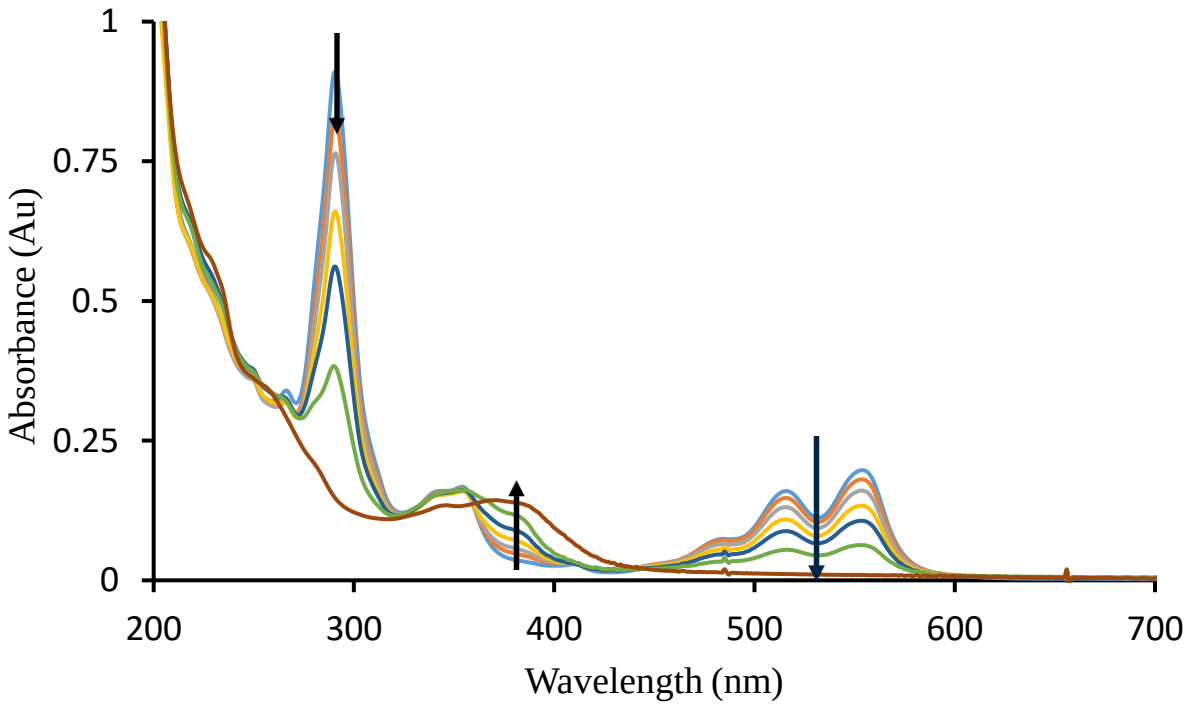

Figure 5.12 UV-vis absorbance of PPC film with 3pphr PAG and BPET exposed to 560 nm light at various time increments.

A film of PPC with 3 pphr PAG and BPET was exposed to 560 nm of light at an intensity of 1.03 mW/cm^2. Changes in BPET absorbance were monitored as a function of time. Figure 5.12 shows the maximum absorbance of BPET occurs at 517 and 556 nm. BPET absorbance at these wavelengths decreases as a function of sunlight exposure until the absorbance is nearly zero. This experiment was repeated with DMBA and the results are similar in Figure A11. These results shows that the electron-transfer process from PAH to PAG is irreversible and the sensitizer is chemically converted to a non-absorbing species, in agreement with Scheme I eq.3 and eq.4. The iodonium radical produced upon activation rapidly decays and prevents back electron-transfer to BPET. The absorption range of BPET's chromophoric is related to the pi-conjugation network. Formation of the highly reactive BPET radical cation can undergo a number of reactions such as photodimerization, which will disrupts its π-conjugation network and decreases the onset absorption wavelength[101].

Cationic and/or radical-based photopolymerization is the common use of sensitizers with onium salts. Formation of non-volatile residue after decomposition is not desirable for transient polymer applications. Transient polymers rely on monomer evaporation following depolymerization. However, the slow evaporation of phthalaldehyde following poly(phthalaldehyde) depolymerization gives ample opportunity for side-reactions with the sensitizer by-products because the phthalaldehyde monomer has a very low vapor pressure and may take an extended time to evaporate [102].

PPHA films with various PAG and DMBA loadings were formulated and cast onto glass substrates to evaluate amount of residue formed during photoexposure, Figure 5.13.

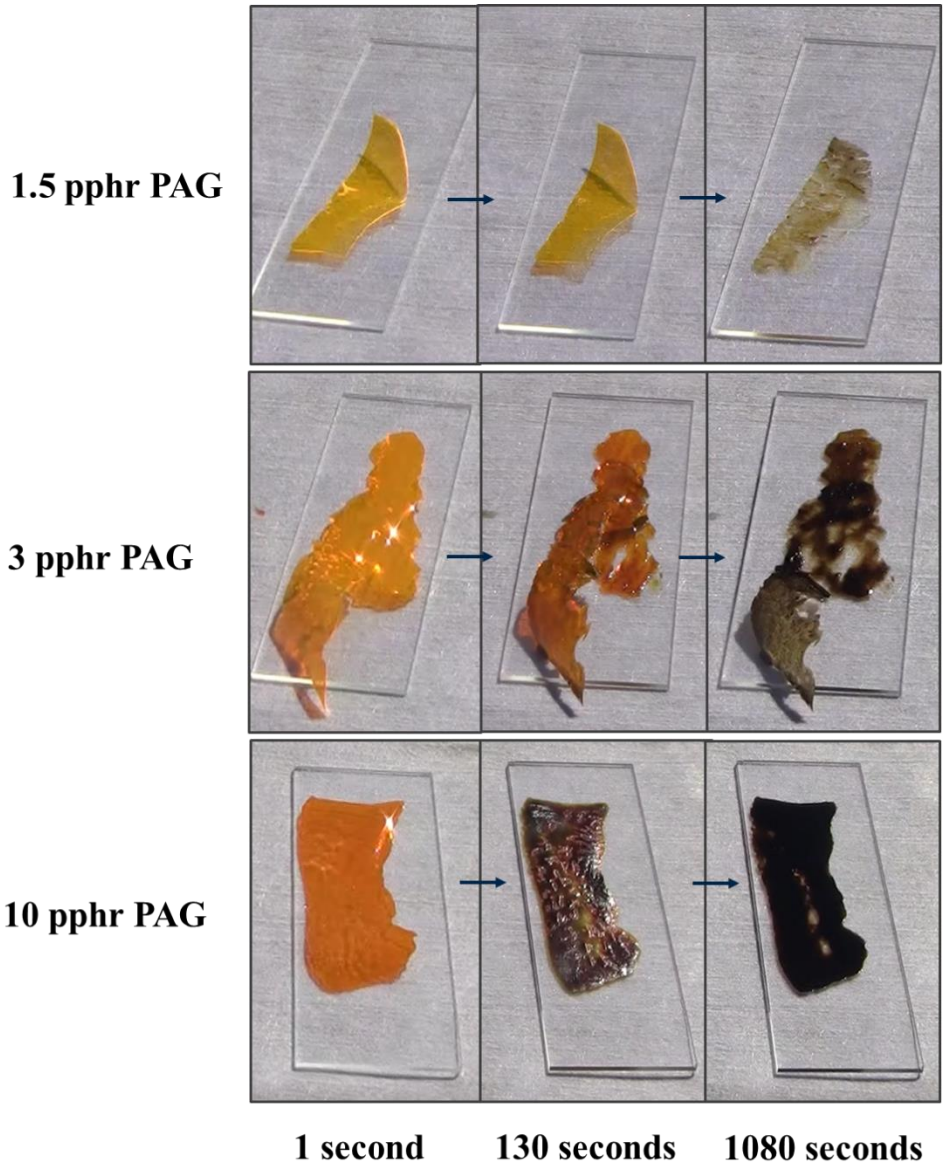

Figure 5.13 Sunlight-induced depolymerization of PPHA films with various loadings of FABA-PAG with DMBA over glass substrate over an 18 minute sunlight exposure at noon.

Films were exposed to mid-day sunlight, 1,034 W/m^2. PPHA can depolymerize by protonation of the PPHA ether linkage creating cationic hydroxyl groups that lead to an unzipping decomposition reaction producing phthalaldehyde [103]. The polymer transforms into liquid during depolymerization followed by evaporation or sublimation of the monomer [104]. The three PPHA films in Figure 5.13 contain 1.5, 3, or 10 pphr PAG with DMBA at a 1.2:1 mole ratio of PAG to DMBA. Photoresponse time for PPHA depolymerization was dependent on PAG loading. PPHA samples with 10, 3, and 1.5 pphr PAG with DMBA began to liquefy after 10 s, 60 s, and 150 s, respectively. Yellow phthalaldehyde is easily observed upon depolymerization. A dark discoloration and presence of solid residue was visible at higher PAG/DMBA loadings. The higher PAG/DMBA loading increased the likelihood for side-reactions with the phthalaldehyde forming black, nonvolatile residue.

Crivello previously proposed multiple decomposition pathways for the photosensitizer radical cation after the PET reaction, as shown in Figure 5.14[69]. Side reactions with phthalaldehyde may occur through similar chemical pathways when PPHA depolymerizes. The sensitizer radical cation can react with the iodonium neutral radical products forming dimers, or they may directly react with phthalaldehyde during or after depolymerization. The formation of the black-colored residue may indicate that the DMBA conjugation has been extended.

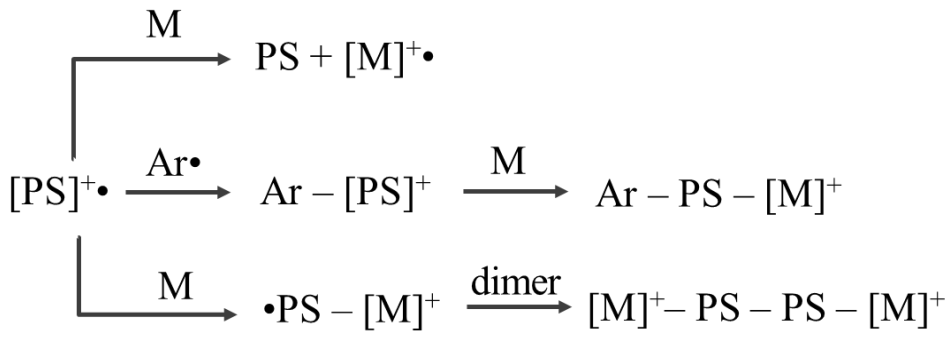

Figure 5.14 Competing Side Reactions of Sensitizer Cation Radical

It is known that the anthracene radical cation can undergo phenylation with the aryl radical from the iodonium to produce 9-phenylanthracene and a proton [100]. The 9-phenylanthracene can absorb another photon and act as an electron donor with another iodonium salt. It was proposed that poly(acenes) can be generated in this manner[100]. The modified PAHs used in this study may also react with aryl radicals or phthalaldehyde in a similar way. The modified PAH appears to induce a larger amount of solid residue at a faster rate than the unmodified parent compound during the PET reaction. Appending phenylethynyl groups onto the acene core likely provides more resonance stability of the radical cation of the sensitizer. The long-lived radical cation may diffuse and form stable products by reaction with phthalaldehyde or other aryl compounds creating an extended conjugated network.

The nonvolatile, black residue from the PHA film with 10 pphr PAG and DMBA was analyzed by ^{1}H-NMR to investigate the chemical structure, as shown in Figure A12. The residue was baked at 175 ºC on a hotplate for 4 hours to evaporate phthalaldehyde while remaining below the melting point of DMBA. The residue had broad peaks from 6-8 ppm indicative of possible aromatic derivatives. Furthermore, the mass of the post-

exposure residue was greater than the original mass of PAG and DMBA in the film. This suggests that phthalaldehyde participates in reactions with the DMBA cation-radical.

The residue after photo-depolymerization of a PHA film loaded with 10 pphr PAG with DMBA was analyzed by ESI to determine the participation of PAG in the side reactions after PET. The results show that the iodonium cation was no longer present (i.e. absence of 337 m/z peak), however the borate anion was present (i.e. 679.1 m/z) suggesting that it does not play a significant role in the side reactions. MALDI-TOF-MS was used to determine the molecular mass of the poly(aromatic) products to evaluate the extent of the conjugated framework, Figure 5.15.

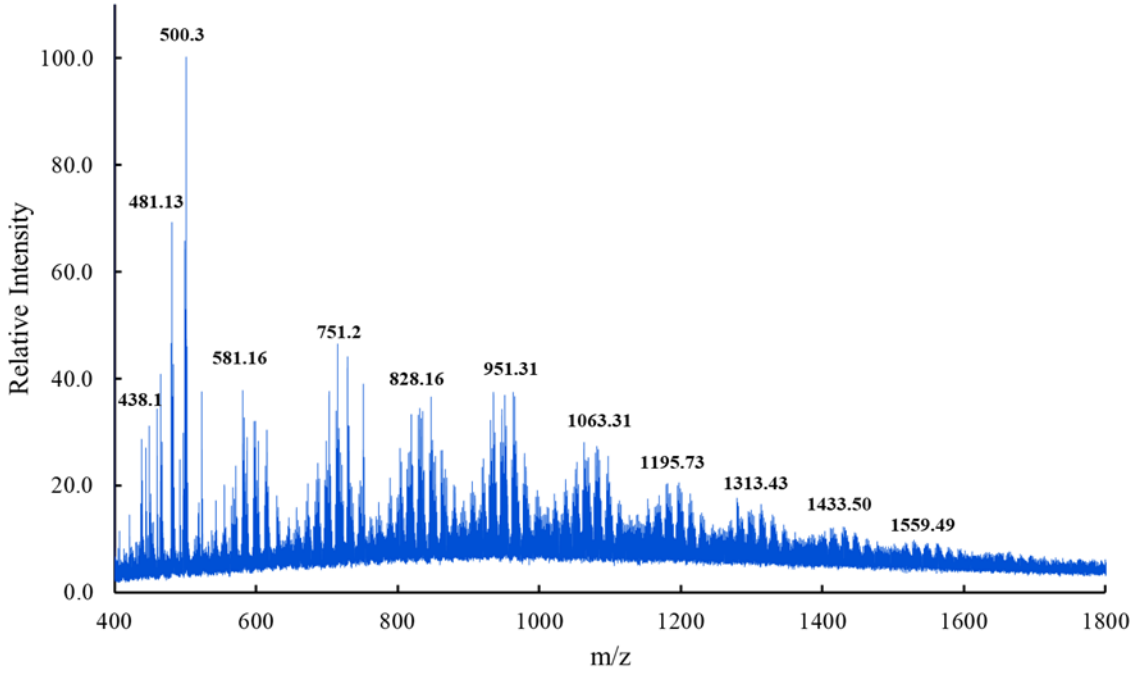

Figure 5.15 MALDI-TOF-MS analysis of residue after full sunlight-induced depolymerization of PPHA film with 10 pphr PAG and DMBA.

The MS spectrum shows a number of aromatic derivatives as a result of the side reactions with the DMBA radical cation. A series of main peaks (denoted in the spectrum) with their corresponding fragmentations were observed. The product formed in the side reaction extends to nearly 1.5 kDa, which is 3.6 times the molar mass of DMBA. The separation between these peaks corresponds to about the molar mass of a phthalaldehyde monomer, ca. 134 Da. It is evident that lower loadings of the PAG and modified PAHs are necessary to mitigate the undesirable side reactions with phthalaldehyde that form nonvolatile, solid poly(aromatics). Faster evaporating copolymers of aldehydes, such as with butanal, could also potentially mitigate side-reactions.

The sunlight-induced 'transience' of the PHA films with optimal loading of photo-catalysts with photosensitizers was exposed mid-day sunlight, as shown in Figure 5.16. Formulations of 1 pphr PAG with anthracene, CPTX, DMBA, BPET, and BTMP (1.2:1 PS to PAG ratio) were solution-cast into film. BTMP loaded films remarkably began to depolymerize in less than 1 minute and underwent complete depolymerization in 5.5 minutes. The PET efficiency (Ecc) of BTMP with iodonium salts are 1 to 2 order of magnitude lower than the other sensitizers according to Table . However, it is likely the higher near-UV absorbance excites BTMP to an upper excited state where electron-transfer is more efficient. This is shown in Table and Figure 5.8 where the bimolecular quenching rate increased by an order of magnitude when evaluated at the second singlet excited state. All of the sensitized PHA films eventually lose their mechanical integrity by during depolymerization.

Figure 5.16 Time-lapse photos of PPHA films with 1 pphr PAG and anthracene, CPTX, DMBA, BPET, BTMP exposed to natural sunlight at noon over a 20 minute period.

5.5 Conclusions and Recommendations

Polynuclear aromatic hydrocarbons with disubstituted phenylethynyl groups were found to be efficient sensitizers of onium salts to induce acid-catalyzed depolymerization of poly(phthalaldehyde) and poly(propylene carbonate) films. Thermodynamically favorable sensitizers for PET reaction, as evaluated by the Rehm-Weller equation, show a strong correlation with the fluorescence quenching rates in solution and contrast-curve efficiency within films. Pentacene derivatives showed long fluorescence lifetimes and high quenching rates in the upper excited singlet state levels. The soluble anthracene, tetracene, and pentacene derivatives were effective in the photodegradation of polymers with short sunlight exposure times. However, the residue formed from the reaction of the rampant, phenylation of the cation-radical of the sensitizer products after PET reaction is problematic for any sacrificial application. Control and mitigation of this side reaction will be beneficial for future projects. The addition of other molecules that could undergo redox reactions to quench the cation-radical may be possible. This study has provided a pathway of developing a class of photochemical triggers whose exposure wavelength can be tuned from the ultraviolet region into the entire visible light region for the purpose of initiating the depolymerization of polymers for a wide variety of transient applications.

CHAPTER 6. PHOTODEGRADABLE POLYALDEHYDES: LIQUID-STATE EXTENSION AND DELAY OF PHOTORESPONSE

6.1 Motivation

In Chapter 5, expanding the absorption wavelength for the photo-acid generator affords a controlled trigger for various transient device applications. However, the 'transient' properties of the poly(phthalaldehyde) which include photoresponse time, depolymerization rate, and vaporization rate of monomer products pose many challenges. The control of the photo-activation time for the depolymerization of PPHA is desired as to not cause accidental exposures. It is also desirable to use the transient device in the presence of the phototrigger until a precise, onset of degradation time. Delaying the depolymerization of PPHA has many potential benefits for transient applications. Furthermore, the sublimation rate of phthalaldehyde is slow. Copolymers of polyaldehydes with more volatile monomers, such as with butanal, have been demonstrated to increase the vaporization time by a factor of 12 for 1 μm films[102]. However, the vaporization time will likely decrease substantially as the overall surface area is reduced with thicker films for more structural applications. An alternative 'transience' mode for these polyaldehydes are needed to avoid detection and reverse-engineering. The liquification of the polyaldehdyes into the environment is pursued as an alternative transience mode of these polymers once photo-triggered.

The acid-catalyzed depolymerisation of poly(phthalaldehyde) is known to undergo a phase transition into a liquid prior to the sublimation of the monomer due to the exothermic nature of the reaction. The liquid-state can potentially absorb into the surrounding environment. However, the liquid-state during depolymerization of PPHA only exists for a few seconds and is not enough time for absorption into the soil. The liquid-state is directly related to the freezing point of the monomer which is highly dependent on ambient temperature. Therefore, additives can be imparted into the solution deposited films to extend the liquid-state time at ambient conditions by depression of the freezing point to subzero temperatures.

6.2 Supercooling of Phthalaldehyde

Three methods can be assessed to inhibit crystallization of phthalaldehyde after depolymerization of PPHA: i) super cooling of the phthalaldehyde, ii) liquid additives such as plasticizers 3) liquid aldehyde co-monomers.

Supercooling is examined by DSC analysis to determine if phthalaldehyde has a temperature range where the monomer is unable to solidify below its melting point. Phthalaldehyde was loaded directly into an aluminium pan and ran at a ramp rate of 5° C/min.

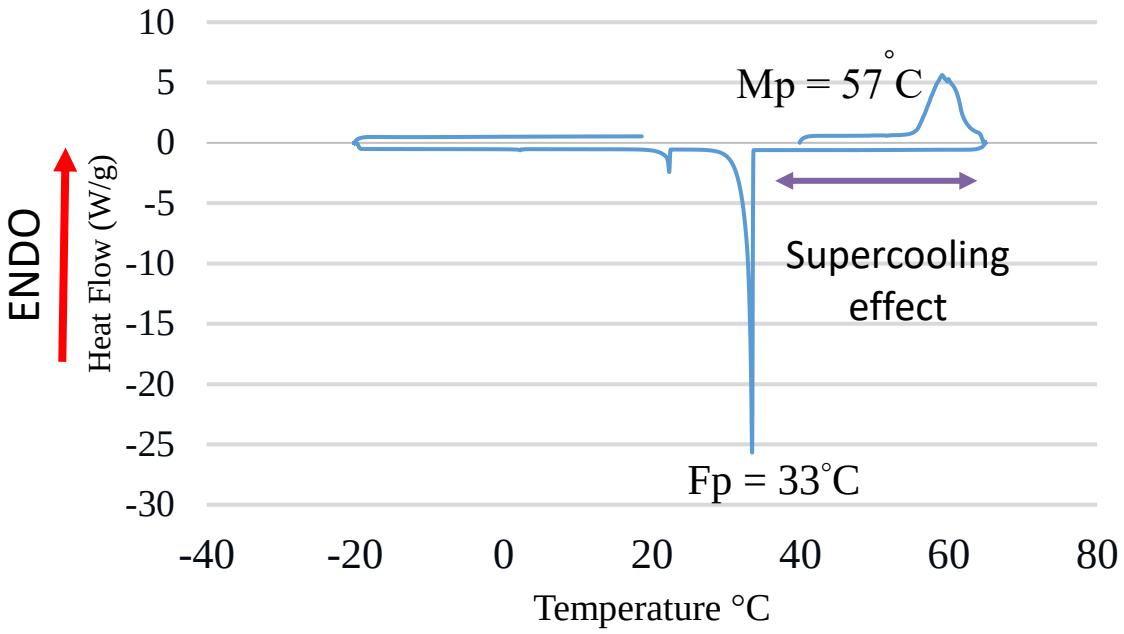

Figure 6.1 DSC trace of phthalaldehyde

The melting point of phthalaldehyde is seen at 57°C while the freezing point exhibits a super-cooling effect to 33°C. The acid-catalyzed depolymerization reaction is thought to be exothermic thereby melting the monomer while it is maintained in a metastable liquid-state at lower temperatures. The supercooling effect of phthalaldehyde is a desirable phenomenon, however, the absorption of the monomer into soil post-depolymerization can only occur in relatively hot environments. Other methods are necessary to expand this temperature range to sub-zero temperatures.

6.3 Non-Ionic and Ionic Plasticizers

Depression of the freezing point of phthalaldehyde can be attempted by a careful selection of plasticizers. Plasticizers are defined as a substance such as an elastomer that can be incorporated into other materials to increase its flexibility and workability. Plasticizers are an excellent choice as freezing point depressants because they are typically

liquids with low vapor pressures and low freezing points. Careful choice of plasticizers with the prior characteristics can potentially disrupt the intermolecular interactions of phthalaldehyde thereby preventing crystallization at lower temperatures. Miscibility of the plasticizers with the polyaldehyde films under solution deposition is necessary for utilization as freeze depression agents. Many classes of plasticizers were evaluated for their miscibility with poly(phthalaldehyde). The plasticization ability of these compounds will likely correlate the ability to extend the liquid state of the monomer after depolymerization. Classes of plasticizers can include adipates, azelates, citrates, ether-ester, glutarates, isobutyrates, phosphates, and sebecates which have melting points ranging from -70°C to -90°C. Most classes of the plasticizers revealed incompatibility in films of PPHA giving opaque films due to the change in refractive index from phase aggregation at loadings of 15 wt% or less. As expected, the ether-ester class of plasticizers exhibited the greatest miscibility with PPHA films. Phase separation with PEO and BEHP was not seen until 20 wt% and 35 wt%, respectively.

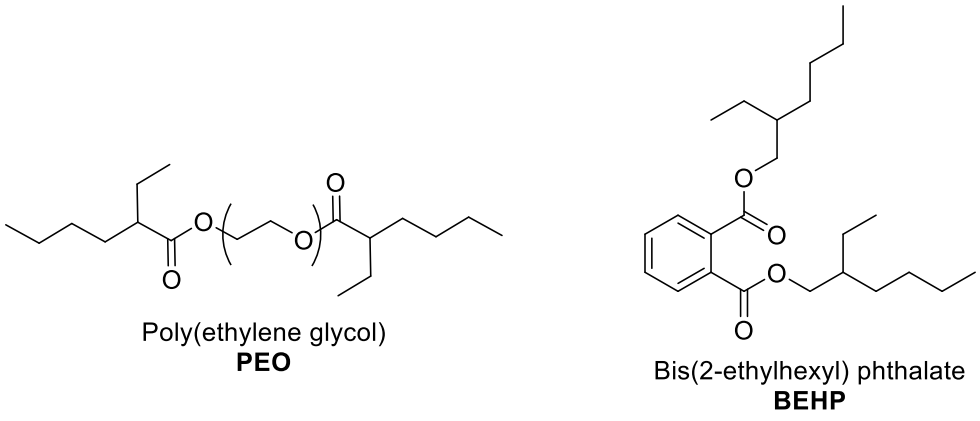

Figure 6.2 Non-ionic plasticizers in the ether-ester class: PEO and BEHP

Alternative plasticizers, such as ionic liquids, have been investigated for phase miscibility with PPHA. Ionic liquids are salts that melt at temperatures of 100°C or lower which are benign to the environment and have negligible vapor pressures at 20°C. The ionic liquids of interest here are liquids at ambient or sub-zero temperatures because they can depress the freezing point of phthalaldehyde. Ionic liquids have previously been employed in films of poly(vinyl chloride) and poly(methacrylates) and has shown to be moderate plasticizers for mechanical properties as well as an excellent glass transition depressing agent[105–108]. Ionic liquids used in this chapter can have ammonium, pyrrolidinium, sulfonium, or imidazolium cations with weak nucleophiles as shown in Figure 6.3.

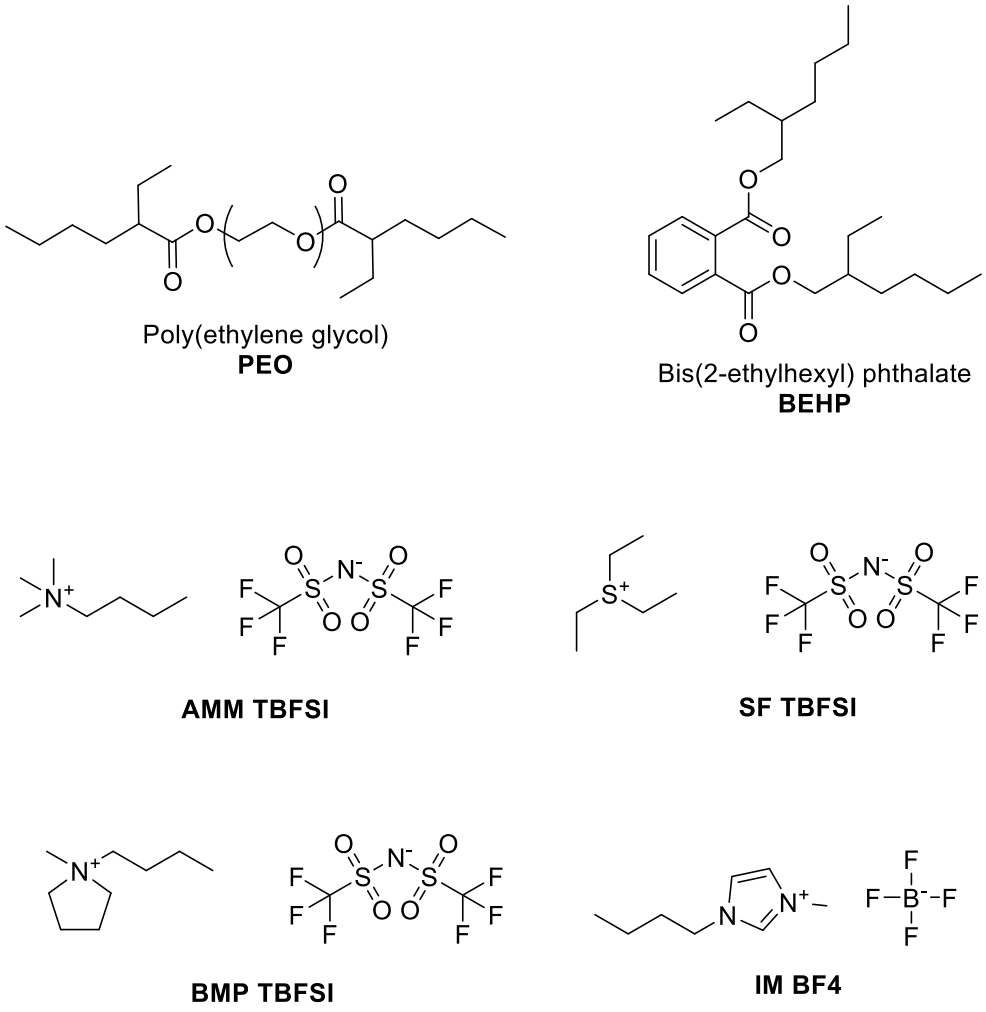

Figure 6.3 Ionic Liquids

The low-leaching rates documented in the previous study are beneficial as the additive can potentially be loaded to relatively high levels without phase separation. The BMP-TBFSI ionic liquid had no observable phase separation as high as 100 pphr loadings. No significant leaching of the ionic liquid from the polymer film was observed after several weeks at room-temperature. The ionic liquids were evaluated in films of PPHA with 1 pphr Anthracene to evaluate the path length. It was shown that in Chapter 5, the addition of

highly absorbing sensitizers decreased the path length of films. In Figure 6.4, it is shown that the increasing addition of plasticizers reduces the relative, volume space of the sensitizer thereby giving films longer path lengths. The ionic and non-ionic plasticizers will have this increasing effect on the path length because they absorb at wavelengths less than 300 nm.

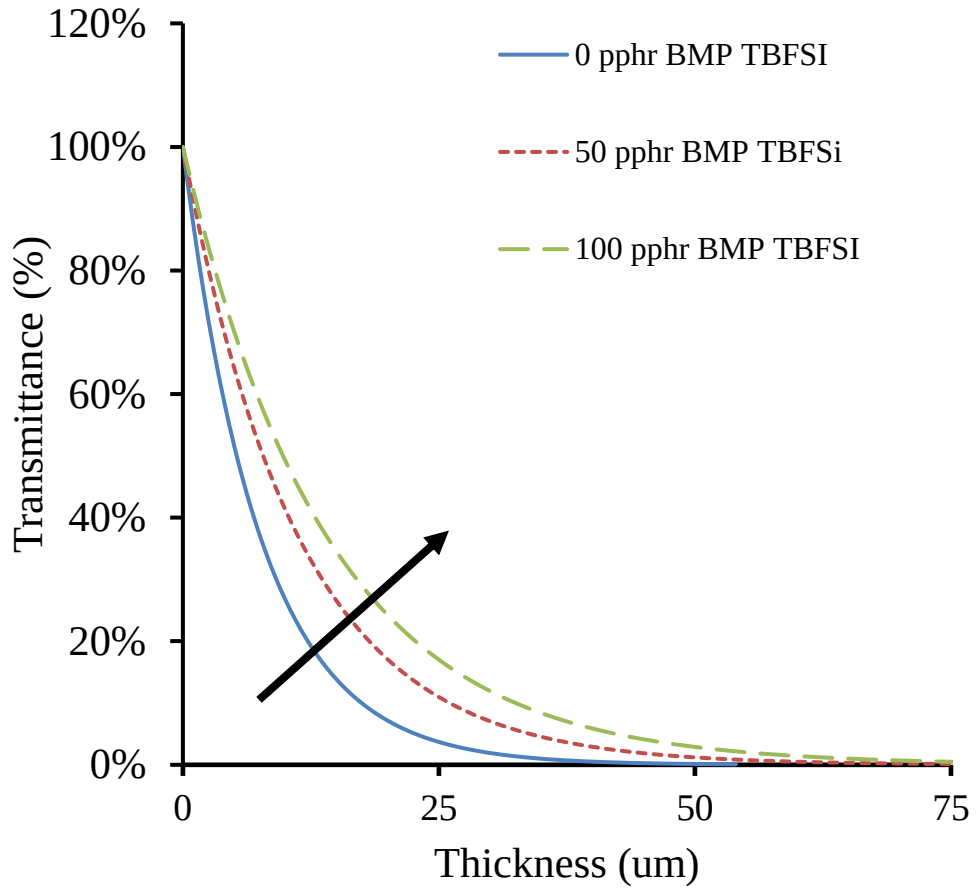

Figure 6.4 Path Length of PPHA and 1 pphr Anthracene with various loadings of BMP TBFSI

6.4 Thermal Stability

The thermal stability of PPHA with 20 pphr loading of the ionic and non-ionic plasticizers were investigated by thermogravimetric analysis (TGA). PPHA and additives

were mixed in solution of THF and casted onto nylon sheets. The films were allowed to dry for 3 days and removed for TGA analysis as shown in Figure 6.5 and Table .

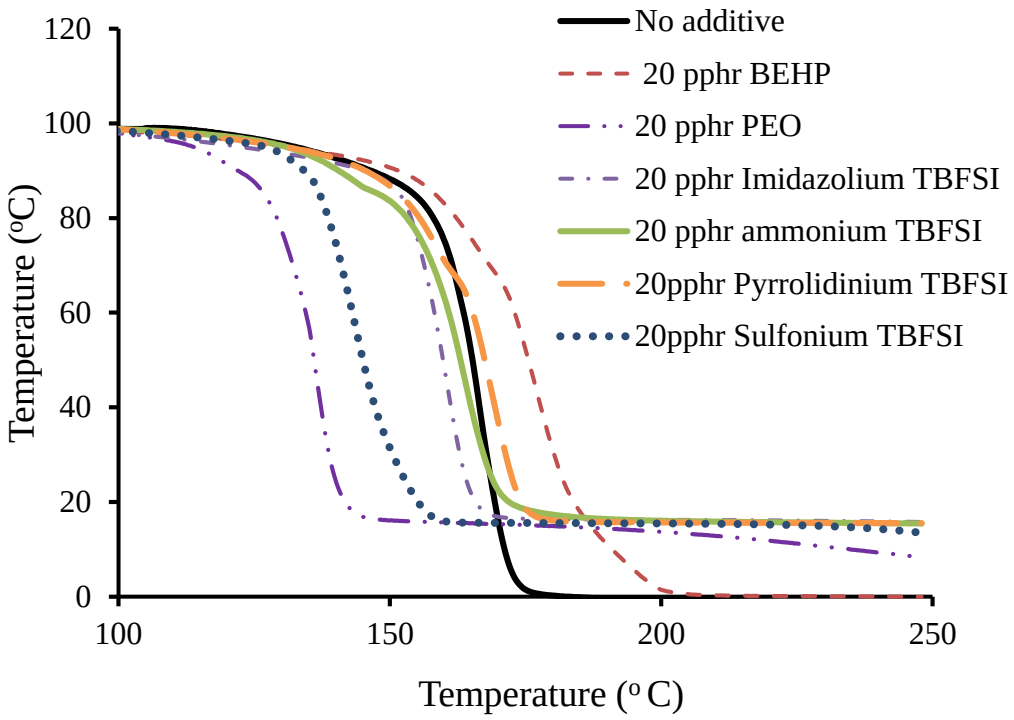

Figure 6.5 TGA plot of PPHA with 20 pphr of loadings of various non-ionic and ionic plasticizers

Table 4 TGA results for the onset and endset of depolymerization of PPHA with 20 pphr loadings of various ionic and non-ionic plasticizers

Sample	Onset °C	Endset °C	Difference
No additive	158	172	14
20 pphr BEHP	165	187	22
20 pphr PEO	126	140	14
20 pphr IM TBFSI	153	165	12
20 pphr AMM TBFSI	149	169	21
20pphr BMP TBFSI	153	174	21
20pphr SF TBFSI	136	152	16

PPHA with no additives had a thermal onset degradation temperature of 158°C which matches previous reports. Most of the ionic liquids had no significant effect on the thermal stability of the polymer. The difference of the onset and endset temperatures show the PPHA films loaded with pyrrolidinium, imidazolium, and ammonium ionic liquids have depolymerize at a slower rate. However, 20 pphr loading of the sulfonium TBFSI reduced the onset degredation temperature by 22°C. The two non-ionic plasticizers (PEO and BEHP) have drastically different effects on the thermal stability of PPHA. The 20 pphr loading of PEO reduced the onset of degradation by 32°C while 20 pphr loading of BEHP stabilized the onset of PPHA degradation by 7°C with a much slower depolymerization rate. PEO was found to be relatively acidic when dropped in aqueous solution (recorded a pH of 2) which is likely the cause of the reduced onset temperature.

6.5 Liquid State Extension and Delay of Photo-response

The kinetics of the ambient depolymerization photodegradable polymers is difficult to measure by differential scanning calorimetry or thermogravimetric analysis. Recently, a novel method of determining the solid-state depolymerization reaction kinetics and photoresponse of transient polymers with a quartz crystal microbalance (QCM) was demonstrated. The Butterworth-van Dyke equivalent circuit model for the electrical response provides information on depolymerization of transient films. The resistance at resonance can change with the elasticity or viscosity of the film that is in contact with the crystal surface. Resistance is normalized to the maximum observed raw value within each experiment and the time is zeroed at the moment of photoexposure. The 'photoresponse delay' was taken as the point of maximum resistance of the QCM. The data was fit to an exponential curve of the form. The resulting data was fit to an exponential curve of the form Rnorm = exp(b(t-c)), where Rnorm is the normalized resistance, t is time in seconds, and b and c are fitting parameters. Both parameters can provide quantitative values for the physical occurrence of depolymerization with b being the rate of depolymerization and c being the delay in the response to light irradiation as shown in Figure 6.6.

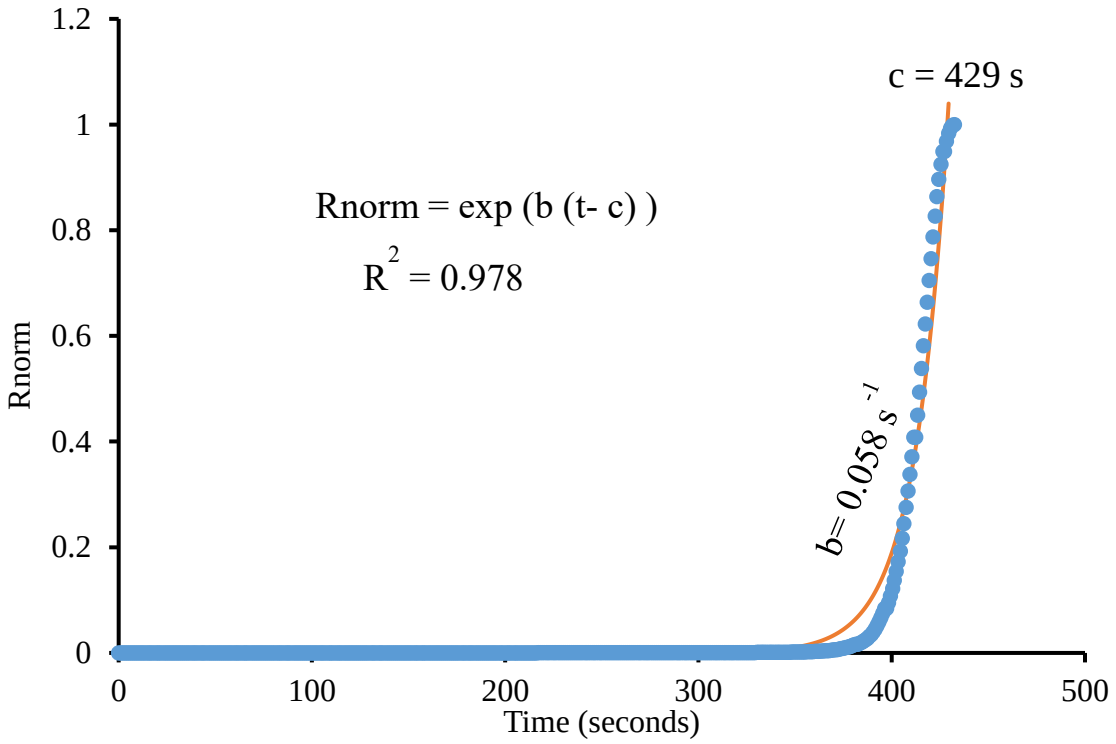

Figure 6.6 QCM plot and exponential fit of the depolymerization of PPHA with 5 pphr PAG and Anthracene after exposure to UV light

In this study, QCM was also used to quantify the liquid state time of the monomer prior to crystallization during the exothermic depolymerization of PPHA. Evaporation is occurring during the depolymerization which is withdrawing heat. Rapid crystallizations occurs as the monomer is cooled past its freezing point while the resistance returns to its original value. As the monomer is cooled below its freezing rapid crystallization into a solid occurs as the resistance returns to its original value. A linear line can be drawn from the intial sharp, increase of the resistance (ie. depolymerization) and the following decrease of the resistance (crystallization) where the Rnorm is zero. The difference of the time points at which the linear slope crosses x-axis can be defined as the liquid-state time as shown in Figure 6.7. Depression of the freezing point of phthalaldehyde below 33^{o}C will give longer liquid state times at ambient temperature as recorded from QCM. Hence, the effect of

plasticizers on the photoresponse delay, depolymerization rate, and liquid-state time of the monomer during the acid-catalyzed depolymerization of PPHA can be evaluated.

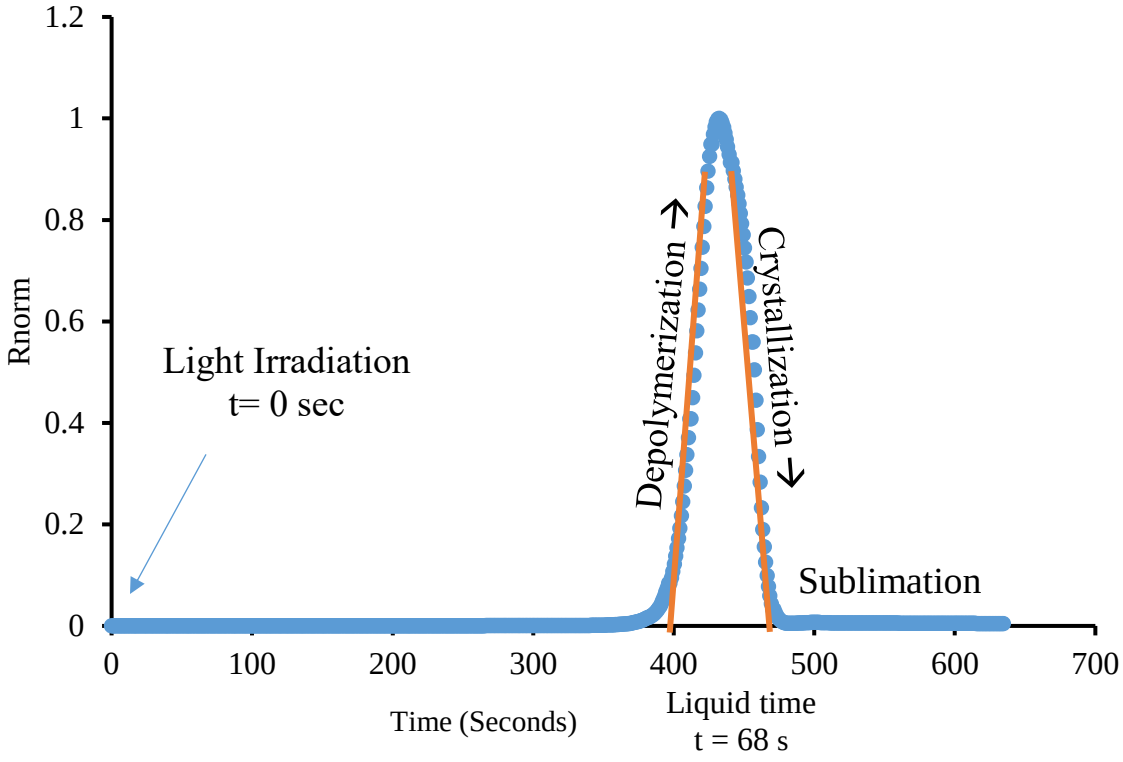

Figure 6.7 QCM plot of the depolymerization, crystallization, and sublimation of PPHA with 5 pphr PAG and Anthracene after exposure to UV light

Table 5 Delay, Rate Constant, and Liquid State Time of PPHA with various additives after UV exposure from QCM

Additive	pphr loading	Delay (s)	Rate Constant ($10^3 s^{-1}$)	Liquid-State Time (s)
None	0	14 ± 1	309 ± 17.9	9.99 ± 0.344
BEHP	10	20.5 ± 2.14	345 ± 70.2	193.3 ± 29.489
	20	19.9 ± 2.90	718 ± 132	4173 ± 1079
PEO	10	364.7 ± 39.3	67.7 ± 20.6	78.2 ± 4.910
	20	1436 ± 73.5	22.3 ± 0.593	300 ± 10
PEO + BMP TBFSI	20	895 ± 7.13	28.2 ± 0.703	>3600
BMP TBFSI	20	23.2 ± 0.122	251 ± 19.8	23.2 ± 0.122
AMM TBFSI	20	23.2 ± 5.33	202 ± 23.9	17.1 ± 0.966
	50	18.1 ± 2	210 ± 21.2	>3600
SF TBFSI	20	19.6 ± 0.470	205 ± 13.7	14.6 ± 0.402
NMP	0.16	34.4 ± 0.517	200 ± 27	---
	0.5	86.2 ± 7.87	139 ± 4.64	---
	1	397 ± 35.4	58.6 ± 5.04	76 ± 13.7
	5	8326 ± 1645	8.36 ± 2.49	228 ± 76.1
	10	11377 ± 3257	8.67 ± 1.29	287 ± 59
	20	15308 ± 1813	3.87 ± 0.282	>3600
	30	16176 ± 2578	7.42 ± 4.89	>3600

PPHA with no additives has a photoresponse delay, rate constant , and liquid state time of 14 ± 1 s, 0.31 ± 0.018s, and 10 ± 0.3s respectively as shown in Table . It is evident that the short-lived, liquid-state time of 10 seconds at ambient temperature is not a reliable transience property and must be extended. The non-ionic plasticizers (PEO and BEHP)

have contrasting effects on the photoresponse delay and depolymerization rate of PPHA from QCM. Loadings up to 20 pphr BEHP appear to have little to no effect on the photoresponse delay, however, the rate constant increases by a factor of 2.32. The acid-diffusion length has likely reduced due to the greater mobility of the acid to protonate various acetal linkages across the backbone of the poly(phthalaldehyde) chain. However, PEO has a notable effect on the increased photoresponse delay and the lower rate constant which correlates with the amount of pphr loadings. This results suggests there are inhibiting reactions that are occurring with the free FABA acid and the ether linkages in the polymeric backbone of PEO. The addition of both plasticizers PEO and BEHP extend the liquid-state time of the monomer at room-temperature by a factor of 10 and 417. As seen in Figure 6.8, the resistance recorded from QCM directly correlates to the viscosity of the liquid after depolymerization. BEHP retains a higher resistance after depolymerization indicative of a very low-viscosity liquid that is ideal for mechanical deformation and rheological properties for absorption into the surrounding environment. The similar phthalate structure of BEHP and the phthalaldehyde monomer likely have great miscibility which reveals a greater effect on the liquid-state retention of phthalaldehyde after depolymerization of PPHA.

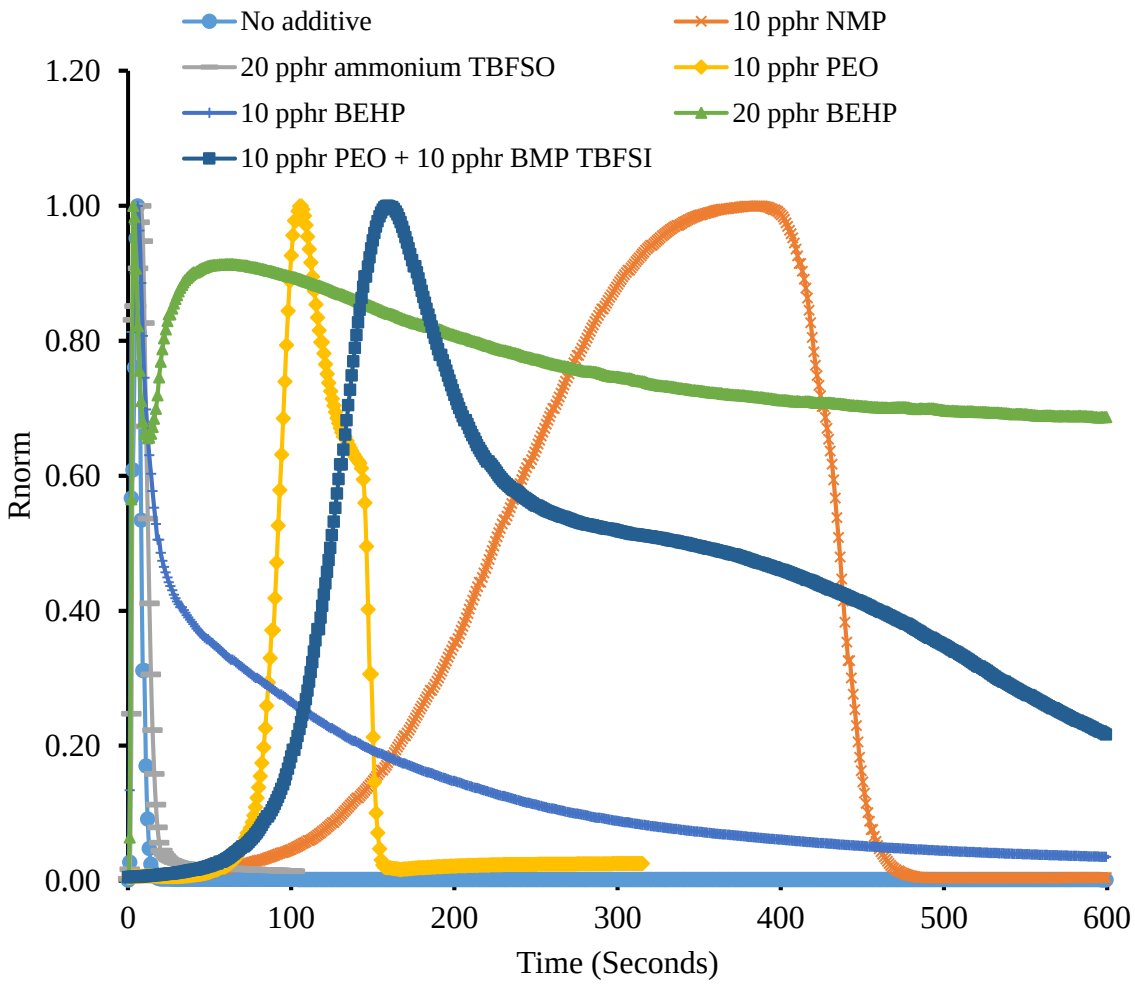

Figure 6.8 QCM plots of PPHA with various loadings of additives indicating the liquid-state extension

Residual solvent also is an important contributor to the transient properties (delay, rate constant, liquid-state time) during the depolymerization of PPHA. PPHA films that were solution-casted from NMP had a drastic effect delaying the response from the light irradiation. In contrast, acetone, tetrahydrofuran, gamma butryalctone (GBL), cyclohexane, and cyclopentanone were found to have little to no effect on the transient

properties. PPHA dissolved in cyclopentanone with the additions of 1, 5, and 10 pphr NMP were solution-casted and evaluated by QCM as seen in Figure 6.9.

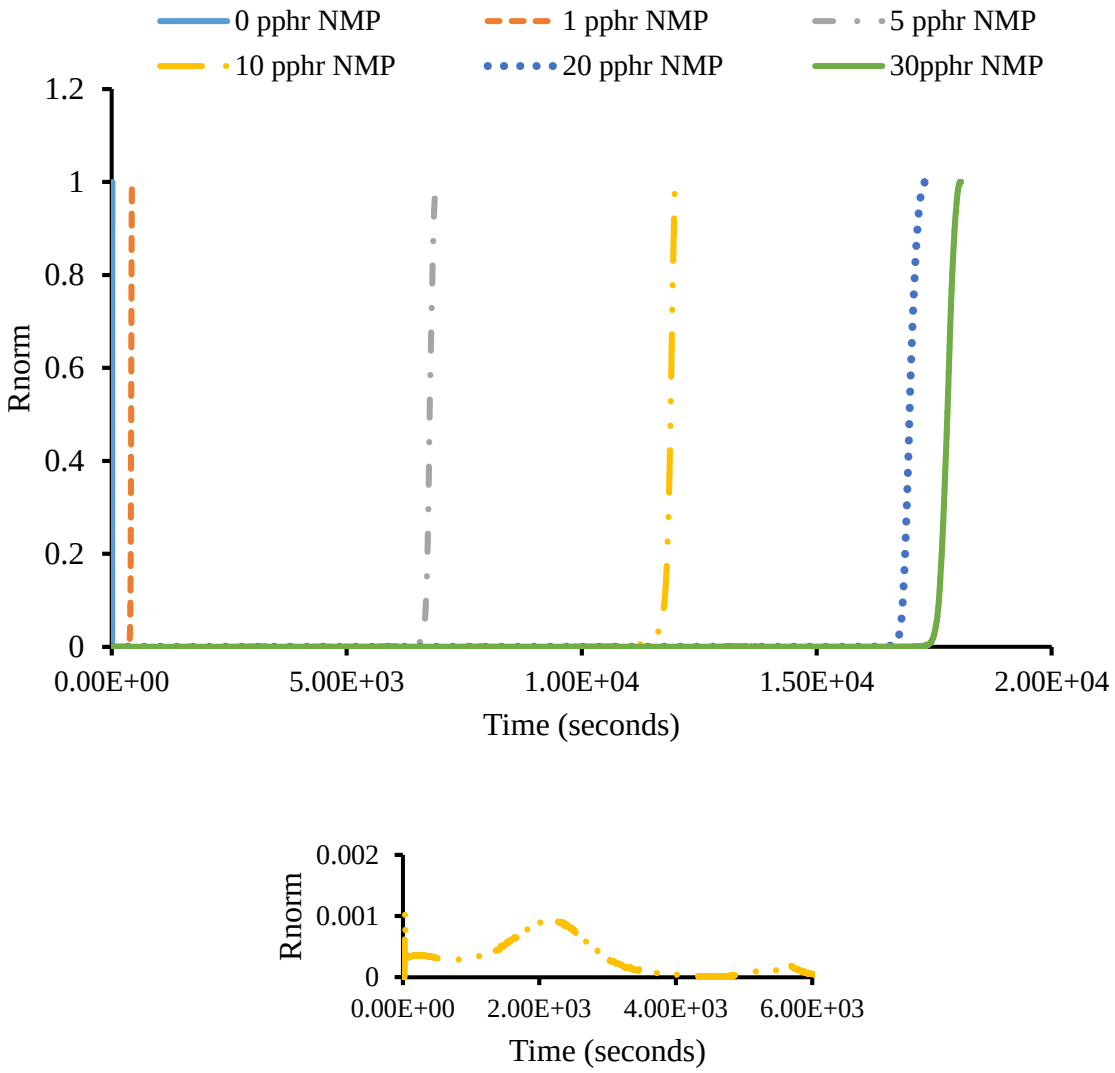

Figure 6.9 QCM plots of PPHA with various loadings of NMP (above), and zoomed-in view of the 10 wt% loaded NMP film (below)

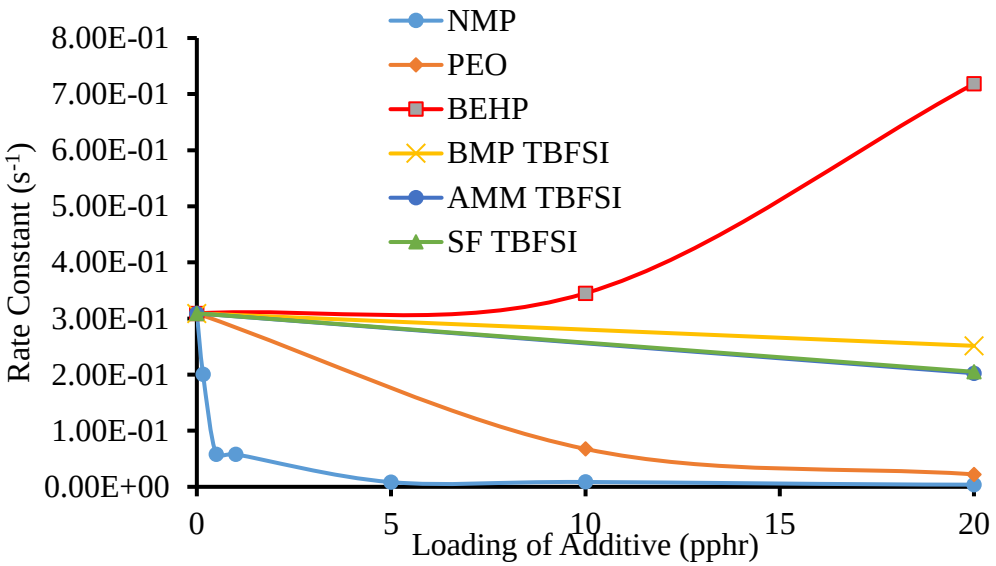

Figure 6.10 Rate Constants for Depolymerization of PPHA with various loadings of additives from QCM

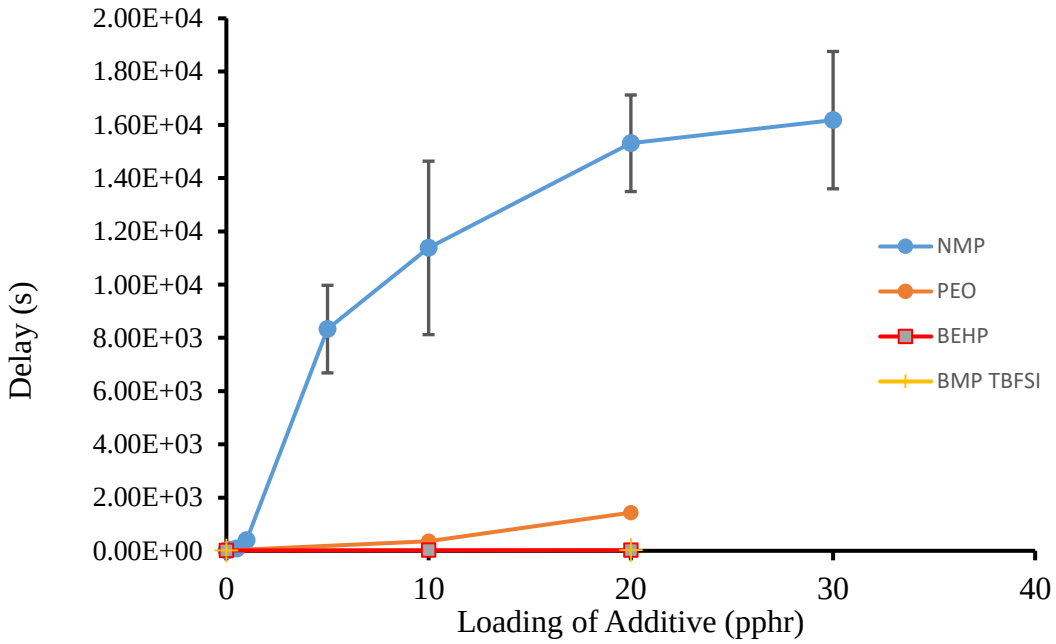

Figure 6.11 Photoresponse delay for the depolymerization of PPHA with various loadings of additives

The photoresponse can be delayed by a factor of 1155 by the simple addition of 30 pphr NMP into PPHA films. This result suggests that the acid is not directly neutralized as NMP is 60 times in molar excess than the FABA acid at 30 pphr loading. A significant delay in the photoresponse was not seen until NMP was in 2 times molar excess than the Rhodorsil-FABA from Table . A plausible theory is that there is likely a competitive reaction between the depolymerization of PPHA (via protonation of the acetal linkages) and NMP that could be protonated by the FABA acid which transitions into a weaker acid as shown in Figure 6.12. An equilibrium may exist between protonated NMP and the monoprotonic acid[109]. The addition of more NMP into the PPHA film may likely force the equilibrium to shift towards the protonated NMP. This relationship is demonstrated in Figure 6.11, as the loading of NMP begins to show no additional effect on the delay as the loading of NMP reached 30 pphr due to the equilibrium shift to NMP-H+.

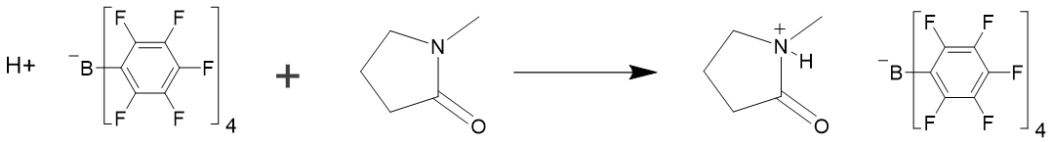

Figure 6.12 Schematic representation of the competing reaction with NMP

The depolymerization rate constant is also slower by a factor of 42, however, it is observed that the bulk of depolymerization has been maintained to relatively short time-scale region. The bottom chart in Figure 6.9, shows that there is some depolymerization occurring at 0.1% of the overall resistance the upon photexposure. The rate constant for depolymerization remains relatively the same after 10 pphr NMP, however a significant increase in the photoresponse delay remains until ~30 pphr NMP. This result suggests that the mechanical integrity of the PPHA film can potentially be maintained for

extended times under irradiation. The tuneable photodegradation based on the loadings of NMP is a desirable characteristic that can potentially be useful transient applications where operational time is needed in the presence of the phototrigger.

NMP also exhibited a significant increase in the liquid-state time prior to the freezing of phthalaldehyde by a factor of 29. Based on the protonation of NMP theory as showed in Figure 6.12, ionic liquids were employed to gain the beneficial properties to the liquid-state extension while maintaining the photoresponse time. The ionic liquid is already in its ion form and should interact with the free FABA acid. As expected, the ionic liquids showed little to no effect on the delay or rate constant of depolymerization. However, the liquid state time of the monomer after depolymerization did not show significant effects until higher loadings to 50 pphr. The effects of the chemical structure of cation appears relatively independent on the transient properties of the PPHA films. Films with 50 pphr loadings of BMP-TBFSI maintained the liquid state of the monomer for greater than 4 hours. The synergistic effects of the non-ionic plasticizer (PEO) with an ionic plasticizer (BMP TBFSI) was investigated. The combination of 10 pphr PEO and 10 pphr BMP TBFSI is shown to exhibit long-lived liquid states at ambient conditions past 4 hours. The combination of 3 dissimilar compounds (PEO, BMP TFSI, o-pha) may exhibit eutectic behaviour as the mixture likely exceeds the freezing points of the separate components.

The extension of the liquid-state after depolymerization of PPHA at sub-zero temperatures is desirable to further expand the thermal window to achieve transience in colder environments. DSC was used to monitor the depression of the freezing point of phthalaldehyde from the addition of non-ionic and ionic plasticizers. PPHA films were made with various concentrations of BMP TBFSI and BEHP with 5 pphr PAG and exposed

to 365 nm UV light in an aluminium pan. The resulting yellow liquid was taken to DSC and the freezing point was evaluated as shown in Figure 6.13. It is evident that the increasing loading of BMP TBFSI from 50 pphr can shift the freezing point of phthalaldehyde to sub-zero temperatures. Non-ionic plasticizers such as PEO and BEHP phase aggregate at relatively low loadings. BEHP must be maintained at 20 pphr loadings to prevent phase aggregation, however, the freezing point of the monomer after depolymerization remains high at 21°C. Ionic liquids, such as BMP TBFSI, can be added at high loadings without significant leaching from polymer films. As seen in Figure 6.13, the increased loadings of BMP-TBFSI from 50 pphr to 100 pphr will shift the freezing point of phthalaldehyde to sub-zero temperatures. The mixture of BEHP and BMP TBFSI can be combined to depress the freezing point of phthalaldehyde to -5.1°C.

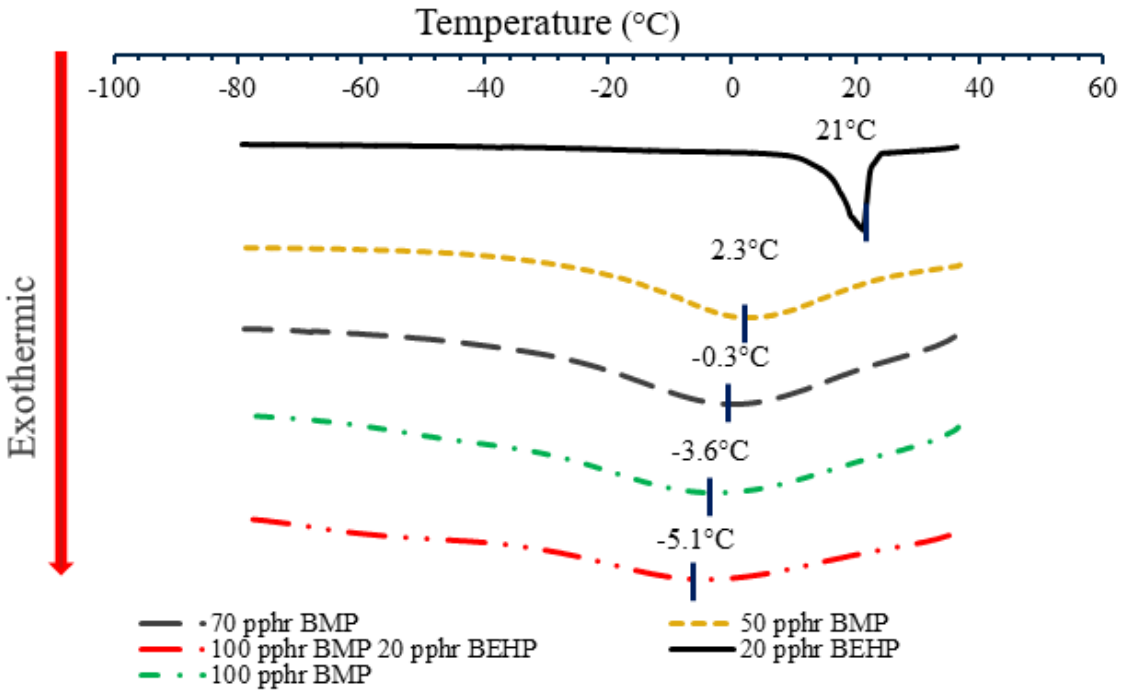

Figure 6.13 DSC traces of the liquid products after depolymerization of PPHA with various additives

6.6 Conclusions

The transient properties of PPHA from the photoresponse delay, depolymerization rate, and liquefaction of the monomer have been controlled with various additives. The addition of NMP to act as a hydrogen acceptor to perform competitive reactions with free acid within films has shown to be a useful method to control the degradation time after exposure. The basic strength can potentially be tuned to further control of the photo response per mole basis. Ionic liquids have been successfully employed without phase segregation in PPHA films for the first time and has been demonstrated to be very beneficial for tuning the freezing point of phthalaldehyde to sub-zero temperatures.

CHAPTER 7. MULTILAYER AND ACID-AMPLIFIED DEGREDATION OF DEPOLYMERIZABLE POLYMERS

7.1 Motivation

Several concerns arises when adding photo-catalysts such as PAGs and sensitizers as additives into the polymer substrate to achieve transience. The salt products produced form the photo-acid generator and the sensitizer can generate a residue that has negligible vapor pressure. Photo-patternable sacrificial polymers utilized in MEMS packaging systems can also potentially benefit from reducing the amount of residue from the salt produced from the photo-acid generators. Furthermore, it is difficult to fabricate devices that are photosensitive to visible light. Thus, it is desirable to add the photosensitive material at the last fabrication process step. The need to amplify the acid response and for targeted thermal triggers are desirable for transient electronics.

7.2 Dual Layer Degradation and Acid Amplification

When a photosensitive polymer is used, it can be problematic to handle materials because they can be inadvertently exposed to the triggering light. Also, the photosensitive polymer may have a limited temperature range where it is stable. This can make processing the final component difficult if high temperature processes are needed, such as for soldering or curing of compounds.

Thus, it is desirable to fabricate a polymer-containing component without it being photosensitive and add a photosensitive layer later, or at the end of the process. In this

invention, it was found that a second, photo-sensitive layer containing a decomposing photo-catalyst can be added after component fabrication. Activation of the second, photo-sensitive layer can be initiated and result in decomposition of the second layer. Further, the photo-catalyst in the second layer can diffuse into the first, non-photosensitive layer resulting in efficient destruction of it. This is particularly effective when the first step in the photo-decomposition process is the liquefaction of the photo-activated materials because the photo-catalyst has a high diffusion coefficient and can easily penetrate into the non-photo sensitive layer.

The concept is demonstrated in Figure 7.1 where a conductive pathway of PPHA with copper nanoparticles was coated. Another photosensitive PPHA layer with a photoacid generator (Rhodorsil-Faba) was coated ontop. The sheet resistance of the film was measured by a four-point probe and found to be about 2 MΩ. The entire film was given a UV exposure dose of $2J/cm^2$. The acid was generated and initiated depolymerization of the top-layer. The acid eventually diffused to the bottom layer shorting the electrical circuit from mechanical deformation of the PPHA polymer as it transitions into phthalaldehyde monomer where evaporation and sublimation will take place.

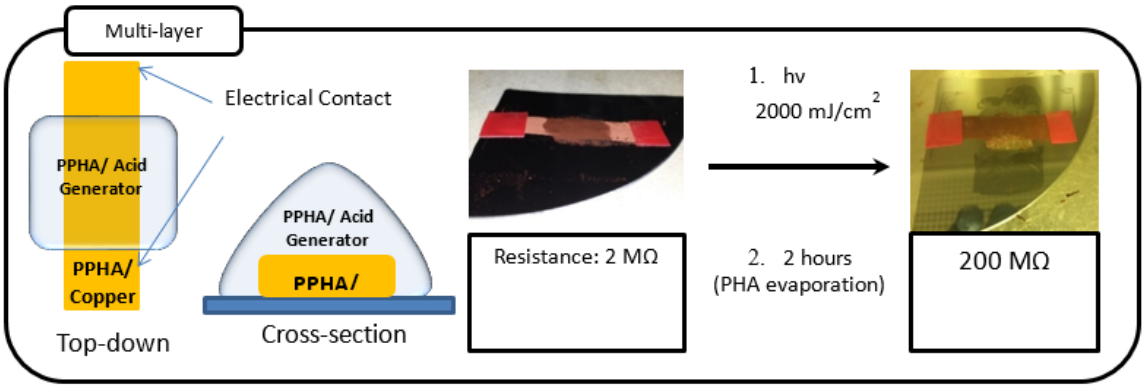

Figure 7.1 Dual layer Concenpt of coating a conductive PPHA layer with copper nanoparticles and a photosensitive PPHA layer with photoacid generator.

One method of analyzing transport properties of the acid amplifiers within a polymer film is to monitor the change in dimensions of features with post-exposure bake times. These methods can consist of lateral changes of the feature under reaction conditions, or vertical depth profiles where an acid layer can diffuse to a non-acid layer underneath[110,111]. The diffusion of acids in photoresist films has been suggested to follow classical Fickian diffusion. The diffusion coefficient (D) of the acid can be determined from this formula: $D = L^2/2t$, where L is the diffusion length and t is the time. Local enhancement of the acid mobility can drastically affect the diffusion of acid which may be beneficial or a hindrance for different applications. This is largely dependent on the thermal properties of the polymer[112,113].

The acid-catalyzed decomposition of PPC is a controlled experiment that occurs at high temperatures (~100°C), making for an ideal candidate for measure diffusion coefficients. The effective diffusion coefficient of acid was evaluated in a two-layer structure of polypropylene carbonate (PPC). An 11.7 µm layer of PPC was spin-coated

onto a silicon substrate. A 2.3 µm layer of PPC with 3 pphr PAG was coated onto another substrate, then lifted off and lightly pressed onto the 11.7 µm layer of PPC without PAG. Too much pressure resulted in a film with no defined interface between PAG-loaded and PAG-free.

The two-layer structure was exposed to 4 J/cm^2 to ensure full activation PAG in the top layer. The sample was held at 100^{o}C (the acid-catalyzed decomposition temperature of PPC) where the depth of the top-layer was recorded with time after the hole had reached the underlying non-PAG layer. The square of the depth in µm was plotted with time as shown in Figure 7.2.

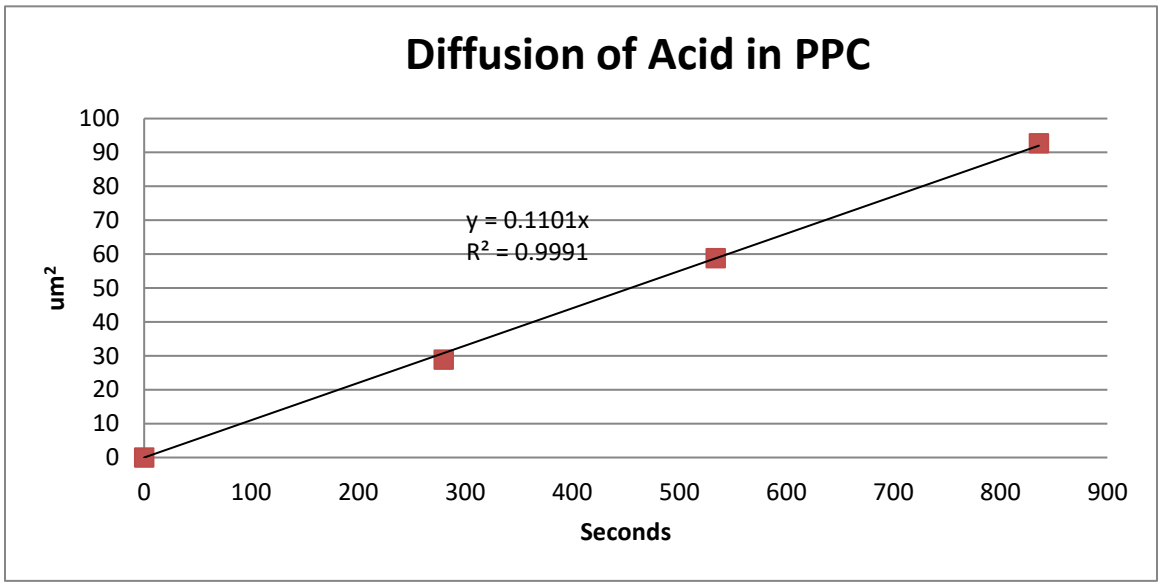

Figure 7.2 Plot of acid diffusion depth squared vs. time at 100°C. The slope of the line corresponds to the effective diffusion coefficient

The linear profile is indicative of one-dimensional Fickian diffusion where the time is proportional to the square of the distance ($D=L^2/t$). The diffusion coefficient of the acid

produced from the iodonium PAG through the decomposing PPC film was taken to be 0.11 $\mu m^2/s$.

The effective diffusion coefficient measured in PPC can be utilized for relatively thin films for use in lithographic packaging systems, however, this may not be fast enough for thicker substrates used in transient applications. Although the depolymerization of PPHA is believed to be catalytic, it is expected that the acid could be readily consumed by impurities. Therefore, potentially one could use compounds that can multiply the number of the acid generated from the catalysts, or chemically amplify the catalyst. The amplifiers can also be used as latent thermal acid generators to trigger the depolymerization of the polyaldehyde substrates Therefore, the amount of acid increases as it diffuses through the polymer matrix. A number of acid amplifiers were synthesized and evaluated for their ability to amplify the acid.

Contrast curves will be evaluated with PPC films with various loadings of PAG and acid amplifiers and presented in Table 6. The D_{100} is expected to decrease with acid amplifier loading. PPC films had 3 pphr and 10 pphr of an acid amplifier. They were exposed to UV light and developed on a hotplate at 80°C for 7 minutes.

Table 6 Contrast Curves of PPC with 3 pphr PAG and 10 pphr of various acid amplifiers

Acid Amplifier	Exposure Dosage (mJ/cm^2)	D_{100} (mJ/cm^2)	Contrast (ϒ)
None – PAG Only	500	173.98	1.73
PAG + 3MO	500	62.42	1.35
PAG + 3HO	2000	120.32	1.28
PAG + 3HMS	500	-	-
PAG + 3MF	500	373.60	1.23
PAG + 3HT	500	76.48	1.61
PAG + 3MT	500	309.20	1.65
PAG + 3MMS	500	361.99	1.17

It is evident 3MO, 3HO and 3HT all produce acid in significant quantities as indicated by their D_{100} values. (They all offer a $D_{100} < D_{100,PAG}$). This can be attributed to the acidic strength of the acid precursor due to the strong electron-withdrawing of the fluorine groups. The acid amplifiers of 3MT and 3HT had contrasting effects on the sensitivity. It is expected that the tosyl acid may not be as reactive for PPC decomposition, however, the 3HT reduced the overall sensitivity of PPC. The hydroxyl trigger may be more susceptible to acid degradation. The acid amplifiers with the mesyl acid precursor (3MMs and 3HMs) both appear to decrease the photosensitivity of PPC. This can be attributed to the volatility and the lower acidic strength of the acid precursor for decomposition of PPC.

It has been observed previously that 3 wt% minimum PAG is needed to develop photo-pattern films of PPC. The Rhodorsil-Faba has negligible vapor pressure which creates involatile salts that can harm MEMS devices in sacrificial polymer applications.

Therefore, the amount of PAG was reduced with an acid amplifier to determine if photo-patterning was still achievable. The sensitivity of a PPC film with a photo-acid generator and a film with a photo-acid generator and acid amplifier were investigated. A film of PPC was exposed with UV light through a multi-density resolution mask. The film was then dry-developed at 100°C (acid-catalyzed decomposition temperature of PPC) and the thickness was recorded at each % transmission of light from the resolution mask as shown below:

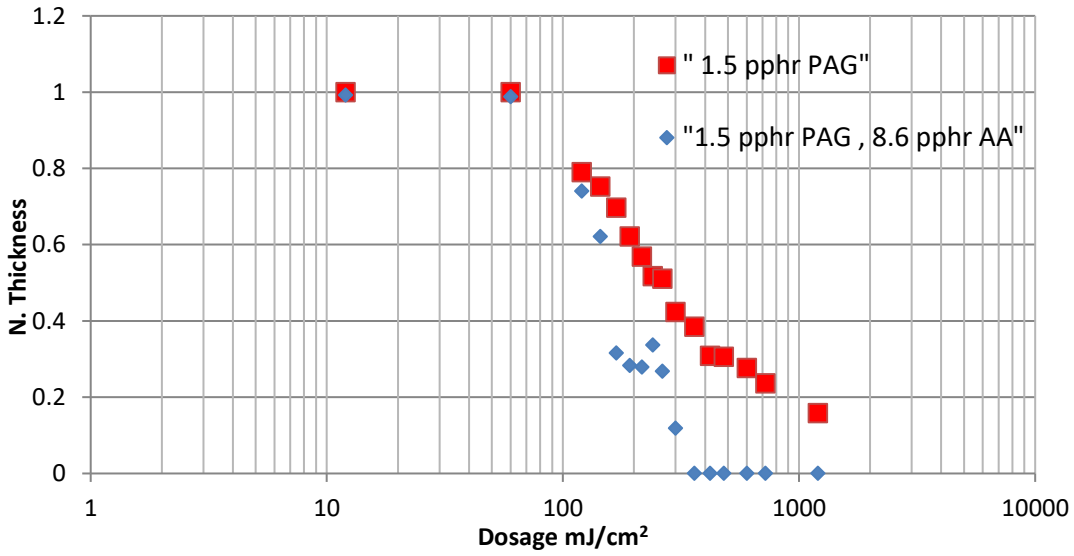

Figure 7.3 Contrast Curve of PPC with 1.5 pphr PAG and 8.6 pphr 3MP

The film of PPC+PAG did not clear through the entire film at the maximum dosage of light. The linear portion can be extrapolated to show that the minimum dosage required to expose through the entire film is 1457 mJ/cm^2. The PPC film with PAG and 8.6 pphr of an acid amplifier only required a minimum dosage of 368 mJ/cm$^{2.}$ The addition of acid amplifiers into the film remarkably showed a 4X increase in acid generation per photon of light.

Analogous experiments were conducted with PPHA homopolymer and dry-developed at room temperature for 24 hours. It was found that the PPHA with 2 pphr PAG required a minimum dosage of 768 mJ/cm^2 to reach through the entire film. However, the addition of 15 pphr acid amplifier reduced the minimum dosage to 420 mJ/cm^2. The PPHA film with acid amplifier was observed to develop at a faster rate than the film with no amplifier. This result reveals a 2X increase in sensitivity of PPHA films and more notably suggests that acid amplifiers can activate in a film at room temperature. However, it is noted that the stability of the amplifier may not be suitable for long periods at room-temperature. The overall film thickness was considerably lower which is indicative of thermal stability concerns of the acid amplifiers in films.

The thermal stability of the acid amplifiers in ambient conditions were stored in containers. 3MO was found to be stable for several months, however, it is found that incorporating 3MO in films of PPHA initiated degradation after 2 weeks. The same acid amplifier by itself was monitored for a week by NMR, which showed no signs of degradation. One possible reason for the short shelf-life of the film is the residual BF_3 catalyst from the synthesis of PPHA. The batch of PPHA used for these films were not purified for the BF3 catalyst post-synthesis.

^{19}F-NMR was used to evaluate potential reactions of BF_3 with the acid amplifier to accelerate the decomposition of these small molecules. A small amount of BF_3 was added to solution of chloroform-D containing an acid amplifier. Over the course of three hours, the solution visibly turned from transparent to black, which indicated that a reaction took place. ^{19}F-NMR was used to confirm the product of this reaction as seen in Figure 7.4.

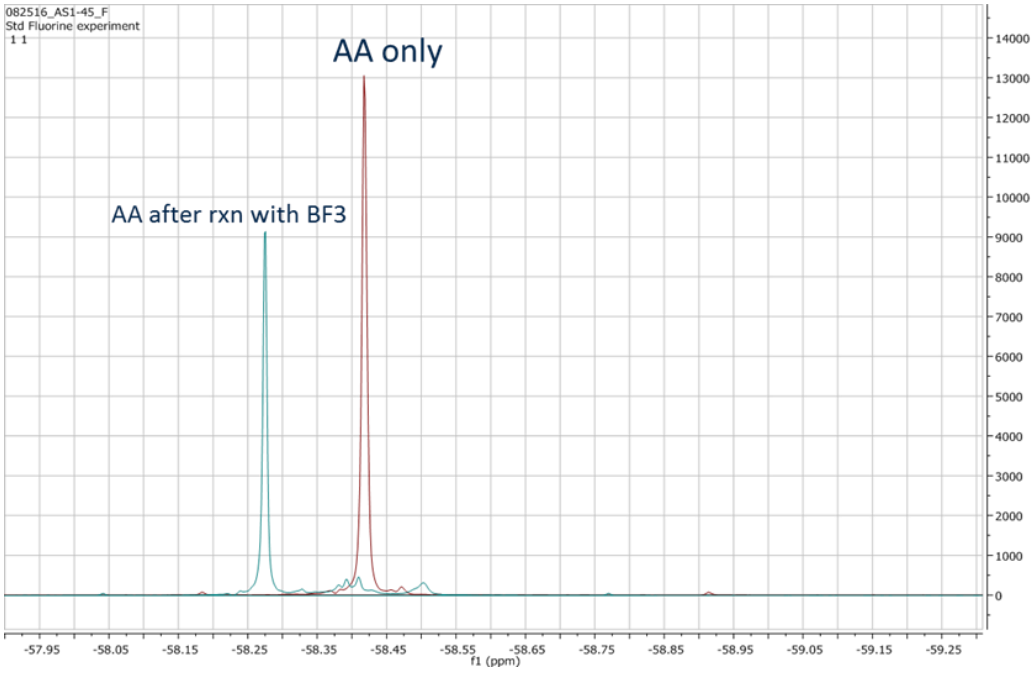

Figure 7.4 ^{19}F-NMR of acid amplifier by itself and after reaction with BF3 catalyst

It is clear that proper purification procedures of PPHA are necessary for the use of acid amplifiers. The product of the reaction between BF3 and the acid amplifier is unknown. However, the result is interesting to note that the BF_3 can initiate auto-catalytic reactions with acid amplifiers at ambient temperatures creating potentially acidic species as products.

7.3 Applications for Electronic Device and Packaging Systems

The two following sections demonstrate applications for the acid amplifiers and dual layers used for two different applications. Poly(aldehydes) has been evaluated as dual-layers for sacrificial bracing applications. This work was supported by Lam Research Inc. I specifically would like to acknowledge Drs. Stephen Sirard, Ratchana Limary, and Diana Hymes for technical discussions and advice towards this project. The other section demonstrates the use of polyaldehydes as the substrate material for the fabrication of

functioning multi-layer transient printed wiring board. I would like to acknowledge the technical contributions of Dr. Gerald Gourdin and the funding support from Honeywell that assisted with the completion of this project.

7.3.1 HAR Structures

The sacrificial bracing of materials has been first proposed from U.S. Patent US20160097590A. As semiconductor devices are scaled down to smaller features there are challenges for high aspect ratio (HAR) structures. Many fabrication techniques are employed such as etching, surface cleaning, planarization, and material deposition. In particular, wet processes such as etching can induce collapse of HAR structures due to capillary forces during drying. A method was developed to prevent collapse of high aspect ratio pillars by the deposition of a sacrificial polymer which can provide mechanical support for these structure. The sacrificial polymer can then be thermally or photo-triggered to depolymerize and vaporize from the HAR structure as depicted in Figure 7.5.

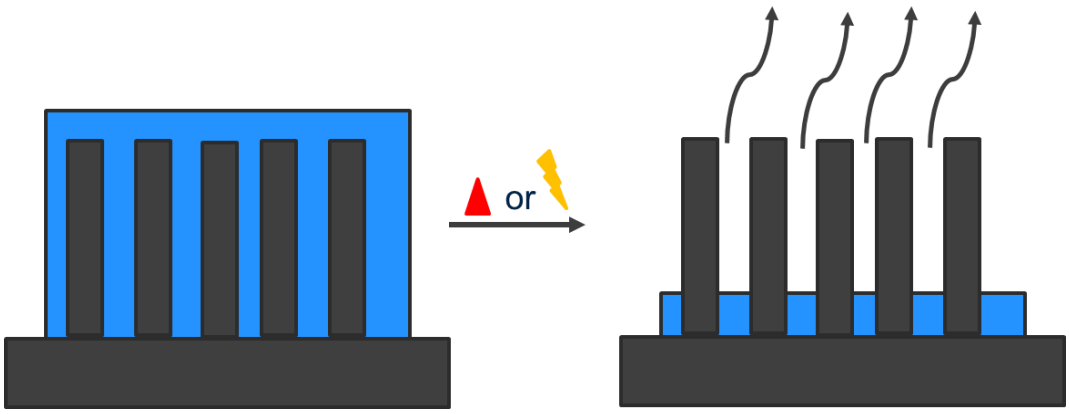

Figure 7.5 Sacrificial Bracing of High Aspect Raito Pillars

Polyaldehydes are an ideal candidate to serve as the sacrificial bracing material for the HAR structures. Poly(phthalaldehyde) (PPHA) has a very 'clean' depolymerization directly into volatile monomer units. The incorporation of thermal or photo-acid generators can afford photo-patternability or tunability of the thermal window for the triggering the release of the sacrificial material. Previous work has focused on single mono-layers of poly(phthalaldehyde)[104]. A freeze drying microscope was used to create a heated environment under high vacuum to bypass the liquid-stage during depolymerization as the polymer transitions from solid to directly to a gas. Anionic poly(aldehydes) with more volatile comonomers such as butanal have been used have been previously evaluated and showed moderate showed success with 9:1 aspect ratio pillars. Higher aspect ratio pillars are more difficult to brace and are prone to collapse. There are some unique challenges that still occur with this sacrificial bracing system with HAR structures with larger aspect ratios. It was hypothesized here that a dual layer structure could be employed to force a top-down depolymerization profile to support the base of the pillar during removal of sacrificial material.

Figure 7.6 Two-Layer for top-down depolymerization profile for sacrificial bracing systems

A careful selection of thermal acid generator can provide a proper thermal window to induce the depolymerization of PPHA. A series of acid amplifiers were evaluated (3MT, 3MMs, and 3MO). Consideration of the reactivity and the volatility of the acid precursor

as needed as the sacrificial bracing material must leave minimal residual products after depolymerisation of PPHA. Therefore, the residual products of the depolymerisation were evaluated by XPS.

Several samples were made of the following: 1) bare Si Wafer, 2) Si wafer soaked in PGMEA, 3) p(PHA-co-BA) film, 4) p(PHA-co-BA) film with 13 wt % 3MT, 5) p(PHA-co-BA) with 13 wt% 3MMs, and p(PHA-co-BA) with 13 wt% 3MO. The samples were thermally treated in an RTA in two different ways. The first way the RTA was ramped at 75°C/min to 425° and held for 3 minutes under reduced pressure of 5 mTorr. The second condition is that the RTA was ramped at 20°C/min to 260°C and held for 30 minutes under reduced pressure of 5 mTorr. The samples were then taken to for XPS analysis characterization where a surface scan was performed. The reported atomic % values from XPS are shown in Table 7.

Table 7 XPS surface scan results of 1) bare SI wafer, 2) bare SI wafer soaked in PGMEA for 10 minutes, 3) , 3) p(PHA-co-BA) film, 4) p(PHA-co-BA) film with 13 wt % 3MT, 5) p(PHA-co-BA) with 13 wt% 3MMs, and p(PHA-co-BA) with 13 wt% 3MO. Table (above) are results from thermally treatment in RTA at 420°C and the table (below) was a separate thermal treatment in RTA at 260°C

Name	Peak (B.E.)	Atomic % (1)	Atomic % (2)	Atomic % (3)	Atomic % (4)	Atomic % (5)	Atomic % (6)
O1s	532.79	34.78	36.29	34.71	37.17	37.24	35.81
Si2p	99.19	57.68	54.69	57.33	56.06	55.07	54.11
C1s	285.25	7.62	8.53	7.59	6.78	7.38	6.81
F1s	688.61	0	0.49	0.37	0.19	0.31	0.35

Name	Peak (B.E.)	Atomic % (1)	Atomic % (2)	Atomic % (3)	Atomic % (4)	Atomic % (5)	Atomic % (6)
O1s	532.79	33.45	-	35.04	34.5	34.66	34.69
Si2p	99.19	55.99	-	55.34	55.37	55.89	55.47
C1s	285.25	10.56	-	9.36	10.05	9.20	9.82
F1s	688.61	0	-	0.26	0.09	0.25	0.03

The native oxide (Si, O) and the possible elements of the residual products of the depolymerisation (C, F) were investigated by XPS. It is seen here in both 420°C and the 260°C, there is not much difference between the control (bare Si wafer) and the samples that contain the acid amplifiers where the control had about 7.62 and 10.56 atomic % of carbon. In many instances, it appears that the overall carbon atomic % decreased after the thermal treatment to remove PPHA. The source of the fluorine detected for samples 4 and 5 that contain 3MT and 3MMs acid amplifiers is unclear. The 3MT and 3MMs acid amplifiers bear no fluorinated substituent groups. Traces of fluorine was also detected in sample 2 of the bare SI wafer that was soaked in the casting solvent PGMEA solvent. These

results suggests that any fluorination detected is likely due to impurities within the solvent as oppose to the acid amplifiers and polyaldehyde films themselves.

7.3.1.1 Dual Layer vs Gradient Layer

Dual layer composition of the sacrificial bracing material do not have to be discrete layers. Rather, they can be graded layers where the concentration of the constituents within each layer changes gradually from one layer blending into the other layer(s). A gradient in concentration from one layer to another can occur experimentally when fabricating a multilayer structure because the constituents in one layer may partially dissolve the constituents in another layer. Or, the gradient may be intentionally added so that there is not a discrete seam between the two layers. The gradient in concentration may occur with structures with more than two layers. Thus, the 'dual' layer is defined here as two discrete layers and 'gradient' layer is defined as dual layers that are partially dissolved with one another. Both methods are assessed for feasibility for the sacrificial bracing materials.

Two methods of a dual layer with two discrete layers are assessed. First, a single layer of a linear p(PHA-co-BA) with a molecular weight of 14 kDA was coated onto the Si wafer. This was followed by two methods: i) the acid amplifiers which is an oil-like substance was spin-casted directly ontop of the polymer film, and ii) the amplifier was dissolved in methanol and spin-casted onto the bottom-layer followed by a soft-bake at 50°C to evaporate residual MeOH. Gradient layers were performed by making 10 wt% solutions of the anionic p(PHA-co-BA) in PGMEA with 5wt% of an acid amplifier and casted directly ontop of the bottom-layer. 3MP, 3MO, and 3MTf were assessed here. The samples were thermally treated in an RTA at a ramp rate of 75^{o}C/min to 425°C and held

for 3 minutes at 5mTorr. The dual and gradient layers were compared to a control of only the anionic p(PHA-co-BA) with no acid amplifier to evaluate any improvements.

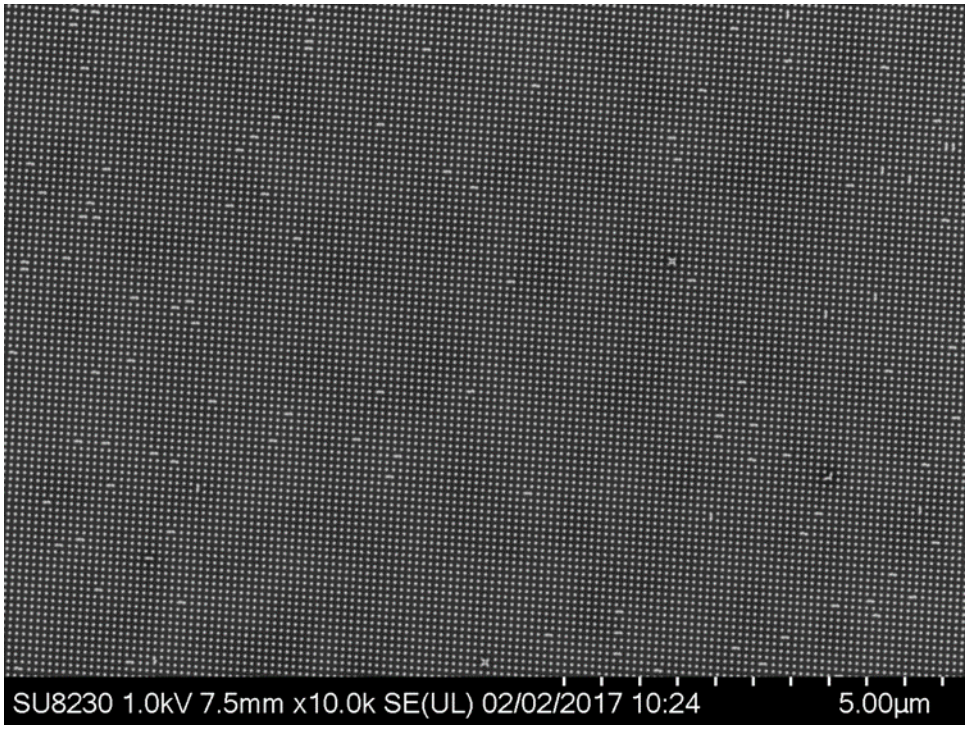

Figure 7.7 Representative SEM image of the thermal decomposition of anionic butyraldehyde copolymer mono-layer after RTA thermal treatment on 9:1 HAR pillars

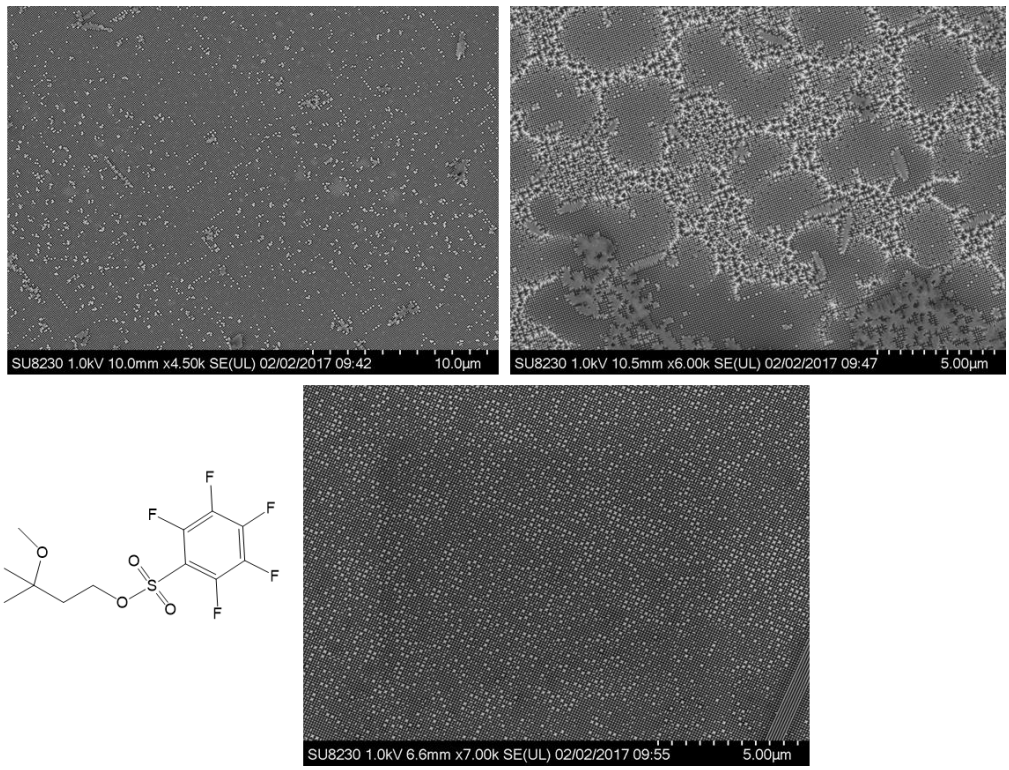

Figure 7.8 Representative SEM image of the thermal decomposition of anionic butyraldehyde copolymer mono-layer after RTA thermal treatment on 9:1 HAR pillars Top-left is the dual layer where 3MP is dropped directly, top-right is the 3MP diluted in methanol and drop-casted, and bottom is the gradient layer where another p(PHA-co-BA) film was coated with 3MP

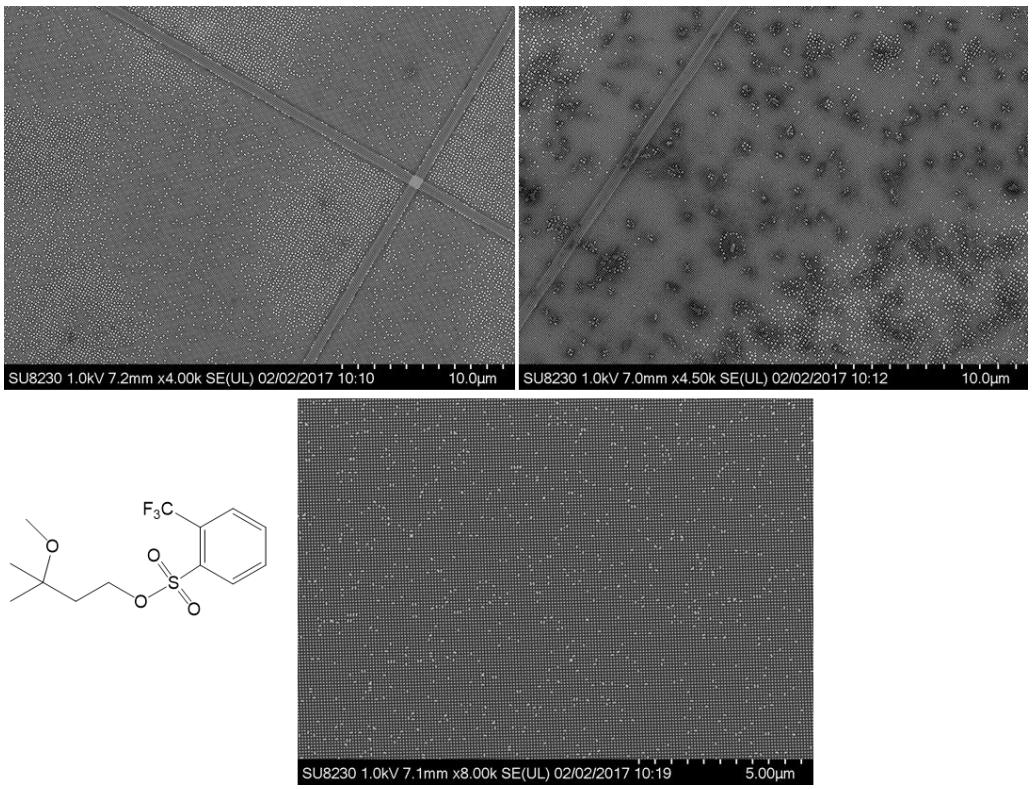

Figure 7.9 Representative SEM image of the thermal decomposition of anionic butyraldehyde copolymer mono-layer after RTA thermal treatment on 9:1 HAR pillars Top-left is the dual layer where 3MO is dropped directly, top-right is the 3MO diluted in methanol and drop-casted, and bottom is the gradient layer where another p(PHA-co-BA) film was coated with 3MO

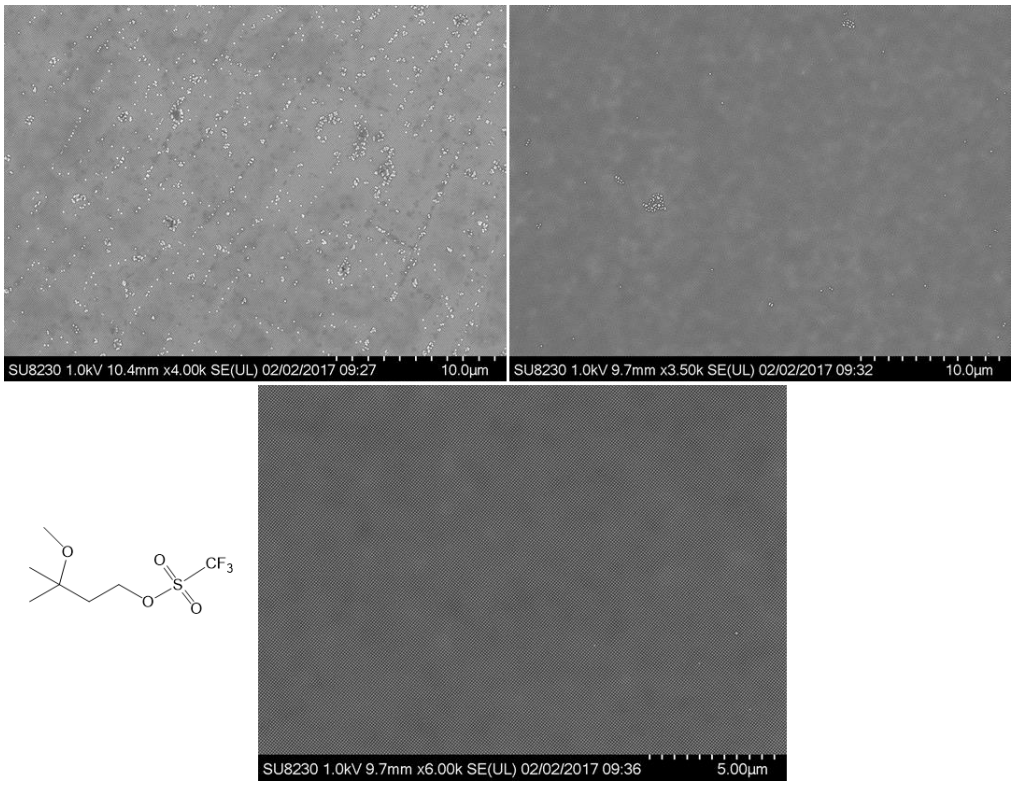

Figure 7.10 Representative SEM image of the thermal decomposition of anionic butyraldehyde copolymer mono-layer after RTA thermal treatment on 9:1 HAR pillars Top-left is the dual layer where 3MO is dropped directly, top-right is the 3MO diluted in methanol and drop-casted, and bottom is the gradient layer where another p(PHA-co-BA) film was coated with 3MO

As seen from the previous figures in Figure 7.7, Figure 7.8, Figure 7.9, and Figure 7.10, the acid amplifier performed better in this pattern 3MTf > 3MO > 3MP from qualitative observation of SEM images for collapsed structures. It is thought that the acid precursors of 3MO and especially 3MP bearing fluorinated substituent groups on a bulky, aromatic ring which will likely induce residue that may contribute to pillar collapse. 3MTf has the volatile acid precursor of triflic acid which has a relatively high vapor pressure in comparison. Furthermore, it appears that the dual layer where the acid amplifer was coated from a solution of methanol and where the acid amplifier loaded in the anionic p(PHA-co-BA) film was coated directly ontop from PGMEA performed the best. It is thought that a

medium such as a polyaldehyde film is needed for the acid amplifier to produce acid and diffuse in a homogenous manner. Successful dual/gradient layers with sacrificial bracing materials were achieved with 9:1 HAR structures.

The control of the ramp rate is necessary for the controlled degradation of the polyaldehyde for use as a sacrificial bracing material. The RTA rapid ramp rate may not be suitable. The freeze drying microscope was used with a heated stage under vacuum. Dual layer with a concentrated solution of acid amplifier with methanol (41 wt% of AA in methanol) was compared with a more dilute solution of acid amplifier with methanol (11wt% of AA in methanol).

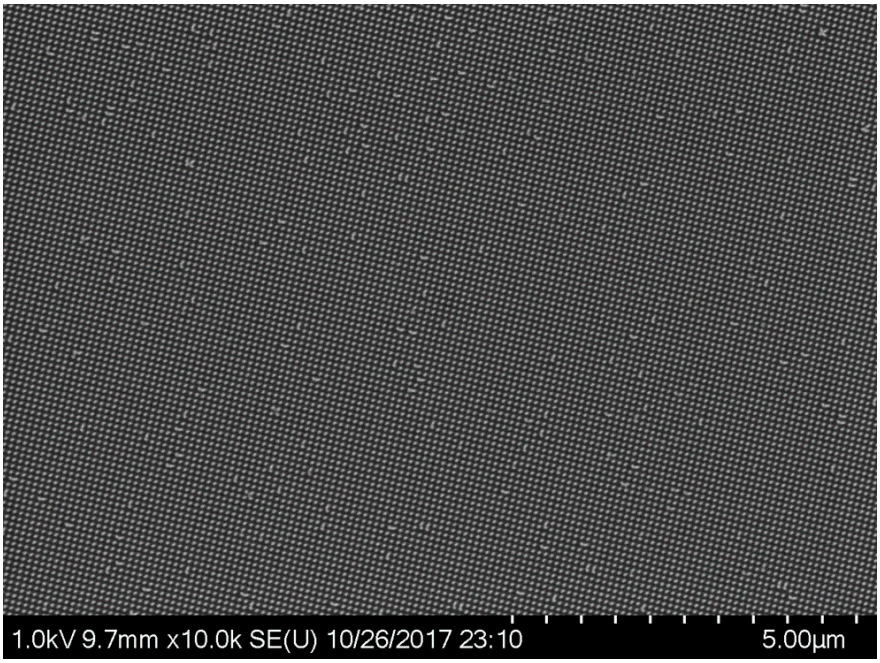

Figure 7.11 Representative SEM image of the thermal decomposition of anionic butyraldehyde copolymer mono-layer after freeze dry microscope thermal treatment on 9:1 HAR pillars

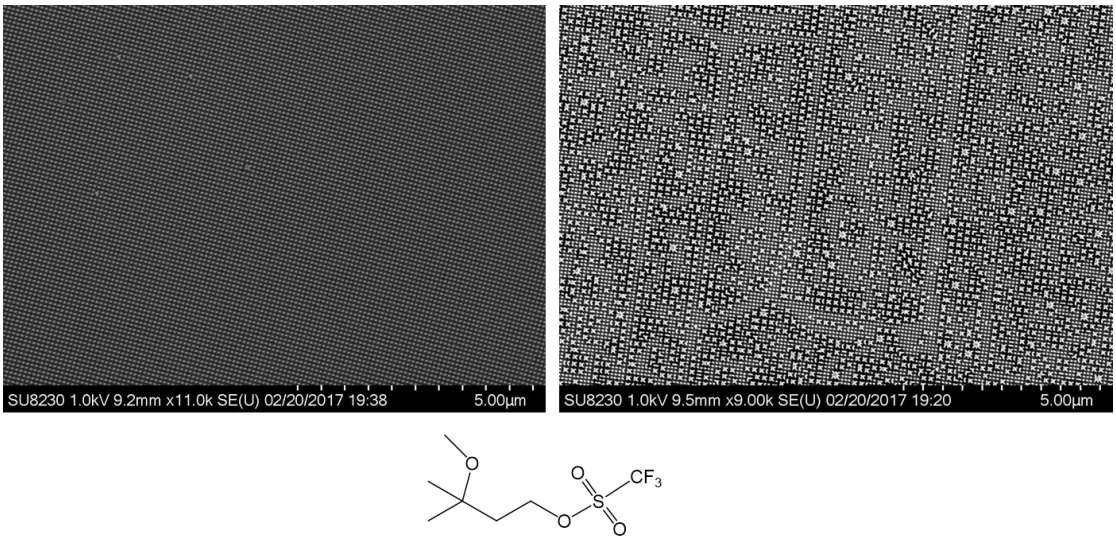

Figure 7.12 Representative SEM image of the thermal decomposition of anionic butyraldehyde copolymer dual layer with freeze dry microscope thermal treatment on 9:1 HAR pillars. Left SEM image is the using 11 wt% 3MTf in methanol formulation. Right SEM image is using the 41 wt% 3MTf in methanol formulation.

There is a significant difference in the performance of the dual layers by variation of the concentration of acid amplifier in the formulation for the top-coat as seen in Figure 7.12. The more concentrated formulation of 41 wt% AA induced significant collapse across the HAR sample. However, the 11 wt% AA induced minimal collapse of structures on the sample. Additionally, it is shown here that the freeze dry microscope remains feasible for a potential top-down decomposition profile.

Dual layer structures were attempted by the 3MT, 3HMMs, and 3MTf were evaluated as dual and gradient layers for higher aspect ratio pillars. The films were solution coated on pillars with aspect ratios of 11:1. The thermal treatment was conducted in a freeze drying microscope under two steps: Ramp 2°C to 80°C hold for 1 hour, and then followed by a ramp of 2°C/min to 250° and hold for 30 minutes to volatize any residual products. The initial low ramp rate was used to give time for the acid amplifiers to begin to thermal

degrade the top polyaldehyde layer followed by diffusion into the bottom-layer. Comparisons of the dual layers to the mono-layer is seen in Figure 7.13

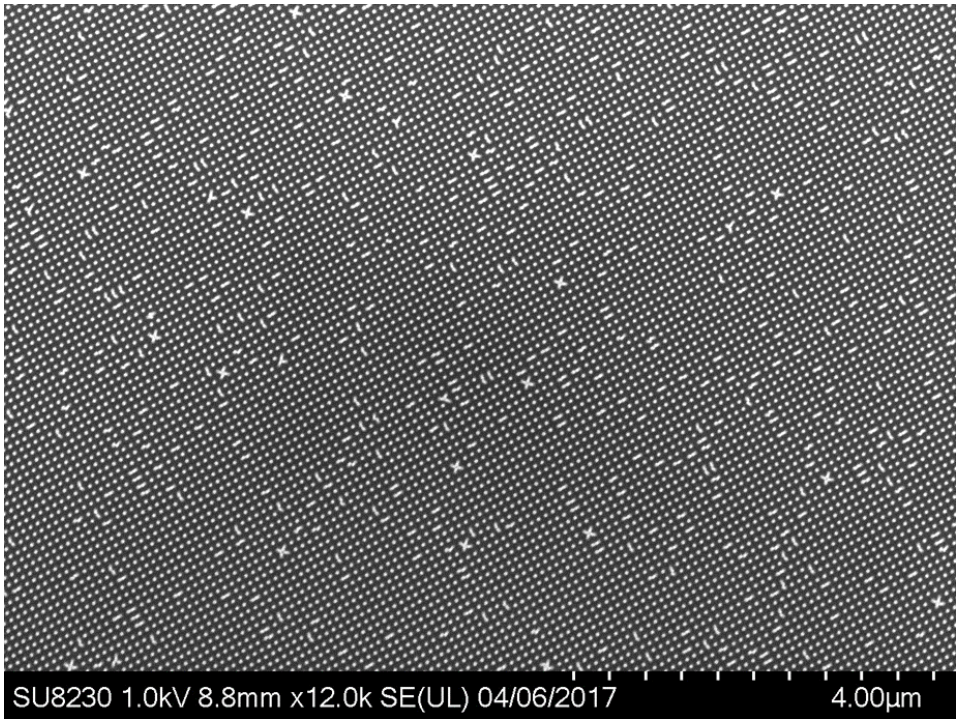

Figure 7.13 Representative SEM image of the thermal decomposition of anionic butyraldehyde copolymer mono-layer freeze drying microscope at 11:1 HAR pillars

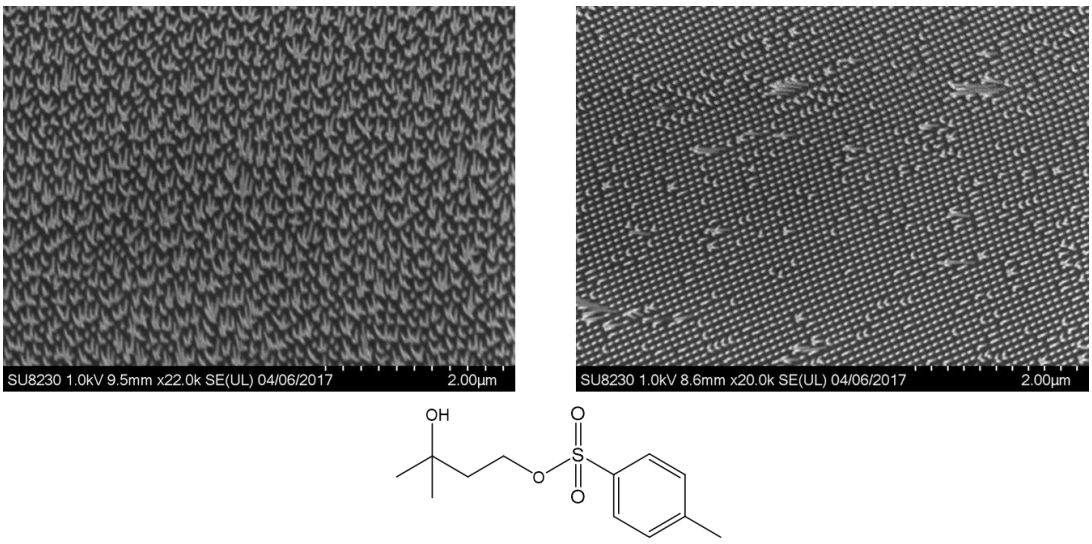

Figure 7.14 Representative SEM image of the thermal decomposition of anionic butyraldehyde copolymer dual layer with 3HT freeze drying microscope at 11:1 HAR pillars. Dual-layer on the left SEM image and gradient layer on the right SEM image.

It is evident in Figure 7.14, that the dual layer causes considerable more collapse of the HAR structures than the gradient layer. The 9:1 HAR structures were not sensitive enough to determine the difference. Therefore, gradient layers were only assessed up to this point. The following gradient layers were assessed with 3MTf and 3HMMs, both of which are have very volatile acid precursors which should not contribute substantially to residual products post-depolymerization. However, these two acid amplifiers caused moderate collapse of HAR structures as seen in Figure 7.15 and Figure 7.16.

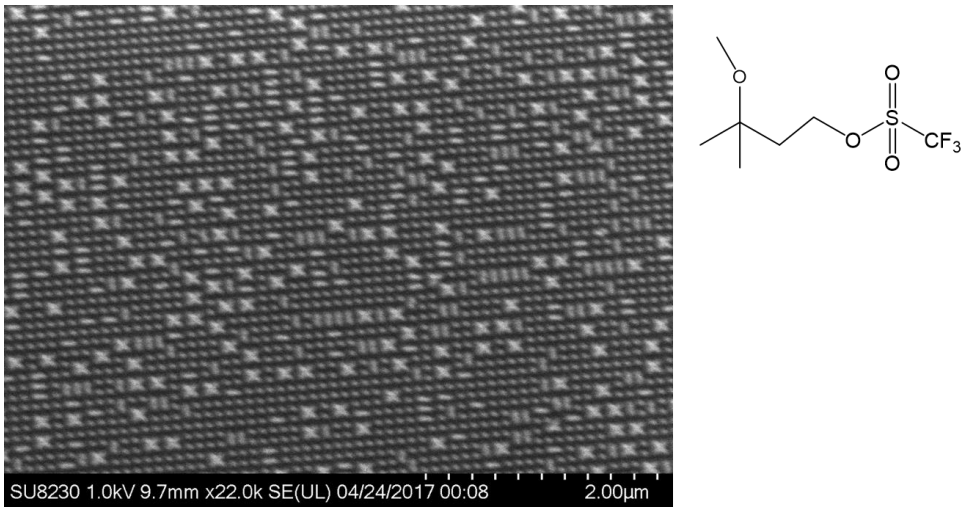

Figure 7.15 Representative SEM image of the thermal decomposition of anionic butyraldehyde copolymer dual layer with 3MTf freeze drying microscope at 11:1 HAR pillars

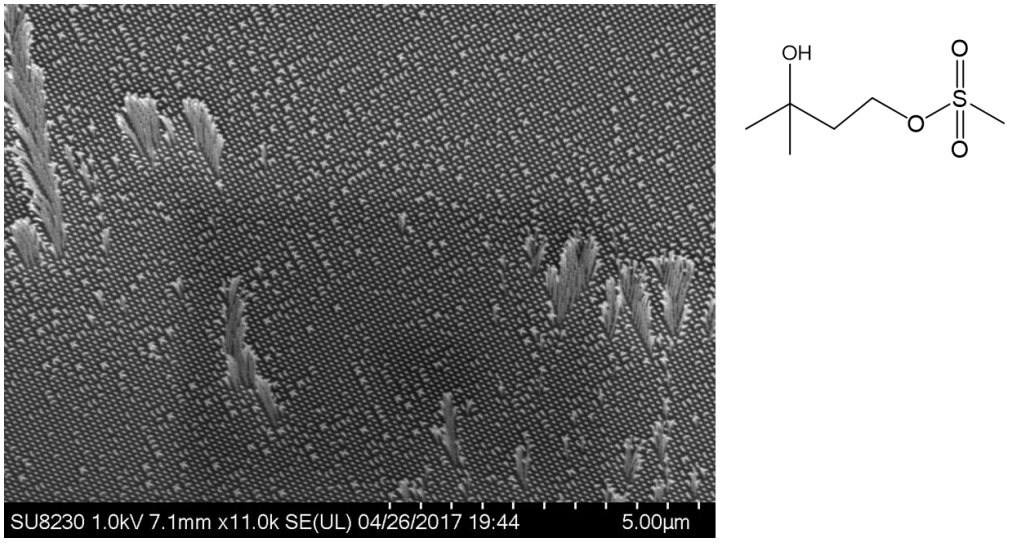

Figure 7.16 Representative SEM image of the thermal decomposition of anionic butyraldehyde copolymer dual layer with 3HMMs freeze drying microscope at 11:1 HAR pillars

7.3.1.2 Kinetics Study of the Copolymers

In general, the gradient layer films with anionic p(PHAco-BA) even with the volatile acid amplifiers of 3MTf and 3HMMs induced moderate pillar collapse of with the more sensitive 11:1 HAR structures. A kinetic study of the amplifiers must be done to understand the thermal process window between the accelerated acid-catalyzed depolymerization rate of the top-coat with acid amplifier against the purely thermal depolymerisation of the bottom-layer with no accelerant. Isothermal theromogravimetric analysis (TGA) was used to study the degradation rates with and without acid amplifier at 80^{o}C as shown in Figure 7.17.

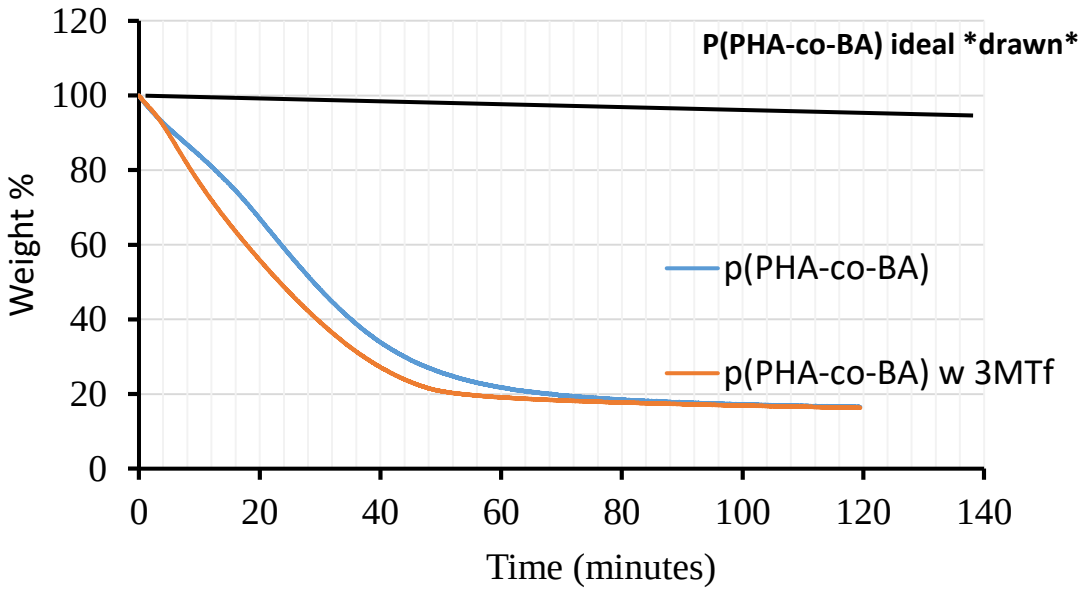

Figure 7.17 Isothermal TGA plot of p(PHA-co-BA) (14 kDa) with 3MTf and no 3MTf at 80°C

Then thermal stability of the anionic p(PHA-co-BA) is not ideal for dual layer structures. The p(PHA-co-BA) must be thermally stable in the temperature range where

the acid amplifier is thermally unstable and decomposes to an acid which can catalyse the depolymerisation of the p(PHA-co-BA) in the top-coat. The top-down depolymerizaiton profile cannot be achieved otherwise. It is evident from the TGA plot that this is a major contributor in the major collapse seen for the gradient layers as sacrificial bracing for the 11:1 HAR structures.

TGA analysis gives a representation of the thermal profile that occurs within the freeze drying microscope. However, the environment is considerably different than within the freeze drying microscope. The sample within the TGA warms from convection and conduction from the platinum pan under inert N_2. The freeze drying microscope heats the sample only through conduction from the heating stage under vacuum. Therefore, films were held isothermally at various temperatures within the freeze drying microscope where the thickness was monitored after 30 minute intervals with a profilometer to understand the kinetics as shown in Figure 7.18.

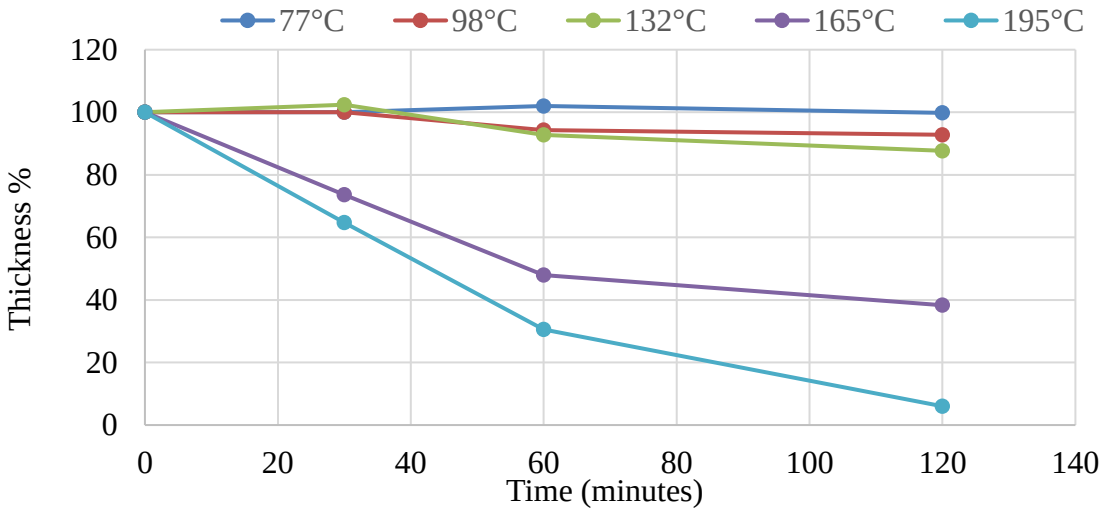

Figure 7.18 The change in the thickness of anionic p(PHA-co-BA) (Mw 34 kDa) films with time heated at various isothermal temperatures in the freeze dry microscope

As seen, the p(PHA-co-BA) is stable up to 132°C giving us our process window to trigger the thermal/acid amplifier in the top-coat to induce depolymerization. The p(PHA-co-BA) begins to depolymerize within one hour at 165°C and 195°C. Therefore, only thermal triggers that can decompose into acids at 135°C or lower are useful here. It is noted that the stability of p(PHA-co-BA) with a molecular weight of 34 kDa in Figure 7.18, is more thermally stable than p(PHA-co-BA) with a molecular weight of 14 kDa in Figure 7.17. The molecular weight is a contributing factor the overall thermal stability of the polymer. However, high molecular weight polymers are likely not ideal for filling the 50 nm gaps between each singular pillar on the HAR structure. TGA was ran on those two samples and is shown in Figure 7.19.

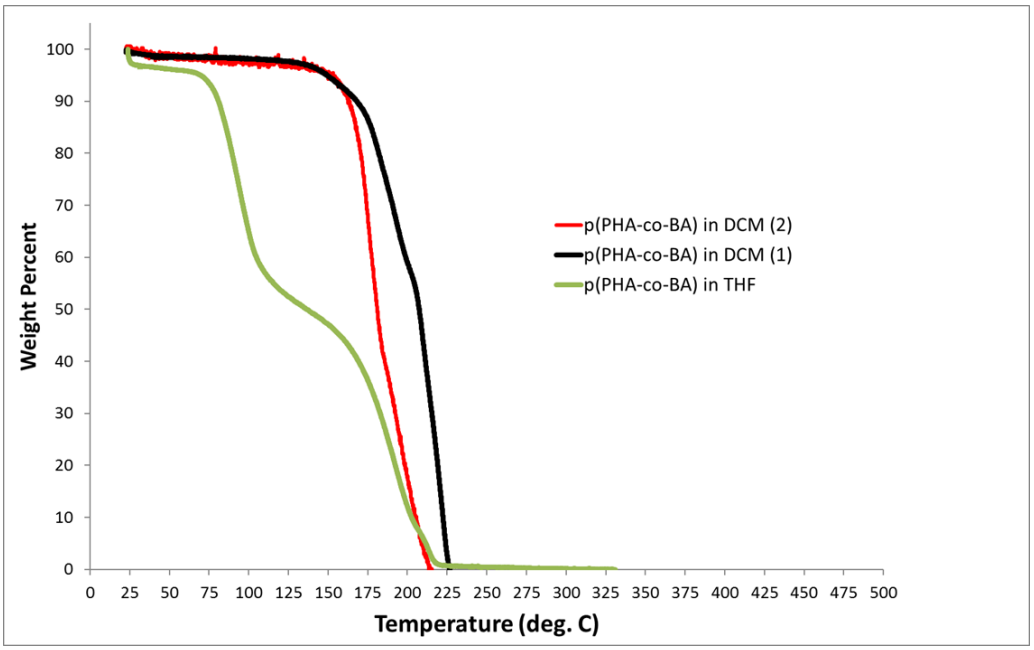

Figure 7.19 TGA plot of anionic p(PHA-co-BA) synthesized in DCM (34-38 kDa) vs THF (14 kDa)

The anionic p(PHA-co-BA) used in Figure 7.19 was synthesized in THF, while the p(PHA-co-BA) used in the other experiment was synthesized in DCM. It is unclear as to

the reason the thermal stability of anioic p(PHA-co-BA) out of the THF is much lower and exhibits a bimodal decomposition profile. This suggests that the termination of the end-groups were likely not sufficient in the THF sample or the particular anionic p(PHA-co-BA) has partially depolymerized over time in storage.

7.3.1.3 Evaluation of Cationic Polyaldehydes for Sacrificial Bracing Materials

The anionic synthesis of high, molecular weight polyaldehyde copolymers has previously shown to be difficult. Low molecular weight polyaldehyde copolymers are ideal for the sacrificial bracing materials of the HAR structures with 50 nm pitches. However, synthesizing reproducible butanal copolymers with high molar incorporation has proven difficult. Additionally, the low thermal stability of the anionic polyaldehydes can only afford a shelf-life of approximately 2 weeks within solution. Therefore, low-molecular weight cationic polyaldehyde copolymers were also assessed as sacrificial bracing materials. Cationic polyaldehyde copolymers have been previously documents to have shelf-life stability of over a year at ambient conditions. The thermal stability of a variety of copolymers was assessed by TGA analysis in Figure 7.20.

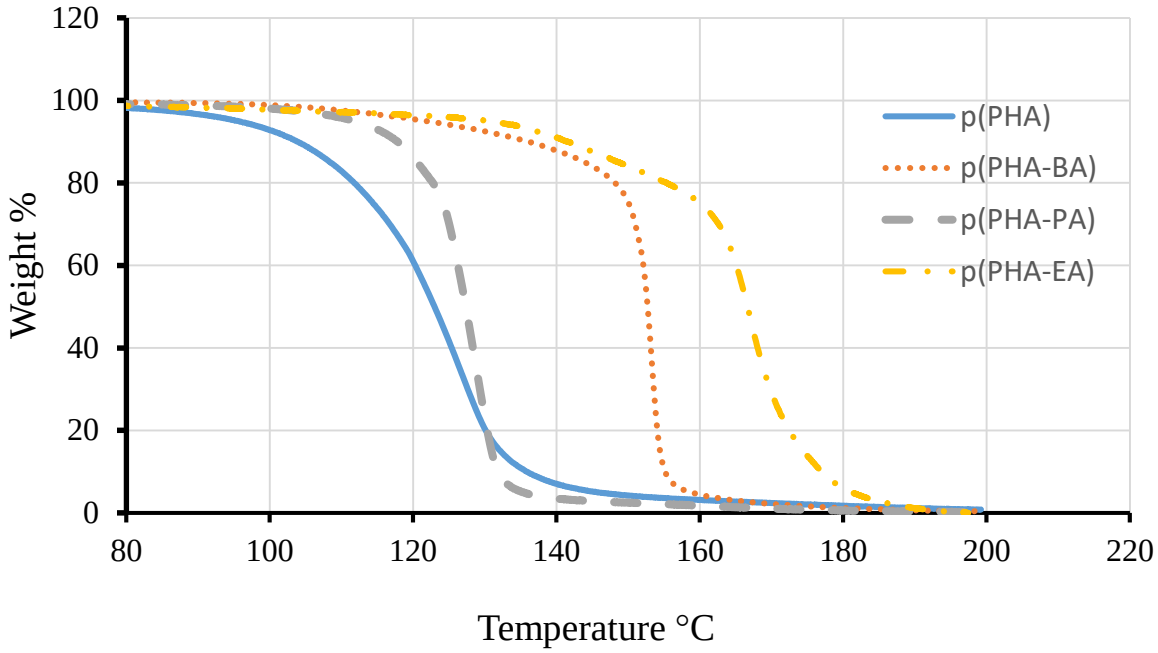

Figure 7.20 TGA Plot of various cationic polyaldehyde copolymers

The p(PHA-co-EA) had the highest thermal stability than the other copolymers. The thermal stability of the copolymer from polymer composition than molecular weight is unclear. However, p(PHA-co-EA) is believed to be the best copolymer as sacrificial bracing materials due to the highly volatile comonomer, ethanal, that boils at 20°C. The thermal stability was also evaluated by monitoring the decrease of film thickness instead the freeze dry microscope in Figure 7.21.

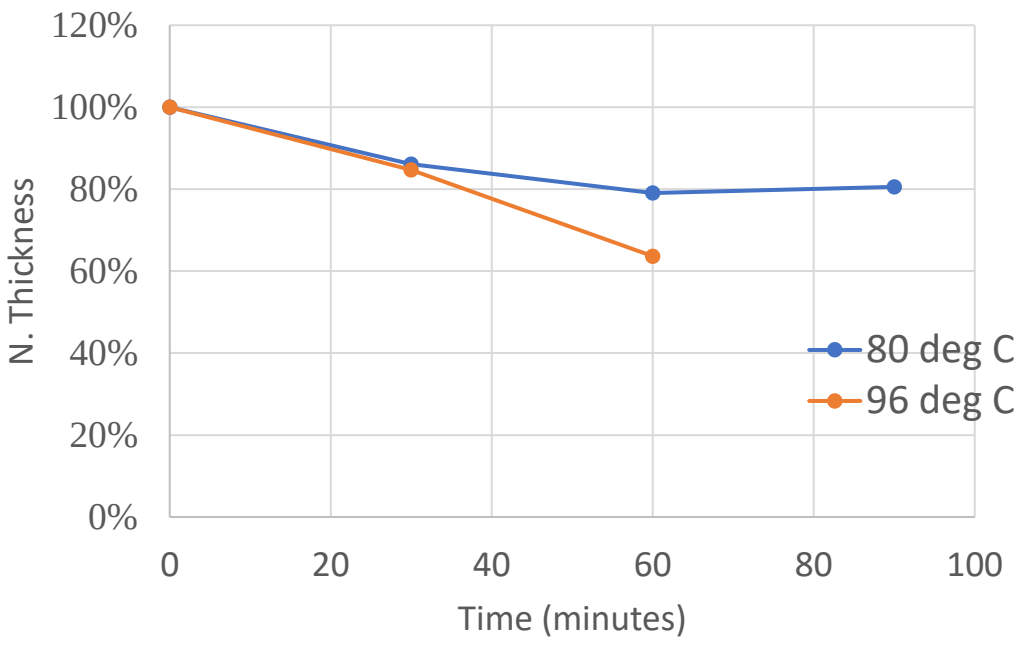

Figure 7.21 The change in the thickness of cationic p(PHA-co-EA) film with time heated at various isothermal temperatures in the freeze dry microscope

The p(PHA-co-EA) film was found to be stable at 80°C for 90 minutes. The initial decrease of the film thickness in the first 30 minute interval is likely due to possible variation in the measurement or solvent removal. The film appeared intact for the following hour. However, the film at 96°C was not stable and clearly began to depolymerize over the course of an hour as shown in Figure 7.22.

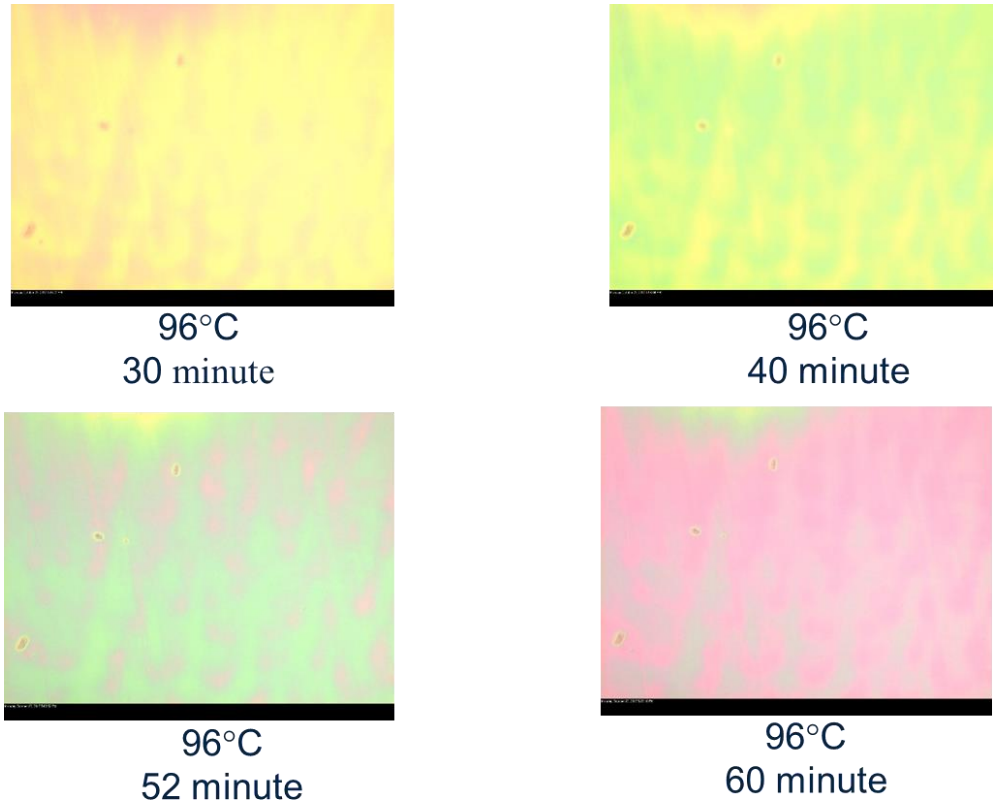

Figure 7.22 Microscope images of p(PHA-co-EA) film heated isothermally at 96° C at time intervals

The color change in the SEM images of the p(PHA-co-EA) film after time intervals at 96°C is the based on the refractive index of the polymer as the thickness decreases from polymer degradation. In conclusion, the thermal process window to induce depolymerisation of the top-layer must be at or below 80°C. The thermal acid generator (TAG-MS) such as 4,5-dimethoxy-2-nitrobenzyl methanesulfonate was used to initiate depolymerization of the top-layer. The TAG-MS was found to initiate depolymerization of polyaldehyde films as low as 60°C.

Gradient cationic p(PHA-co-EA) films were solution coated on pillars with aspect ratios of 11:1. The thermal treatment was conducted in a freeze drying microscope with a single ramp of 30°C/min to 80°C and held for 3 hours to volatize any residual products.

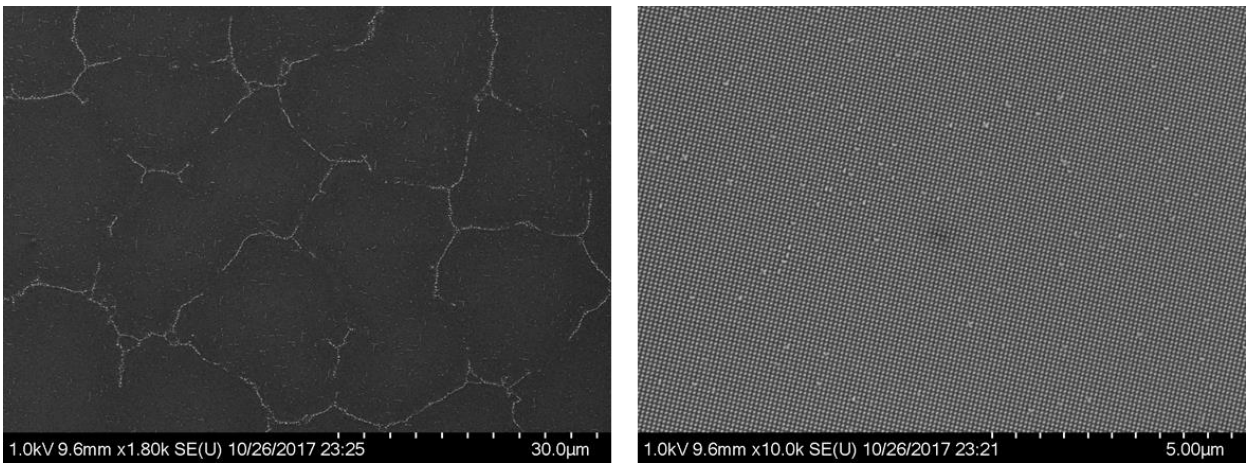

Figure 7.23 SEM image of HAR structure after thermal treatment of gradient Layer for cationic p(PHA-co-EA) with TAG-MS

As seen from the SEM images from Figure 7.23, the gradient film of using p(PHA-co-EA) and TAG-MS produced the best results for the 11:1 HAR structures with minimal collapse. However, it is noted that the low magnification SEM image suggests that dewetting is occurring with the films form the visual appearance of connected lines of collapsed pillars.

7.3.2 Triggered Depolymerization of Transient Printed Wiring Boards

A representative electronic component, i.e. a multilayer, interconnect board, was fabricated using a cyclic p(PHA) substrate that was designed for triggerable transience through the addition of a photo-acid generator (PAG). The p(PHA) material was used to

fabricate the dielectric that acts as the support substrate for the metal routing layers, where the conductive 'wiring' was composed of a silver nanoparticle-filled p(PHA) formulation. Interlayer routing was achieved through the use of vias, which were cut using an IR laser with the aid of a mask to properly align the via pattern. The final multilayer, interconnect board was manufactured layer-by-layer to ensure sufficient connectivity between routing layers during each stage of assembly. Physical properties (elastic modulus, resistivity, etc.) of the individual material components were evaluated and complete transience was demonstrated.

The physical properties of the component materials can be organized into two topics of interest: (1) the dielectric properties of the layer substrate and (2) the electrical properties of the printed wiring. Those measured values ultimately determine the applicability of these materials for use in the fabrication of electronic devices. Long strips of the polymer substrate were prepared as described in the Experimental Methods section. Polymer films of different molecular weights and both unfilled and filled with glass fibers were evaluated. Data from a typical analysis is presented in Figure 7.24

Not unexpectedly, the measurements showed that higher molecular weight polymers produced higher modulus polymer. The best measured modulus values were obtained from polymers with molecular weights between 90 and 130 kDa, which produced values that ranged from 0.5 to 0.7 GPa. Furthermore, the addition of glass fibers were also shown to increase the values obtained from the lower molecular weight by 90-120%, but seemed to offer only modest increases for the higher molecular weight polymers. While significantly lower than the Young's modulus of FR4 (23 GPa), these values compare quite favorably to the values for polypropylene and polyimide, 1.3 and 2.5 GPa, respectively.

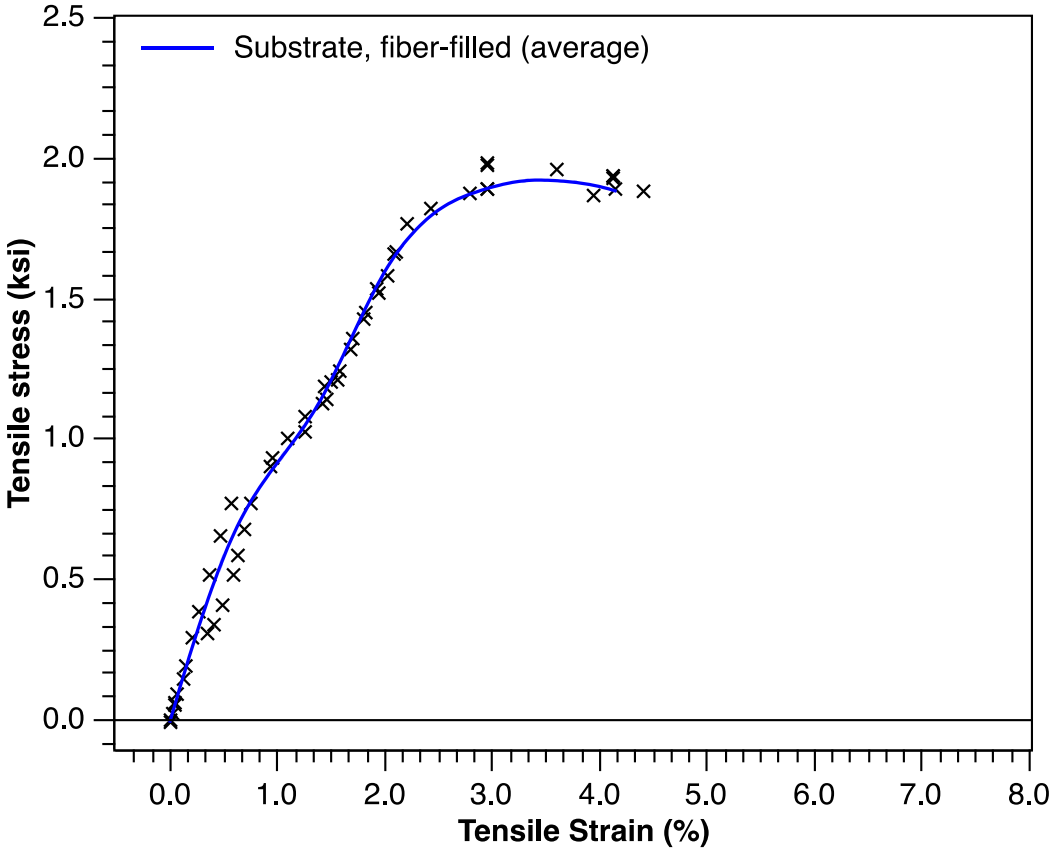

Figure 7.24 Young's Modulus Analysis. Typical results from a dynamic mechanical analysis to determine the Young's Modulus of the polymer substrate.

The dielectric properties of the film were also determined by measuring the capacitance and dissipation factor of the polymer substrate layer using conductive discs printed onto the film as electrodes, as described in the Experimental Methods section. The relative permittivity was calculated using these measured capacitance values and the capacitance value for a representative vacuum-filled space of similar dimensions. The average dissipation factor was measured at 0.033 and the average relative permittivity was calculated to be 9.1. This compares to FR4, which has a dissipation factor of 0.017 and a relative permittivity of 4.4.

A thin film was prepared on plain FR4 board using the conductive (Ag-filled polymer) formulation. Once dry, the thickness of the film was measured and the average was 13 μm. The sheet resistance was measured and the average was found to me 62 mΩ square-1. Using these values, the average resistivity was calculated to be 7.8 x 10^{-7} Ω m, while the resistivity of pure silver is 1.59 x 10^{-8} Ω m. Other metals that have previously been used as conductive materials in transient electronic devices have included magnesium, tungsten, and molybdenum which possess resistivity values of 4.39 x 10^{-8}, 5.28 x 10^{-8}, and 5.34 x 10^{-8} Ω m, respectively[114,115].

The conductivity of the metal wiring printed on a polymer substrate was also measured using the LCR-800 instrument configured for two probe operation. While it is understood that more accurate measurements can be made using a four-point probe array, the dimensions of the printed wiring deposited on a polymer substrate were not conducive to that method. The resistance of printed lines of various lengths were measured and using the lengths, widths and thicknesses of those lines, values for the sheet resistance and resistivity were calculated. The average sheet resistance and resistivity were 26.9 mΩ/square and 1.1 x 10^{-6} Ω m, respectively. The values are comparable to the values obtained from the standalone film and, while somewhat higher than that for pure silver, the materials are still suitable for use in the fabrication of electronics with the desired transient properties.

7.3.2.1 Fabrication of Printed Wiring Board

The multilayer board fabricated in this report consisted of two substrate layers with three metal layers. For each substrate layer, a film of the p(PHA) polymer with dimensions

of approximately 7 x 7 cm was prepared by casting an appropriate amount of polymer-only formulation onto a piece of prepared Cu:FR4 board using the doctor blade technique (see Experimental Methods). Each prepared polymer substrate was of a size that could accommodate four 1.5 x 1.5 cm board substrate layers in a 2x2 (four up) arrangement. The drying process generally took approximately 23 hours after which the film substrates were stored in a refrigerator until the next step in the fabrication process.

Vias were cut through each polymer substrate layer using a CO2 laser and a stainless steel mask ~102 μm in thickness to align the vias in their proper location. In addition, a perforated outline was cut around each board layer, which was used to cut the completed multilayer boards free from the extraneous surrounding polymer substrate. Lastly, four guide holes were also cut through each substrate layer, which were used to align the layer when depositing the metal wiring and during final assembly of the multilayer board. An example layout is shown in Figure 7.25.

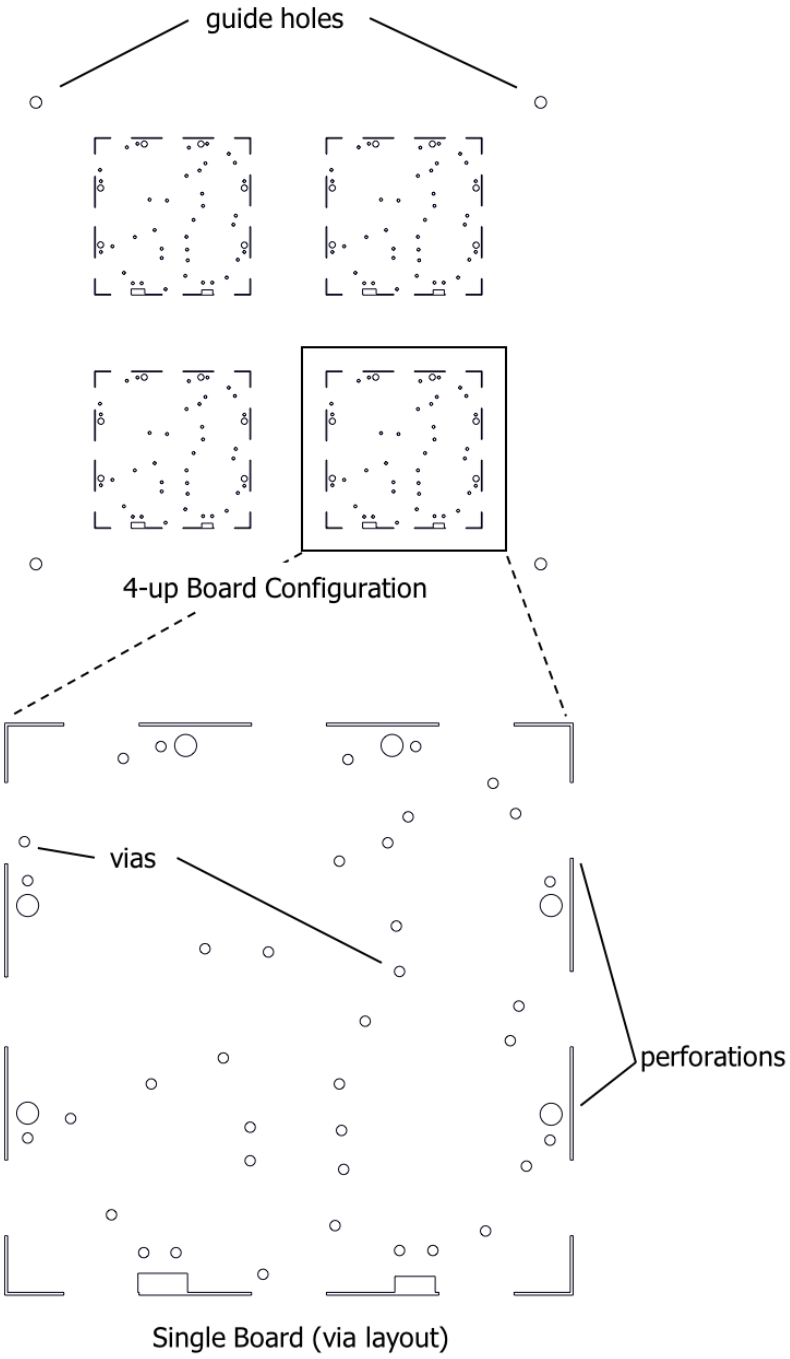

Figure 7.25 Typical Stencil Mask for Vias. Layout pattern and detail of a single board that was used to create the vias stencil mask.

After the vias have been laser cut, 1 mm diameter holes were drilled through the Cu:FR4 support at the positions where the guide holes had been laser cut in the polymer

substrate. These holes were used to support the film-on-Cu:FR4 in a jig with guide posts. Those guide posts allow for the proper alignment of stencils and materials during the remainder of the fabrication process. The fabrication of each metalized board layer is illustrated in Figure 7.26.

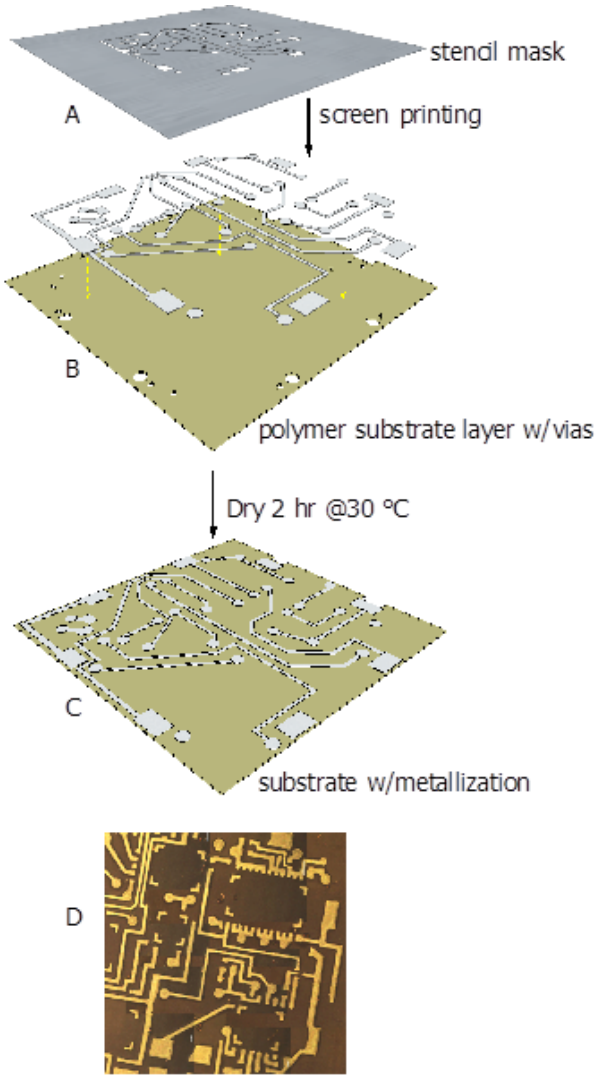

Figure 7.26 Fabrication of Metalized Layer (illustration). (A) Stencil mask directs deposition of Ag-filled formulation to form conductive traces (B), which are bonded to polymer substrate layer after drying (C). Example of printed wiring on polymer substrate is shown in (D).

For each metal layer, a stainless steel stencil, 76 µm thick, was laser cut with the desired wiring diagram. This was used as a mask to direct and control deposition of the conductive, Ag-filled formulation. In addition, the stencil mask was aligned over the laser cut vias by placing it over the guideposts in the support jig. The appropriate metal wiring diagram was then printed onto its corresponding polymer substrate layer using the screen printing technique to form the electronic pathways.

After printing the metal wiring, each printed polymer substrate layer was first dried in the microwave for 1-2 hours at 30 °C and then removed from its Cu:FR4 support as described in the Experimental Methods section by soaking in a dilute solution of ammonium persulfate. The reaction of the copper layer with the ammonium persulfate converts the copper metal to soluble copper ions thereby releasing the polymer substrate from the underlying support. The now free printed polymer layers were allowed to dry overnight and, to ensure that the layers remained flat while drying, each was placed on a support jig where the guideposts would kept the layer stretched taut.

After drying, the non-printed side of each printed layer was inspected to ensure that the vias were sufficiently filled with the conductive formulation. If necessary, addition formulation was added to the vias to form a larger pad such that electrical continuity between layers where needed was assured. The complete multilayer board was assembled by laminating the two layers together, as illustrated in Figure 7.27.

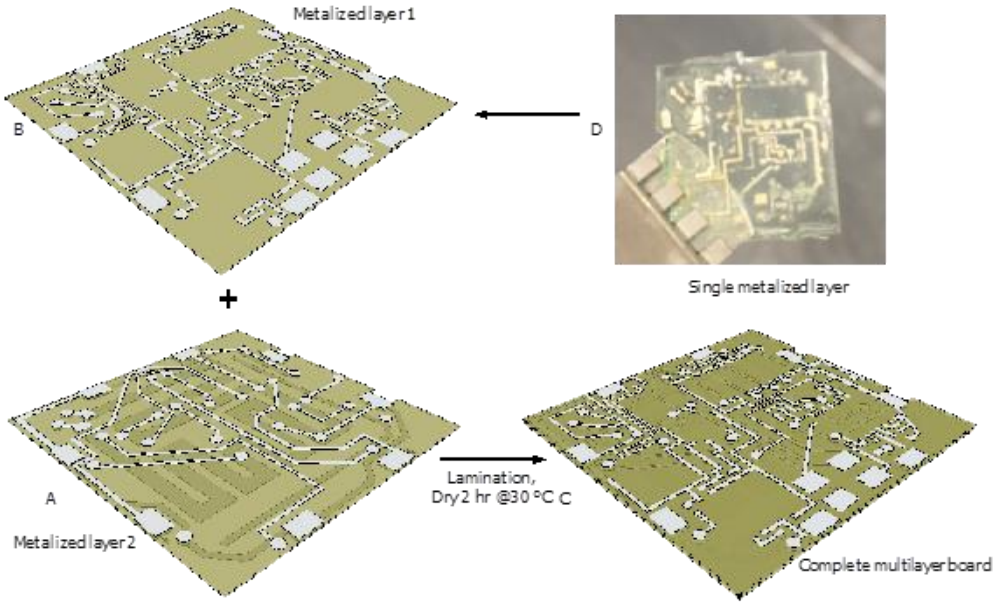

Figure 7.27 Final Assembly of Multilayer Board (illustration). (A) and (D) A thin coat of NMP is sprayed onto the first metalized layer to which is added the second metalized (B). The two layers are gently pressed together and then dried to complete the lamination process to form the multilayer board (C).

The lower layer was placed in the support jig and then a thin layer of the NMP solvent was applied to that layer. The upper layer was then aligned over the lower layer using the guideposts in the support jig and gently pressed to the lower layer ensuring even contact across the entire surface. The laminated layers were dried in the microwave for 1-2 hours at 30 °C.

A demonstration multilayer board is shown in Figure 7.28A with the detail of the surface and internal (middle layer) printed wiring shown in Figure 7.28B. This detail of the multilayer board is of a board that has partially depolymerized. While not clearly seen in this photo, cracks in the printed wiring are evident.

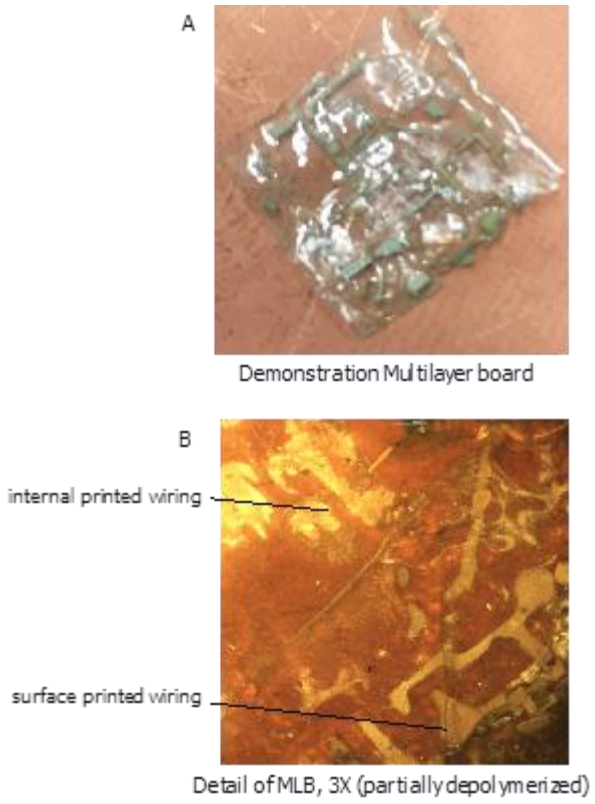

Figure 7.28 Demonstration MLB. (A) Complete demonstration multilayer board with the (B) detail of the surface and internal printed wiring in a partially depolymerized MLB.

7.3.2.2 Accelerated Transience of Printed Wiring Board

The transience properties of the polymer was evaluated in two ways: (1) temperature ramp from 70 °C to 175 °C and (2) at constant temperature of 120 and 140 °C. Both the homopolymer and the copolymer (90% phthalaldehyde/10% butyraldehyde) were evaluated with and without the addition of the acid amplifier. The results from the temperature ramp experiments for the homopolymer and the copolymer are shown in Figure 7.29 and Figure 7.30, respectively.

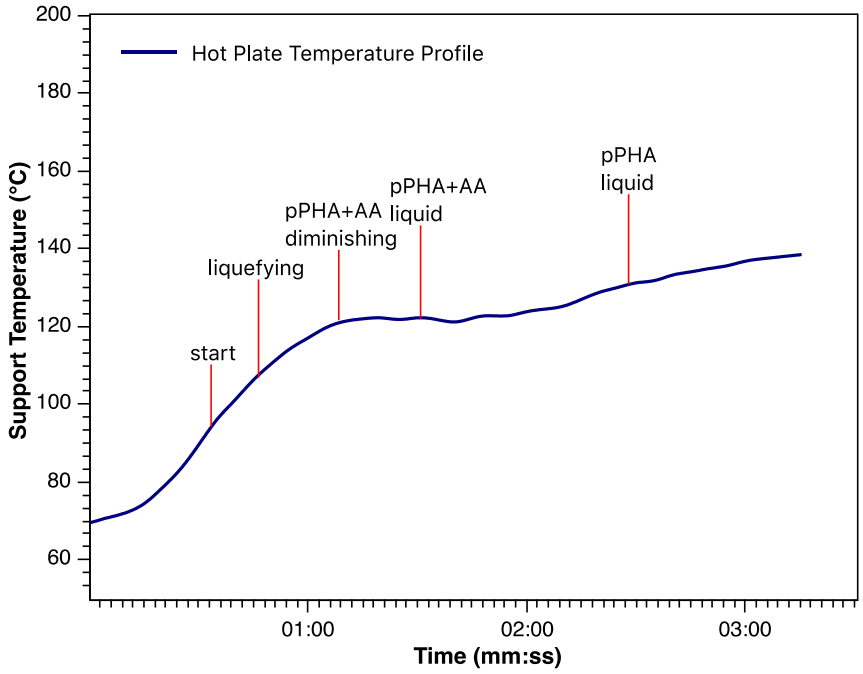

Figure 7.29 Cationic PPHA with 3 wt% acid amplifier

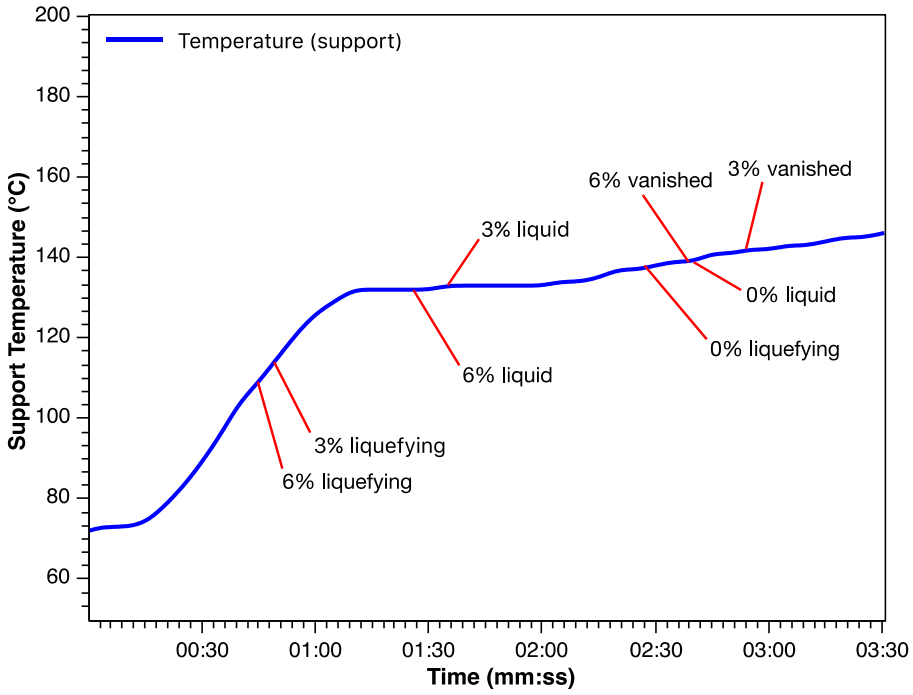

Figure 7.30 Cationic p(PHA-co-BA) with 3 pphr and 6 pphr of an acid amplifier

For the homopolymer, the addition of acid amplifier at 3 wt% significantly reduces time to complete transience after reaching trigger temperature. While the copolymer, without an acid amplifier, initiates at a higher temperature than the homopolymer it liquefies and evaporate faster than homopolymer. The addition of the acid amplifier at 3 and 6 wt% catalyze liquefaction and significantly lowers the triggering temperature for the materials.

Table 8 Transience times at constant temperature

Polymer Composition	120 °C	140 °C
copolymer (PHA-BA)	>7 min	3 min, 30 sec
copolymer (PHA-BA) + 3 wt% AA	2 min, 45 sec	70 sec
copolymer (PHA-BA) + 6 wt% AA	2 min, 30 sec	83 sec
homopolymer (PHA)	>10 min	3 min, 40 sec
homopolymer (PHA) + 3 wt%AA	~6 min	1 min, 40 sec

Pulse heating was also evaluated to determine the minimum thermal energy requirement to induce depolymerization of PPHA. Two homopolymers, PPC and PPHA, were tested to determine how they respond to brief exposures to heat. Both polymers contained approximately 7 wt% catalyst (acid amplifier), respectively. The hot plate was set at 160 °C. Samples were placed on the hot surface at 150 °C and then removed after the requisite time. It should be noted that the Si wafer alone requires 20-24 seconds to reach 150 °C. In all tests, the PPC softened but did not liquefy (depolymerize). However, the results indicate that only an 8-sec pulse is required to trigger the catalyst-loaded PPHA. The observations for increases exposure times for the pPHA homopolymer are listed in Table 9.

Table 9 Pulse times and observations of degraded PPHA films with 3wt% acid amplifier

Pulse Time (s)	Observations
4	Polymer softened
6	Polymer partially liquefied
8	Polymer liquefied
12	Polymer liquefied, started to evaporate, dry
20	Polymer liquefied, evaporating but drying and baking
30	Polymer liquefied, evaporating but drying and baking

Furthermore, there was evidence that depolymerization had continued after 18 hours as the materials showed additional discoloration over that time period.

APPENDIX A. PHOTO-INDUCED ELECTRON TRANSFER ANALYSIS

A.1 Cyclic Voltammograms of Photosensitizers

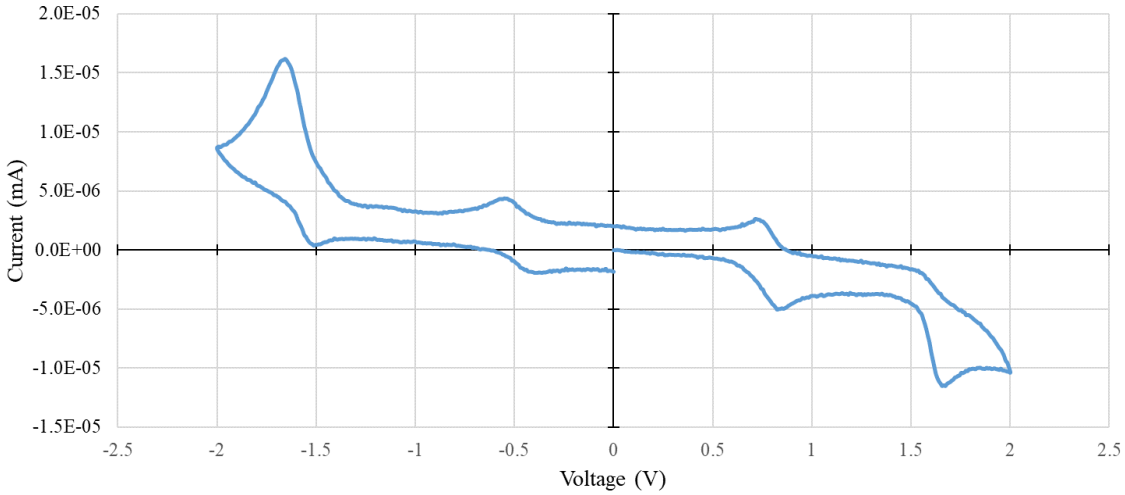

Fig A1. Cyclic voltammogram of anthracene in DMF solution. Ferrocene was used as an internal reference with an oxidation potential at 0.77 V. Anthracene has two reversible reduction potentials at –0.47V and -1.58 V and an oxidation potential at 1.59 V

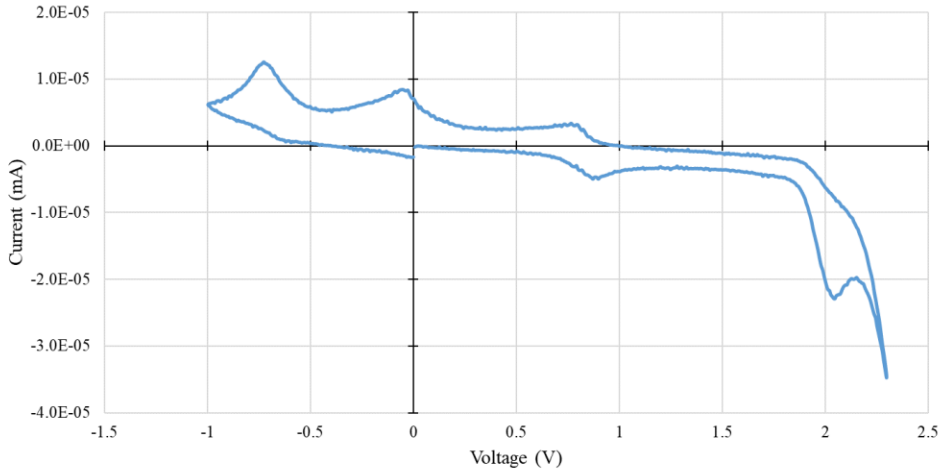

Fig A2. Cyclic voltammogram of CPTX in DMF solution. Ferrocene was used as an internal reference with an oxidation potential at 0.83 V. CPTX has two reversible reduction potentials at 0.04V and -0.64 V and an oxidation potential at 1.95 V.

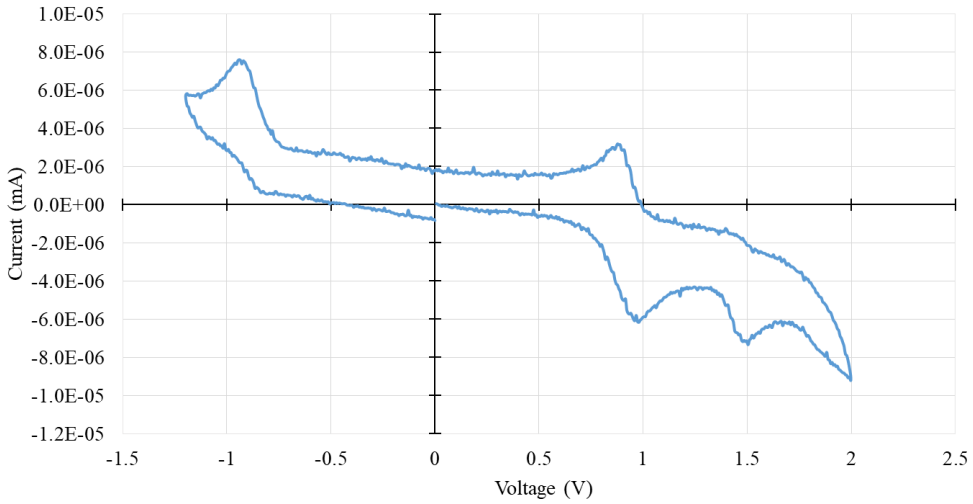

Fig A3. Cyclic voltammogram of DMBA in DMF solution. Ferrocene was used as an internal reference with an oxidation potential at 0.93 V. DMBA has a reversible reduction potentials at -0.88 V and an oxidation potential at 1.42 V.

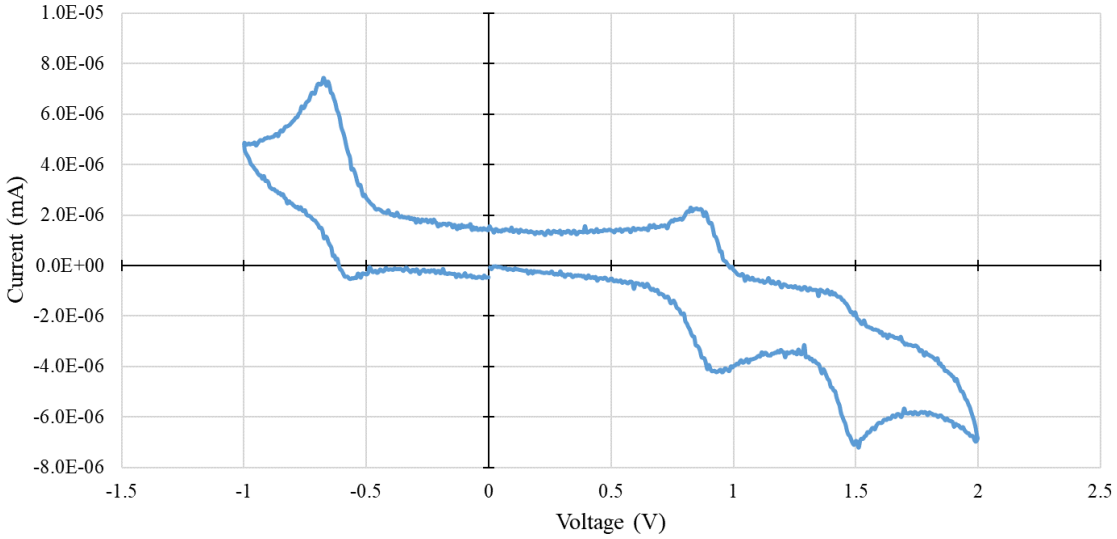

Fig A4. Cyclic voltammogram of BPET in DMF solution. Ferrocene was used as an internal reference with an oxidation potential at 0.89 V. BPET has a reversible reduction potentials at -0.62 V and an oxidation potential at 1.43 V.

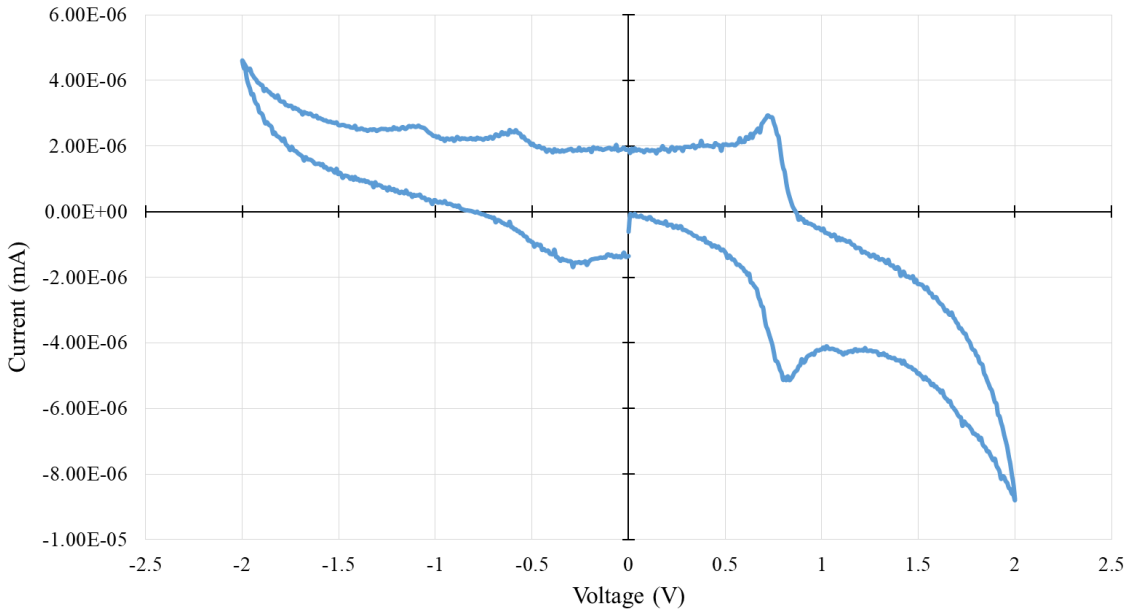

Fig A5. Cyclic voltammogram of BPEP in DMF solution. Ferrocene was used as an internal reference with an oxidation potential at 0.77 V. BPEP has a reversible reduction potential at -1.04 V and an oxidation potential at 1.08 V. Note that the additional reduction potential is a verified impurity.

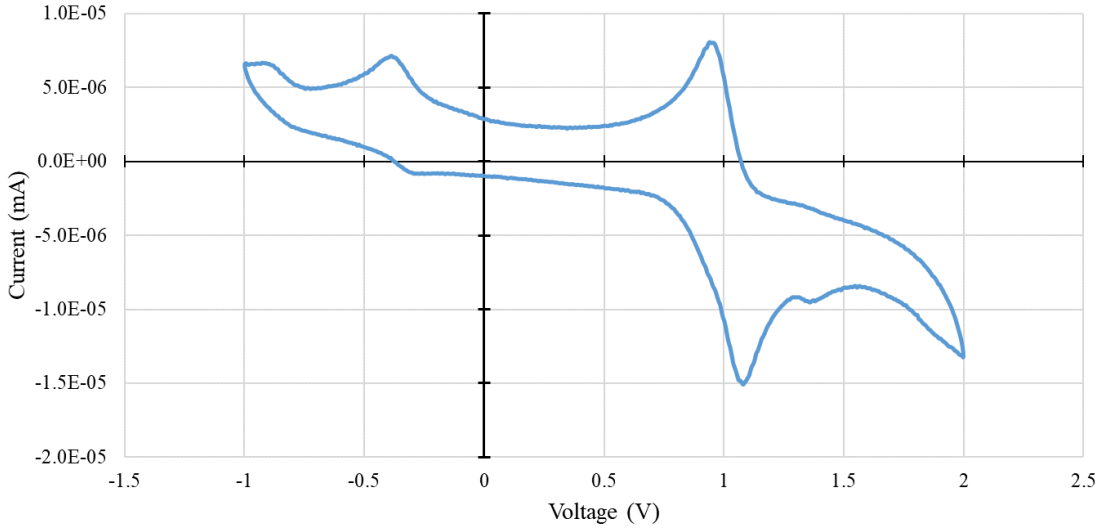

Fig A6. Cyclic voltammogram of BTMP in DMF solution. Ferrocene was used as an

internal reference with an oxidation potential at 1.02 V. BTMP has a reversible reduction potential at -0.34 V and an oxidation potential at 1.33 V.

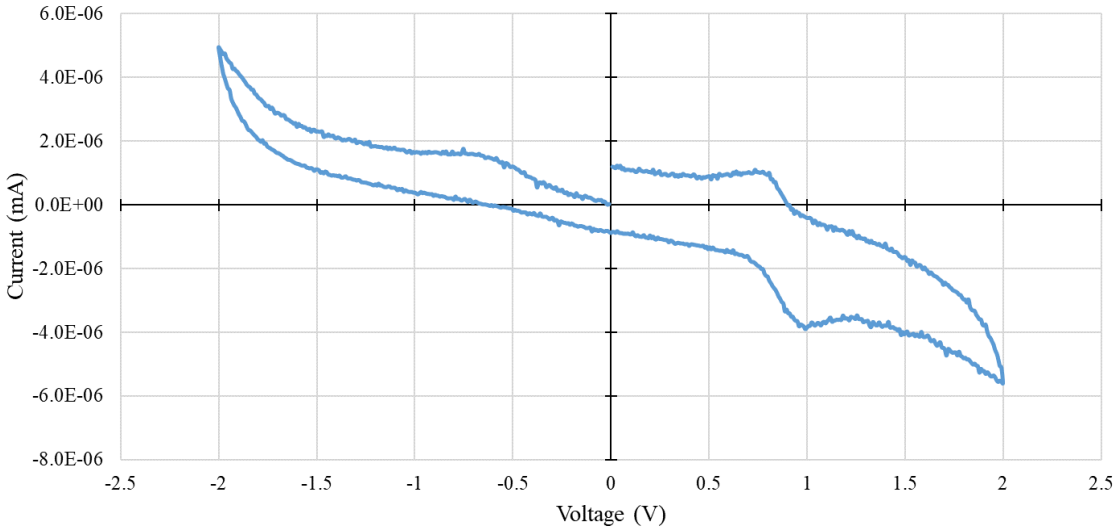

Fig A7. Cyclic voltammogram of FABA-PAG in DMF solution. Ferrocene was used as an internal reference with an oxidation potential of 0.99 V. FABA-PAG has an irreversible reduction potential at -0.43 V

A.2 Fluorescence Lifetime Decay of Photosensitizers

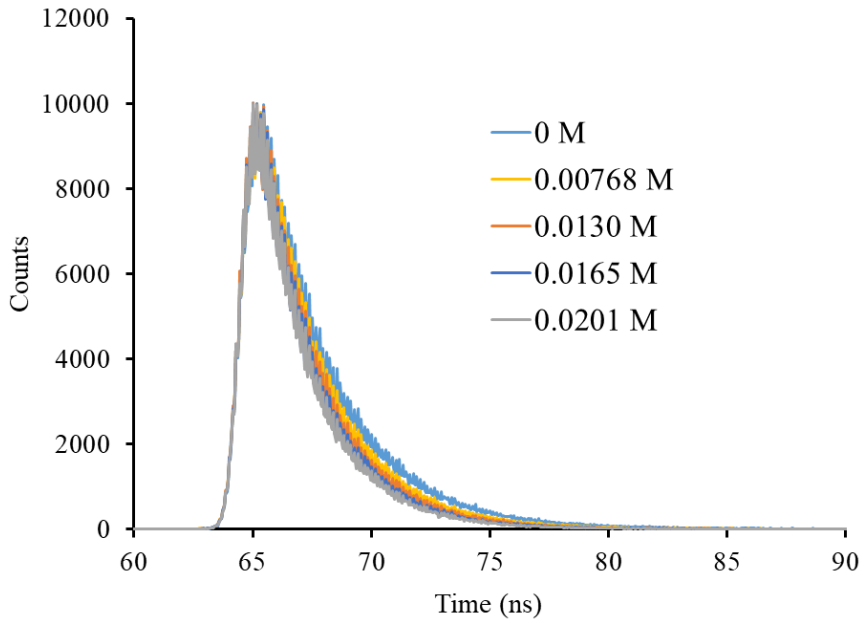

Fig A8. The effects of various concentrations of FABA-PAG on the fluorescence lifetime decay of anthracene. Fitted to a mono-exponential decay with $2.097 < \chi 2 < 2.198$

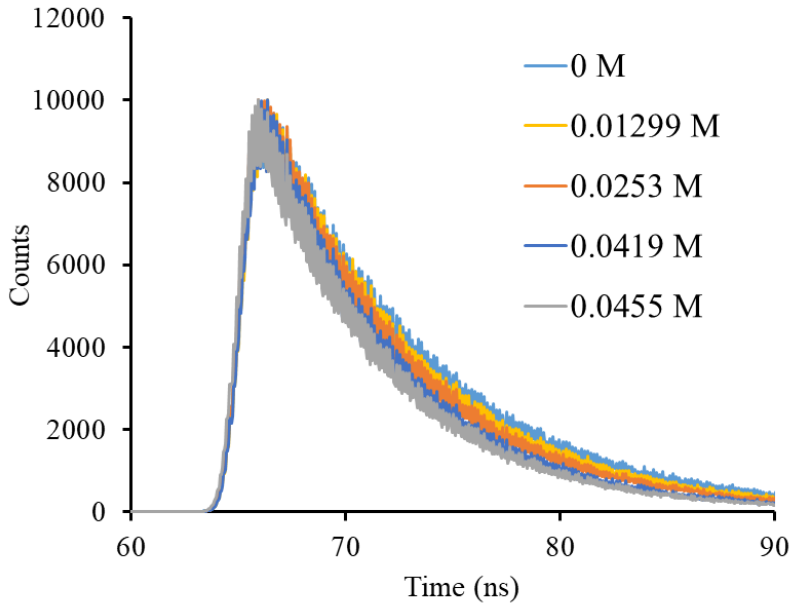

Fig A9. The effects of various concentrations of FABA-PAG on the fluorescence lifetime decay of BPET. Fitted to a mono-exponential decay with $3.178 < \chi^2 < 3.751$

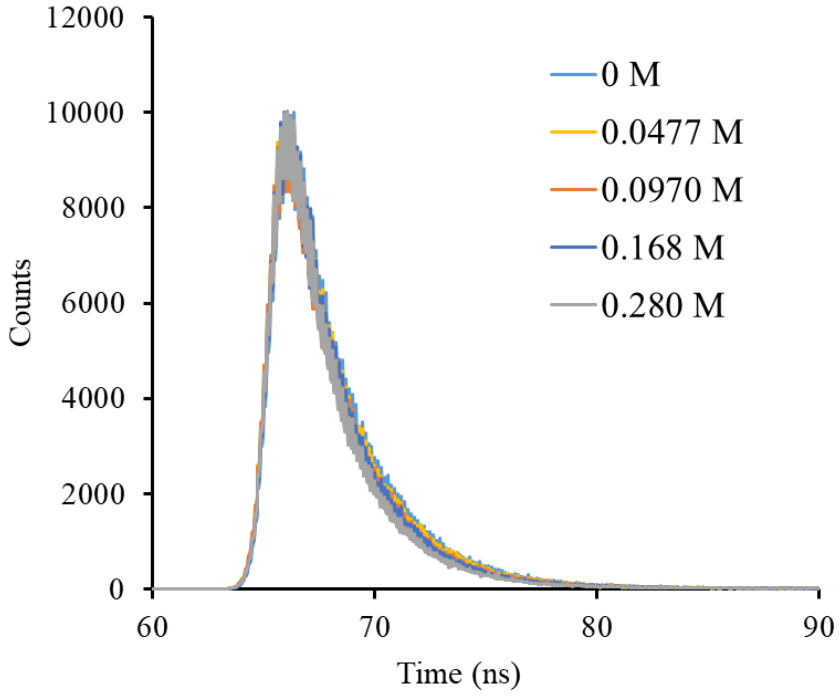

Fig A10. The effects of various concentrations of FABA-PAG on the fluorescence lifetime decay of BTMP. Fitted to a monoexponential decay with $2.45 < \chi^2 < 2.64$

A.2 Contrast-Curve Efficiency (Ecc)

The contrast-curve efficiency (Ecc) was developed as a method to compare the effectiveness of PET reactions between sensitizers in decomposable polymer films. Ecc measurements in this study is defined as the number of photo-active compounds divided by the number of absorbed photons in a unit volume space of PPC from the D_{100} region. Equivalent loadings of PAG and development time provides direct comparison between sensitized samples. In this case, the development method is a post-exposure bake where the PPC films are held at 100 ℃ for 7 minutes.

A description of the calculation is described below:

$$\text{Ecc} = \frac{\text{Number of PAC molecules}}{\text{Number of Absorbed Photons from } D_{100}}$$

$$\text{Number of PAC compounds} = \text{pphr PAC (solids)} \times \frac{\text{FT x Exp Area x } \rho}{\text{PAC Mw}} \times N_A$$

PAC = photo-active compounds, PAG or Sensitizer depending on absorption wavelength

Where, pphr PAC = % of PAC loading relative to polymer solids

PAC MW= Molecular weight of PAC (g/mol)

FT = Film Thickness (cm)

Exp. Area = Exposure area (1 cm^2)

Na= Avogadro's number (mol^{-1})

ρ = density of film (g/cm^3)

$$\text{No. of Absorbed Photons} = \frac{\text{Min. Energy to Expose Through Film}}{\text{Energy of a single photon}} \times \text{Fraction of Absorbed Light}$$

$$\text{No. of Absorbed Photons} = \frac{D_{100} x\ \lambda}{hc} \times (1 - 10^{-a \times FT})$$

Where D_{100} is the minimum dosage required to expose through an entire film

h =Planck's constant (J s)

c = speed of light (cm/s)

λ = Exposure wavelength (cm)

FT= Film Thickness (μm)

a = absorption coefficient (μm^{-1})

The photo-active compound is a general term that is described as the FABA-PAG or modified PAHs, depending on the exposure wavelength of interest. For unsensitized film, the FABA-PAG was used. For sensitized films, the modified PAHs and their corresponding molecular weights were used. Films were spin-coated onto quartz wafers for UV/vis measurements where the absorbance and film thickness were recorded to calculate absorption coefficients at exposure wavelength. A summary for the Ecc calculations is collected for the PAG and sensitizers are recorded in Table A1.

Table A1 Contrast-Curve Efficiency Calculations for sensitized PPC films. PPC films all contained 3 pphr PAG and a PS to PAG molar ratio of 1.2:1 for sensitized films.

	PAG only	Anthracene	CPTX	DMBA	BPET	BTMP
Wavelength (nm)	248	365	365	500	560	650
Absorption Coeff (μm^{-1})	0.070	0.011	0.021	0.098	0.081	0.016
D_{100} (mJ/cm^2)	35.7	432.5	573.4	283.6	269.8	6179.5
Transmittance	0.73	0.95	0.91	0.64	0.69	0.93
Dose absorbed (mJ/cm^2)	9.24	20.92	48.85	97.15	79.56	408.27
No. of Photons /cm^2	1.2E+16	3.8E+16	9.0E+16	2.4E+17	2.2E+17	1.3E+18
No. of PAC	4.8E+15	5.1E+15	5.0E+15	5.0E+15	5.2E+15	5.0E+15
Photons/PAC	2.40	7.56	17.87	48.52	43.49	265.91
PAC/photon "E_{cc}"	0.42	0.13	0.056	0.021	0.023	0.004

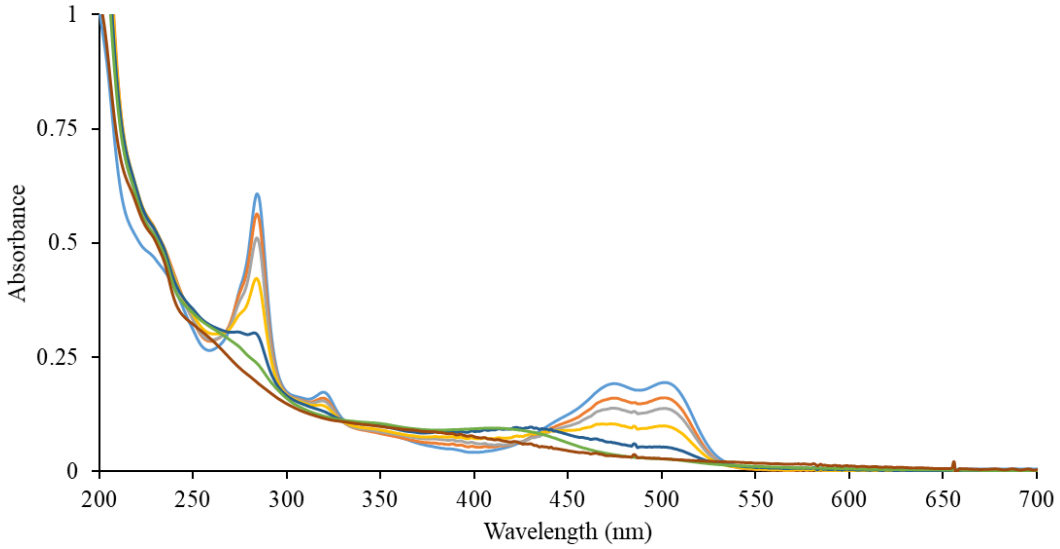

Fig A11. UV-vis absorbance of PPC film with 3pphr PAG and DMBA exposed to 500 nm light at various time increments.

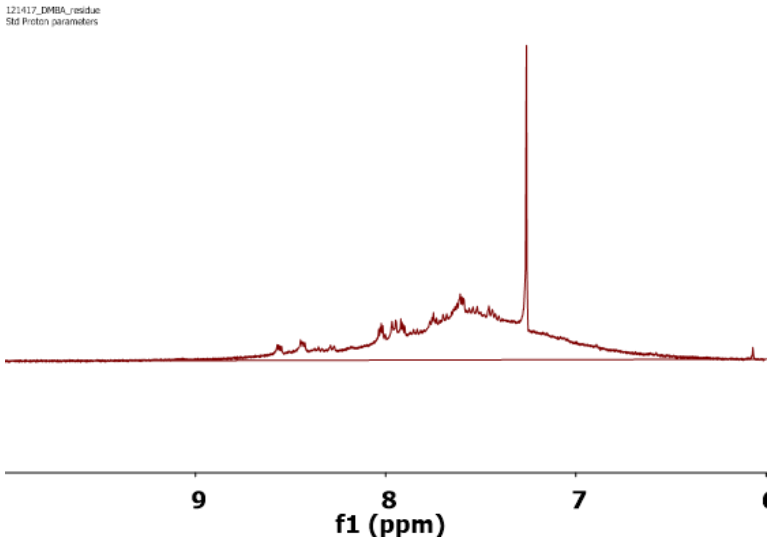

Fig A12. ^{1}H-NMR analysis of residue after full sunlight-induced depolymerization of PPHA film with 10 pphr PAG and DMBA.

REFERENCES

(1) Chan, K.; Gleason, K. K. Air-Gap Fabrication Using a Sacrificial Polymeric Thin Film Synthesized via Initiated Chemical Vapor Deposition. *J. Electrochem. Soc.* **2006**, *153*, C223.

(2) Wu, X.; Reed, H. a.; Wang, Y.; Rhodes, L. F.; Elce, E.; Ravikiran, R.; Shick, R. a.; Henderson, C. L.; Bidstrup Allen, S. A.; Kohl, P. a. Fabrication of Microchannels Using Polynorbornene Photosensitive Sacrificial Materials. *J. Electrochem. Soc.* **2003**, *150*, H205.

(3) Hua, Y.; Henderson, C. Photodefinable Thermally Sacrificial Polycarbonate Materials and Methods for MEMS and Microfluidic Device Fabrication. *J. Chem. Inf. Model.* **2013**, *53* (10), 1689–1699.

(4) Uzunlar, E.; Kohl, P. a. Size-Compatible, Polymer-Based Air-Gap Formation Processes, and Polymer Residue Analysis for Wafer-Level MEMS Packaging Applications. *J. Electron. Packag.* **2015**, *137* (December), 041001.

(5) Monajemi, P.; Joseph, P. J.; Kohl, P. A.; Ayazi, F. Characterization of A Polymer-Based MEMS Packaging Technique. In *2006 11th International Symposium on Advanced Packaging Materials: Processes, Properties and Interface*; IEEE; pp 139–144.

(6) Saha, R.; Fritz, N.; Bidstrup-Allen, S. A.; Kohl, P. a. Packaging-Compatible Wafer Level Capping of MEMS Devices. *Microelectron. Eng.* **2013**, *104*, 75–84.

(7) Joseph, P. J.; Monajemi, P.; Ayazi, F.; Kohl, P. a. Wafer-Level Packaging of Micromechanical Resonators. *IEEE Trans. Adv. Packag.* **2007**, *30* (1), 19–26.

(8) Jayachandran, J. P.; Reed, H. a.; Zhen, H.; Rhodes, L. F.; Henderson, C. L.; Bidstrup, S. A.; Kohl, P. a. Air-Channel Fabrication for Microelectromechanical Systems via Sacrificial Photosensitive Polycarbonates. *J. Microelectromechanical Syst.* **2003**, *12* (2), 147–159.

(9) Reed, H. a; White, C. E.; Rao, V.; Allen, S. A. B.; Henderson, C. L.; Kohl, P. a. Fabrication of Microchannels Using Polycarbonates as Sacrificial Materials. *J. Micromechanics Microengineering* **2001**, *11*, 733–737.

(10) Li, W.; Tegenfeldt, J. O.; Chen, L.; Austin, R. H.; Chou, S. Y.; Kohl, P. a; Krotine, J.; Sturm, J. C. Sacrificial Polymers for Nanofluidic Channels in Biological Applications. *Nanotechnology* **2003**, *14*, 578–583.

(11) Lau, J. H. Design and Process of 3D MEMS System-in-Package (SiP). *J. Microelectron. Electron. Packag.* **2010**, *7*, 10–15.

(12) He, R.; Kim, C. C. On-Wafer Monolithic Encapsulation by Surface Micromachining With Porous Polysilicon Shell. *J. Microelectromechanical Syst.* **2007**, *16* (2), 462–472.

(13) Fu, K. K.; Wang, Z.; Dai, J.; Carter, M.; Hu, L. Transient Electronics: Materials and Devices. *Chem. Mater.* **2016**, *28* (11), 3527–3539.

(14) Hwang, S. W.; Kim, D. H.; Tao, H.; Kim, T. Il; Kim, S.; Yu, K. J.; Panilaitis, B.; Jeong, J. W.; Song, J. K.; Omenetto, F. G.; et al. Materials and Fabrication Processes for Transient and Bioresorbable High-Performance Electronics. *Adv. Funct. Mater.* **2013**, *23* (33), 4087–4093.

(15) Hwang, S.; Huang, X.; Seo, J.; Song, J.; Kim, S.; Hage-ali, S.; Chung, H.; Tao, H.; Omenetto, F. G.; Ma, Z.; et al. Materials for Bioresorbable Radio Frequency Electronics. **2013**, 3526–3531.

(16) Bettinger, C. J.; Bao, Z. Organic Thin-Film Transistors Fabricated on Resorbable Biomaterial Substrates. *Adv. Mater.* **2010**, *22* (5), 651–655.

(17) Hwang, S. W.; Lee, C. H.; Cheng, H.; Jeong, J. W.; Kang, S. K.; Kim, J. H.; Shin, J.; Yang, J.; Liu, Z.; Ameer, G. A.; et al. Biodegradable Elastomers and Silicon Nanomembranes/nanoribbons for Stretchable, Transient Electronics, and Biosensors. *Nano Lett.* **2015**, *15* (5), 2801–2808.

(18) Park, C. W.; Kang, S.-K.; Hernandez, H. L.; Kaitz, J. a.; Wie, D. S.; Shin, J.; Lee, O. P.; Sottos, N. R.; Moore, J. S.; Rogers, J. a.; et al. Thermally Triggered Degradation of Transient Electronic Devices. *Adv. Mater.* **2015**, n/a – n/a.

(19) Zhu, Q.; Meng, Y.; Tjong, S.; Zhao, X.; Chen, Y. Thermally Stable and High Molecular Weight Poly(propylene Carbonate)s from Carbon Dioxide and Propylene Oxide. *Polym. Int.* **2002**, *51* (10), 1079–1085.

(20) Hernandez, H. L.; Kang, S.-K.; Lee, O. P.; Hwang, S.-W.; Kaitz, J. A.; Inci, B.; Park, C. W.; Chung, S.; Sottos, N. R.; Moore, J. S.; et al. Triggered Transience of Metastable Poly(phthalaldehyde) for Transient Electronics. *Adv. Mater.* **2014**, *26* (45), 7637–7642.

(21) Uzunlar, E.; Schwartz, J.; Phillips, O.; Kohl, P. a. Decomposable and Template Polymers: Fundamentals and Applications. *J. Electron. Packag.* **2016**, *138* (2), 020802.

(22) Devlin, N. R.; Brown, D. K.; Kohl, P. a. Patterning Decomposable Polynorbornene with Electron Beam Lithography to Create Nanochannels. *J. Vac. Sci. Technol. B Microelectron. Nanom. Struct.* **2009**, *27* (2009), 2508.

(23) Bhusari, D.; Reed, H. a.; Wedlake, M.; Padovani, A. M.; Allen, S. A. B.; Kohl, P. a. Fabrication of Air-Channel Structures for Microfluidic, Microelectromechanical, and Microelectronic Applications. *J. Microelectromechanical Syst.* **2001**, *10* (3), 400–408.

(24) Joseph, P. J.; Kelleher, H. a; Allen, S. A. B.; Kohl, P. a. Improved Fabrication of Micro Air-Channels by Incorporation of a Structural Barrier. *J. Micromechanics Microengineering* **2004**, *15*, 35–42.

(25) Allen, S. D.; Moore, D. R.; Lobkovsky, E. B.; Coates, G. W. High-Activity, Single-Site Catalysts for the Alternating Copolymerization of CO2 and Propylene Oxide. *J. Am. Chem. Soc.* **2002**, *124* (48), 14284–14285.

(26) Chisholm, M. H.; Navarro-Llobet, D.; Zhou, Z. Poly(propylene Carbonate). 1. More about Poly(propylene Carbonate) Formed from the Copolymerization of Propylene Oxide and Carbon Dioxide Employing a Zinc Glutarate Catalyst. *Macromolecules* **2002**, *35* (17), 6494–6504.

(27) Gao, L. J.; Xiao, M.; Wang, S. J.; Du, F. G.; Meng, Y. Z. Copolymerization of Carbon Dioxide and Propylene Oxide with Zinc Glutarate as Catalyst in the Presence of Compounds Containing Active Hydrogen. *J. Appl. Polym. Sci.* **2007**, *104* (1), 15–20.

(28) Luinstra, G. a; Haas, G. R.; Molnar, F.; Bernhart, V.; Eberhardt, R.; Rieger, B. On the Formation of Aliphatic Polycarbonates from Epoxides with chromium(III) and aluminum(III) Metal-Salen Complexes. *Chemistry* **2005**, *11* (21), 6298–6314.

(29) Zhu, Q.; Meng, Y.; Tjong, S.; Zhao, X.; Chen, Y. Thermally Stable and High Molecular Weight Poly(propylene Carbonate)s from Carbon Dioxide and Propylene Oxide. *Polym. Int.* **2002**, *51* (September 2001), 1079–1085.

(30) Darensbourg, D. J. Chemistry of Carbon Dioxide Relevant to Its Utilization : A Personal Perspective. *Inorg. Chem.* **2010**, *49* (10), 10765–10780.

(31) Kember, M. R.; Buchard, A.; Williams, C. K. Catalysts for CO2/epoxide Copolymerisation W. *Chem. Commun.* **2011**, *47*, 141–163.

(32) Luinstra, G. Poly(Propylene Carbonate), Old Copolymers of Propylene Oxide and Carbon Dioxide with New Interests: Catalysis and Material Properties. *Polym. Rev.* **2008**, *48* (August 2015), 192–219.

(33) Michel, A.; Allen, S. Polycarbonate Polyol Compositions. *US Pat. Appl.* **2013**, *US 2013033*.

(34) Peng, S.; An, Y.; Chen, C.; Fei, B.; Zhuang, Y.; Dong, L. Thermal Degradation Kinetics of Uncapped and End-Capped Poly(propylene Carbonate). *Polym. Degrad. Stab.* **2003**, *80*, 141–147.

(35) Li, X. H.; Meng, Y. Z.; Chen, G. Q.; Li, R. K. Y. Thermal Properties and Rheological Behavior of Biodegradable Aliphatic Polycarbonate Derived from Carbon Dioxide and Propylene Oxide. *J. Appl. Polym. Sci.* **2004**, *94* (2), 711–716.

(36) Guo, C.; Zhou, L.; Lv, J. Improved Thermal Stability and Mechanical Propertiesof Poly(propylene Carbonate) by Reactive Blendingwith Maleic Anhydride. *Polym. Polym. Compos.* **2013**, *21*, 449–456.

(37) Li, X. H.; Meng, Y. Z.; Zhu, Q.; Tjong, S. C. Thermal Decomposition Characteristics of Poly(propylene Carbonate) Using TG/IR and Py-GC/MS Techniques. *Polym. Degrad. Stab.* **2003**, *81* (1), 157–165.

(38) Lu, X. L.; Zhu, Q.; Meng, Y. Z. Kinetic Analysis of Thermal Decomposition of Poly(propylene Carbonate). *Polym. Degrad. Stab.* **2005**, *89*, 282–288.

(39) Chisholm, M. H.; Navarro-Llobet, D.; Zhou, Z. Poly(propylene Carbonate). 1. More about Poly(propylene Carbonate) Formed from the Copolymerization of Propylene Oxide and Carbon Dioxide Employing a Zinc Glutarate Catalyst. *Macromolecules* **2002**, *35*, 6494–6504.

(40) Kember, M. R.; Buchard, A.; Williams, C. K. Catalysts for CO 2 / Epoxide Copolymerisation W. **2011**, 141–163.

(41) Dixon, D. D.; Ford, M. E.; Mantell, G. J. Thermal Stabilization of Poly(alkylene Carbonate)s. *J. Polym. Sci. Polym. Lett. Ed.* **1980**, *18* (2), 131–134.

(42) Barreto, C.; Hansen, E.; Fredriksen, S. Novel Solventless Purification of Poly(propylene Carbonate): Tailoring the Composition and Thermal Properties of PPC. *Polym. Degrad. Stab.* **2012**, *97* (6), 893–904.

(43) Guo, C.; Zhou, L.; Lv, J. Improved Thermal Stability and Mechanical Propertiesof Poly(propylene Carbonate) by Reactive Blendingwith Maleic Anhydride. *Polym. Polym. Compos.* **2013**.

(44) Qin, Y.; Chen, L.; Wang, X.; Zhao, X.; Wang, F. Enhanced Mechanical Performance of Poly(propylene Carbonate) via Hydrogen Bonding Interaction with O-Lauroyl Chitosan. *Carbohydr. Polym.* **2011**, *84* (1), 329–334.

(45) Chen, L.; Qin, Y.; Wang, X.; Li, Y.; Zhao, X.; Wang, F. Toughening of Poly(propylene Carbonate) by Hyperbranched Poly(ester-Amide) via Hydrogen Bonding Interaction. *Polym. Int.* **2011**, *60* (January), 1697–1704.

(46) Yu, T.; Zhou, Y.; Liu, K.; Zhao, Y.; Chen, E.; Wang, F.; Wang, D. Improving Thermal Stability of Biodegradable Aliphatic Polycarbonate by Metal Ion Coordination. *Polym. Degrad. Stab.* **2009**, *94* (2), 253–258.

(47) Yu, T.; Zhou, Y.; Zhao, Y.; Liu, K.; Chen, E.; Wang, D.; Wang, F. Hydrogen-Bonded Thermostable Liquid Crystalline Complex Formed by Biodegradable Polymer and Amphiphilic Molecules. *Macromolecules* **2008**, *41*, 3175–3180.

(48) Schwartz, J. M.; Engler, A.; Phillips, O.; Lee, J.; Kohl, P. a. Determination of Ceiling Temperature and Thermodynamic Properties of Low Ceiling Temperature Polyaldehydes. *J. Polym. Sci. Part A Polym. Chem.* **2018**, *56* (2), 221–228.

(49) Lee, O. P.; Lopez Hernandez, H.; Moore, J. S. Tunable Thermal Degradation of Poly(vinyl Butyl Carbonate Sulfone)s via Side-Chain Branching. *ACS Macro Lett.* **2015**, 665–668.

(50) Wang, W.; Alexander, C. Self-Immolative Polymers. *Angew. Chemie - Int. Ed.* **2008**, *47* (41), 7804–7806.

(51) McBride, R. A.; Gillies, E. R. Kinetics of Self-Immolative Degradation in a Linear Polymeric System: Demonstrating the Effect of Chain Length. *Macromolecules* **2013**, *46* (13), 5157–5166.

(52) Bowden, M. J.; Thompson, L. F. Effect of Olefin Structure on the Vapor-Development of Poly (olefin Sulfones) under Electron Irradiation. *Polym. Eng. Sci.* **1977**, *17* (4), 269–273.

(53) Robbins, J. S.; Schmid, K. M.; Phillips, S. T. Effects of Electronics, Aromaticity, and Solvent Polarity on the Rate of Azaquinone − Methide-Mediated Depolymerization of Aromatic Carbamate Oligomers. **2013**.

(54) Fan, B.; Trant, J. F.; Wong, A. D.; Gillies, E. R. Polyglyoxylates: A Versatile Class of Triggerable Self-Immolative Polymers from Readily Accessible Monomers. *J. Am. Chem. Soc.* **2014**, *136* (28), 10116–10123.

(55) Walsh, S. E.; Maillard, J. Y.; Russell, A. D. Ortho-Phthalaldehyde: A Possible Alternative to Glutaraldehyde for High Level Disinfection. *J. Appl. Microbiol.* **1999**, *86* (6), 1039–1046.

(56) De Winter, J.; Dove, A. P.; Knoll, A.; Gerbaux, P.; Dubois, P.; Coulembier, O. Control over Molar Mass, Dispersity, End-Groups and Kinetics in

Cyclopolymerization of Ortho-Phthalaldehyde: Adapted Choice of a Phosphazene Organocatalyst. *Polym. Chem.* **2014**, *5* (3), 706.

(57) Tanaka, A.; Hozumi, Y.; Hatada, K.; Endo, S.; Fujishige, R. Isomorphism Phenomena in Polyaldehydes. *Polym. Lett.* **1964**, *2*, 181–186.

(58) Kubisa, P.; Neeld, K.; Starr, J.; Vogl, O. Polymerization of Higher Aldehydes. *Polymer (Guildf).* **1980**, *21* (12), 1433–1447.

(59) Brame, E. G.; Sudol, R. S. Polymerization of Higher Aldehydes . Tacticity of Elastomeric Polyacetaldehyde. **1965**, *2* (January), 5337–5346.

(60) Vogl, O. Addition Polymers of Aldehydes. *J. Polym. Sci. Part A Polym. Chem.* **2000**, *38* (13), 2293–2299.

(61) Kaitz, J. A.; Lee, O. P.; Moore, J. S. Depolymerizable Polymers : Preparation , Applications , and Future Outlook. **2017**, *5* (2), 191–204.

(62) Cupta, M. G. Photoacid Generators for Catalytic Decomposition of Polycarbonate, Georgia Institute of Technology, 2006.

(63) White, C. E.; Balogun, A.; Henderson, C. L. Effects of the Photoacid Generator Type on the Imaging and Thermal Decomposition Properties of Photodefinable, Thermally Sacrificial Poly(propylene Carbonate) Materials. *J. Appl. Polym. Sci.* **2006**, *102*, 266–271.

(64) Spencer, T. J.; Kohl, P. a. Decomposition of Poly(propylene Carbonate) with UV Sensitive Iodonium Salts. *Polym. Degrad. Stab.* **2011**, *96* (4), 686–702.

(65) Sun, X.; Gao, J. P.; Wang, Z. Y. Bicyclic Guanidinium Tetraphenylborate: A Photobase Generator and a Photocatalyst for Living Anionic Ring-Opening Polymerization and Cross-Linking of Polymeric Materials Containing Ester and Hydroxy Groups. *J. Am. Chem. Soc.* **2008**, *130*, 8130–8131.

(66) Sun, X. Development of Tetraphenylborate-Based Photobase Generators and Sacrificial Polycarbonates for Radiation Curing and Photoresist Applications, Carleton University, 2008.

(67) Crivello, J. V. The Discovery and Development of Onium Salt Cationic Photoinitiators. *J. Polym. Sci. Part A Polym. Chem.* **1999**, *37* (DECEMBER 1999), 4241–4254.

(68) Shi, S.; Croutxé-Barghorn, C.; Allonas, X. Photoinitiating Systems for Cationic Photopolymerization: Ongoing Push toward Long Wavelengths and Low Light Intensities. *Prog. Polym. Sci.* **2017**, *65*, 1–41.

(69) Crivello, J. V.; Jang, M. Anthracene Electron-Transfer Photosensitizers for Onium Salt Induced Cationic Photopolymerizations. *J. Photochem. Photobiol. A Chem.* **2003**, *159*, 173–188.

(70) Kavarnos, G. J.; Turro, N. J. Photosensitization by Reversible Electron Transfer : Theories , Experimental Evidence , and E Xamples. *Chem. Rev.* **2002**, *86* (May), 401–449.

(71) Lee, S.; Armitsu, K.; Park, S.-W.; Ichimura, K. Synthesis and Evaluation of Novel Acid Amplifiers Acids Liberating Fluoroalkanesulfonic Acids. *J. Photopolym. Sci. Technol.* **2000**, *13* (2), 215–216.

(72) Hosoi, K.; Cardineau, B.; Kruger, S.; Miyauchi, K.; Brainard, R. Fluorine-Stabilized Acid Amplifiers for Use in EUV Lithography. *J. Photopolym. Sci. Technol.* **2012**, *25* (5), 575–581.

(73) Arimitsu, K.; Kudo, K.; Ichimura, K. Autocatalytic Fragmentation of Acetoacetate Derivatives as Acid Amplifiers to Proliferate Acid Molecules. *J. Am. Chem. Soc.* **1998**, *120* (4), 37–45.

(74) Gallatin, G. M.; Naulleau, P.; Niakoula, D.; Brainard, R. L.; Hassanein, E.; Matyi, R.; Thackeray, J.; Spear, K.; Dean, K. Resolution, LER, and Sensitivity Limitations of Photoresists. *Proc. SPIE* **2008**, *6921* (2008), 69211E – 69211E – 11.

(75) Schwartz, J. M.; Phillips, O.; Engler, A.; Sutlief, A.; Lee, J.; Kohl, P. A. Stable, High-Molecular-Weight Poly(phthalaldehyde). *J. Polym. Sci. Part A Polym. Chem.* **2017**, *55* (7), 1166–1172.

(76) Schmidt, R.; Göttling, S.; Leusser, D.; Stalke, D.; Krause, A.-M.; Würthner, F. Highly Soluble Acenes as Semiconductors for Thin Film Transistors. *J. Mater. Chem.* **2006**, *16*, 3708.

(77) Pramanik, C.; Miller, G. P. An Improved Synthesis of Pentacene: Rapid Access to a Benchmark Organic Semiconductor. *Molecules* **2012**, *17* (4), 4625–4633.

(78) Kruger, S. A.; Higgins, C.; Cardineau, B.; Younkin, T. R.; Brainard, R. L. Catalytic and Autocatalytic Mechanisms of Acid Amplifiers for Use in EUV Photoresists. *Chem. Mater.* **2010**, *22* (19), 5609–5616.

(79) Campbell, S. a. The Science and Engineering of Microelectronic Fabrication. *Oxford University Press*. 2001, p 688.

(80) White, C. E.; Henderson, C. L.; White, C. E.; Henderson, C. L. Development of Improved Photosensitive Polycarbonate Systems for the Fabrication of Microfluidic Devices Development of Improved Photosensitive Polycarbonate

Systems for the Fabrication of Microfluidic Devices. *J. Vac. Sci. Technol. B* **2003**, *21*, 2926.

(81) Kodiyan, J.; Jae, S.; Hae, J.; Woo, D.; Yang, I.; Yeoul, B. Thermal and Weathering Degradation of Poly (Propylene Carbonate). *Polym. Degrad. Stab.* **2010**, *95* (6), 1039–1044.

(82) Kuran, W.; Górecki, P. Degradation and Depolymerization of Poly(propylene Carbonate) by Diethylzinc. *Die Makromol. Chemie* **1983**, *184*, 907–912.

(83) Liu, B.; Chen, L.; Zhang, M.; Yu, A. Degradation and Stabilization of Poly (Propylene Carbonate). *Macromol. Rapid Commun.* **2002**, *23*, 881–884.

(84) Seo, J.; Jeon, G.; Jang, E. S.; Khan, S. B.; Han, H. Preparation and Properties of Poly (Propylene Carbonate) and Nanosized ZnO Composite Films for Packaging Applications. *J. Appl. Polym. Sci.* **2011**, *122* (2), 1101–1108.

(85) Wyrzykowski, D.; Hebanowska, E.; Nowak-Wiczk, G.; Makowski, M.; Chmurzynski, L. Thermal Behaviour of Citric Acid and Isomeric Aconitic Acids. *J. Therm. Anal. Calorim.* **2011**, *104* (2), 731–735.

(86) Fischer, J. W.; Merwin, L. H.; Nissan, R. A. NMR Investigation of the Thermolysis of Citric Acid. *Appl. Spectrosc.* **1995**, *49* (1), 120–126.

(87) Barbooti, M. M.; Al-Sammerrai, D. A. Thermal Decomposition of Citric Acid. *Thermochim. Acta* **1986**, *98*, 119–126.

(88) Crivello, J. V. Design and Synhesis of Photoacid Generating Systems. *Journal of Photopolymer Science and Technology*. 2008, pp 493–497.

(89) Crivello, J. V.; Bulut, U. Curcumin: A Naturally Occurring Long-Wavelength Photosensitizer for Diaryliodonium Salts. *J. Polym. Sci. Part A Polym. Chem.* **2005**, *43* (May), 5217–5231.

(90) Dadashi-Silab, S.; Doran, S.; Yagci, Y. Photoinduced Electron Transfer Reactions for Macromolecular Syntheses. *Chem. Rev.* **2016**, *116* (17), 10212–10275.

(91) Wallraff, G.M.; Allen, R.D.; Hinsberg, W.D.; Willson, C.G.; Simpson, L.L.; Webber, S.E.; Sturteveant, J. L. A Chemically Amplified Photoresist for Visible Laser Direct Imaging. *Journal of Imaging Science and Technology*. 1992, pp 468–476.

(92) Patra, D.; Malaeb, N. N.; Haddadin, M. J.; Kurth, M. J. Influence of Substituent and Solvent on the Radiative Process of Singlet Excited States of Novel Cyclic Azacyanine Derivatives. *J. Fluoresc.* **2012**, *22* (2), 707–717.

(93) Brömme, T.; Oprych, D.; Horst, J.; Pinto, P. S.; Strehmel, B. New Iodonium Salts in NIR Sensitized Radical Photopolymerization of Multifunctional Monomers. *RSC Adv.* **2015**, *5* (86), 69915–69924.

(94) Brömme, T.; Schmitz, C.; Moszner, N.; Burtscher, P.; Strehmel, N.; Strehmel, B. Photochemical Oxidation of NIR Photosensitizers in the Presence of Radical Initiators and Their Prospective Use in Dental Applications. *ChemistrySelect* **2016**, *1* (3), 524–532.

(95) Kabatc, J.; Ortyl, J.; Kostrzewska, K. New Kinetic and Mechanistic Aspects of Photosensitization of Iodonium Salts in Photopolymerization of Acrylates. *RSC Adv.* **2017**, *7* (66), 41619–41629.

(96) Schmitz, C.; Halbhuber, A.; Keil, D.; Strehmel, B. NIR-Sensitized Photoinitiated Radical Polymerization and Proton Generation with Cyanines and LED Arrays. *Prog. Org. Coatings* **2016**, *100*, 32–46.

(97) Shiraishi, A.; Kimura, H.; Oprych, D.; Schmitz, C. Comparison between NIR and UV-Sensitized Radical and Cationic Reactivity of Iodonium Salts Comprising Anions with Different Coordination Behavior. **2017**, *30* (6), 633–638.

(98) Lakowicz, J. R. *Principles of Fluorescence Spectroscopy Principles of Fluorescence Spectroscopy*; 2006.

(99) Turley, W. D.; Offen, H. W. Diffusion-Controlled Quenching in Solutions at High Pressures. *J. Phys. Chem.* **1984**, *88* (16), 3605–3607.

(100) Dektar, J. L.; Hacker, N. P. Photochemistry of Diaryliodonium Salts. *J. Org. Chem.* **1990**, *55* (2), 639–647.

(101) Breton, G. W.; Vang, X. Photodimerization of Anthracene. *J. Chem. Educ.* **1998**, *75* (1), 81.

(102) Phillips, O.; Schwartz, J. M.; Engler, A.; Gourdin, G.; Kohl, P. A. Phototriggerable Transient Electronics: Materials and Concepts. *Proc. - Electron. Components Technol. Conf.* **2017**, 772–779.

(103) Tsuda, M.; Hata, M.; Nishida, R. I. E.; Oikawa, S. Acid-Catalyzed Degradation Mechanism of Poly (Phthalaldehyde): Unzipping Reaction of Chemical. 77–89.

(104) Schwartz, J. M. Advances in Low-K and Transient Polymers. *Georg. Inst. Technol.* **2017**, No. August.

(105) Scott, M. P.; Brazel, C. S.; Benton, M. G.; Mays, J. W.; Holbrey, D.; Rogers, R. D. Application of Ionic Liquids as Plasticizers for Poly (Methyl Methacrylate). *Chem. Commun.* **2002**, 1370–1371.

(106) Rahman, M.; Brazel, C. S. Ionic Liquids: New Generation Stable Plasticizers for Poly(vinyl Chloride). *Polym. Degrad. Stab.* **2006**, *91* (12), 3371–3382.

(107) Scott, M. P.; Rahman, M.; Brazel, C. S. Application of Ionic Liquids as Low-Volatility Plasticizers for PMMA. *Eur. Polym. J.* **2003**, *39* (10), 1947–1953.

(108) Sankri, A.; Arhaliass, A.; Dez, I.; Gaumont, A. C.; Grohens, Y.; Lourdin, D.; Pillin, I.; Rolland-Sabaté, A.; Leroy, E. Thermoplastic Starch Plasticized by an Ionic Liquid. *Carbohydr. Polym.* **2010**, *82* (2), 256–263.

(109) Geng, Y.; Li, J.; Jing, X.; Wang, F.; Academy, C. Interaction of N-Methylpyrrolidone with Doped Polyaniline. *Synth. Met.* **1997**, *84*, 97–98.

(110) Schlegel, L.; Ueno, T.; Hayashi, N.; Iwayanagi, T. Determination of Acid Diffusion in Chemical Amplification Positive Deep-UV Resists. *Japanese J. Appl. Physics, Part 1 Regul. Pap. Short Notes Rev. Pap.* **1991**, *30* (1991), 3132–3137.

(111) Fedynyshyn, T. H.; Thackeray, J. W.; Georger, J. H.; Denison, M. D. Effect of Acid Diffusion on Performance in Positive Deep Ultraviolet Resists. *J. Vac. Sci. Technol. B* **1994**, *12* (1994), 3888.

(112) Postnikov, S. V.; Stewart, M. D.; Tran, H. V.; Nierode, M. a.; Medeiros, D. R.; Cao, T.; Byers, J.; Webber, S. E.; Wilson, C. G. Study of Resolution Limits due to Intrinsic Bias in Chemically Amplified Photoresists. *J. Vac. Sci. Technol. B Microelectron. Nanom. Struct.* **1999**, *17* (1999), 3335.

(113) Stewarta, M. D.; Somervella, M. H.; Tranb, H. V.; Postnikovb, S. V; Willsonab, C. G. Study of Acid Transport Using IR Spectroscopy and SEM. *Processing* **2000**, *3999*, 665–674.

(114) Kang, S. K.; Hwang, S. W.; Yu, S.; Seo, J. H.; Corbin, E. a.; Shin, J.; Wie, D. S.; Bashir, R.; Ma, Z.; Rogers, J. a. Biodegradable Thin Metal Foils and Spin-on Glass Materials for Transient Electronics. *Adv. Funct. Mater.* **2015**, *25* (12), 1789–1797.

(115) Yin, L.; Cheng, H.; Mao, S.; Haasch, R.; Liu, Y.; Xie, X.; Hwang, S. W.; Jain, H.; Kang, S. K.; Su, Y.; et al. Dissolvable Metals for Transient Electronics. *Adv. Funct. Mater.* **2014**, *24* (5), 645–658.